Detection of an Experimental Mass Grave over Time and at Different Spatial Scales in a Temperate Environment

Gabriela Ifimov

Department of Geography

McGill University

Montreal, Quebec, Canada

A thesis submitted to McGill University
In partial fulfillment of the requirement of the degree of
Master of Science

Abstract

In the past decades, the detection of clandestine mass graves has become a topic of high interest for the international forensic community. Hyperspectral remote sensing may provide complementary and novel techniques to detect mass graves in regions with human conflict by detecting changes in site surface reflectance, which can potentially be different from a non-grave area. In this research study, I assessed differences in spectral reflectance between an experimental mass grave and a non-grave in a temperate environment at three different spatial scales: leaf level and plot level using field spectroscopy and airborne hyperspectral imagery.

To test the application of hyperspectral remote sensing as a tool in the detection of mass graves, three experimental study sites were established in Ottawa, Ontario, Canada: an experimental mass grave containing pig carcasses (*Sus Scrofa domesticus)* at one meter depth, a reference site containing only disturbed soil, and an undisturbed control site. Soil and vegetation samples and spectral data using field spectrometry and airborne hyperspectral imagery were collected in the first 15 months post-disturbance.

The main findings of this research show that differences in spectral reflectance depend on spatial scale, disturbance stage and time in the growing season. Overall differences were found between the grave and control in soil chemistry, vegetation pigmentation and spectral reflectance throughout the study period. In the first 13 months post-disturbance, differences in soil chemistry (e.g. calcium and manganese), vegetation pigmentation (i.e. chlorophyll and carotenoids), and spectral reflectance between the mass grave and reference can be attributed to the overall site disturbance and not as a result of the decomposition process. In contrast, 13 months after burial there are differences in soil chemistry (i.e. ammonium, nitrate, and available phosphorus) and vegetation pigmentation between the mass grave and reference. In terms of spectral reflectance, differences were found along the 400 – 700 nm wavelength range between mass grave and reference during this period. It was also found that the combination of different vegetation indices on airborne imagery increases the spectral separation between mass grave, reference and control depending on time since disturbance. Given that spectral differences emerge towards the end of the data collection, detectable differences between the mass grave and the reference may be delayed due to (1) a slow cadaver decomposition rate and/or (2) the depth of burial that provides a greater barrier to nutrient uptake in surficial plants as previously shown in others studies for deep and shallow graves.

Résumé

Au cours des dernières décennies, la détection des fosses communes clandestines a pris une grande importance au sein de la communauté médico-légale internationale. La télédétection hyperspectrale fournit des techniques complémentaires et nouvelles concernant la détection des fosses communes dans des zones de conflits humanitaires en détectant des changements dans la signature spectrale des surfaces qui peuvent potentiellement être différentes de celles n'ayant pas de fosses communes. Dans cette étude, je vise à évaluer les variations dans les signatures spectrales entre une fosse commune expérimentale et un site neutre dans un environnent à climat tempéré à trois échelles spatiales: au niveau de la végétation et du site en utilisant la spectrométrie du terrain et d'images aériennes hyperspectrales.

Pour tester l'utilisation de la télédétection hyperspectrale en tant qu'outil complémentaire dans la détection des fosses communes enfouies profondément, trois sites expérimentaux ont été établis à Ottawa en Ontario au Canada: une tombe expérimentale ayant carcasses de porcs (*Sus Scrofa domesticus)* a une profondeur d'un mètre, un site neutre ayant seulement un sol mélangé, et un site de contrôle où aucune altération n'a été faite. Des échantillons du sol et végétation et données sur les signatures spectrales, utilisant la spectrométrie du terrain et l'image aérienne hyperspectrale, ont été recueillies pendant les 15 premiers mois suivant la création des sites.

Les principaux résultats de cette étude montrent que les différences en signatures spectrales dépendent de l'échelle spatiale, l'ancienneté du site, ainsi que les conditions environnementales. Des différences ont été trouvées entre la fosse commune et le contrôle dans la chimie du sol, la pigmentation de la végétation et en signatures spectrales pendant toute la période de l'étude. Dans les premiers 13 mois suivant la création des sites, les différences dans la chimie du sol (ex. présence de calcium et manganèse), la pigmentation de la végétation (ex. les concentrations de chlorophylle et caroténoïdes), et les signatures spectrales entre la fosse commune expérimentale et le site neutre sont dues aux effets causés par le mélange du sol. Cependant, les données recueillies après le 13ème mois suggèrent des différences dans la chimie du sol (ex. présence de phosphore, ammonium et nitrate), les concentrations de chlorophylle et caroténoïdes, et les signatures spectrales. Des différences dans les signatures spectrales dans la gamme de longueur d'onde de 400-700 nm ont été découvertes entre la fosse commune expérimentale et le site neutre durant la période d'étude. Nous pouvons aussi ajouter que la combinaison des différents indicateurs de la végétation pour les images aériennes

hyperspectrales peut augmenter la séparation spectrale entre la fosse commune, le site neutre et le contrôle dépendamment de l'avancement temporelle de celle-ci. Puisque les changements des signatures spectrales ont été trouvés pendant les derniers mois de la collection des données (c.d.a. après 13 mois de la création des sites), la possibilité de différencier la fosse commune profonde d'un site neutre peut être retardée à cause de (1) une lente décomposition des cadavres, et/ou (2) de la profondeur de la tombe qui est une barrière pour l'absorption des nutriments par la végétation en comparaison avec des études précédentes sur les fosses communes en surface ou peu profondes.

Acknowledgements

First and foremost, I would like to express my gratitude to my co-supervisors, Dr. Margaret Kalacska and Dr. George Leblanc, for their support and guidance throughout this thesis. The completion of this thesis would not have been possible without their constant feedback during all stages of the project. I will always be grateful for the opportunities they have giving me over the past two years, which allowed me to grow and develop my academic and professional skills. I would further want to extend my thanks to Dr. Tim Moore for being part of this project and for all his feedback and support throughout my studies. I would also like to thank Mike Dalva for his help given during the process of my thesis.

I would like to recognize the help of Ray Soffer in processing the airborne images and for his valuable input during data collection. Further, I would like to thank to everyone who has helped with the data collection process, without which the completion of this thesis would have been near to impossible.

This research would have not been possible without the financial support of the DRDC-Valcartier, the Flight Research Laboratory of the National Research Council Canada, Fonds Quebecois de la Recherché sur la Nature et les Technologies, and Social Sciences and Humanities Research Council Canada. Further, many thanks goes to my supervisor, Dr. Margaret Kalacska, and her lab for providing me with the necessary computer power and instrumentation to conduct all my research.

I would like to mention and acknowledge the support and understanding of my family throughout my study. A big thank you goes to those taking the time to help with the editing of this thesis. Many thanks and appreciations go to my friends and colleagues for their support and moments of laughter. I will always cherish them!

Table of Contents

List of Tables

List of Figures

List of Equations

List of Abbreviations

AOD	Aerosol Optical Depth
AGL	Above Ground Level
ASD	Analytical Spectral Device
ANOVA	Analysis of Variance
CASI	Compact Airborne Spectrographic Imager
FLAASH	Fast Line-of-Sight Atmospheric Analysis of Spectral Hypercube
FOV	Field of View
FRL - NRC	Flight Research Laboratory – National Research Council Canada
FWHM	Full Width at Half Maximum
GIS	Geographic Information Systems
NDPI	Normalized Difference Pigment Index
NDVI1	Normalized Difference Vegetation Index 1
NDVI2	Normalized Difference Vegetation Index 2
PSRI	Plant Senescence Reflectance Index
RENDVI	Red Edge NDVI
REP	Red-edge Position Index
ROI	Region of Interest
RVSI	Red-Edge Vegetation Stress Index
SASI	Shortwave Infrared Airborne Spectrographic Imager
SGI	Sum Green Index
SIPI	Structure Insensitive Pigment Index
VC	Vicarious Calibration Process
VOG1	Vogelmann Red Edge Index 1
VOG2	Vogelmann Red Edge Index 2

1. Introduction

Events such as war crimes, human right abuses, and political instability can lead to the creation of mass graves. For instance, countries such as Argentina (Fondebrider and Doretti 2004), East Timor (Blau and Skinner 2005), Guatemala (Schmitt 2001), Rwanda (Haglund et al. 2001a), and Bosnia Herzegovina (Skinner et al. 2001) are only a few of the locations where mass burials have been reported. Criminal proceedings for mass graves have led the international community to focus on the detection and exhumation of mass burials (Jessee and Skinner 2005). An emphasis is placed on least invasive detection methods and techniques to ensure the integrity of the site and evidence during investigations (Cox 2008).

A mass grave can be defined as a burial unit in soil containing two or more bodies in close contact with each other (Jessee and Skinner 2005). Clandestine burial detection represents a difficult task and mandates the employment of multiple investigation sources, as the search of burial sites requires the location of a small disturbance in a larger environment (Cox 2008; Gleason 2008). An understanding of a clandestine grave's characteristics and local environment is necessary during search investigations. Even though it is challenging to predict changes over multiple environments in which clandestine graves occur, there are key indicators that can indicate potential location areas (Gleason 2008; Powell 2006). Investigators require an understanding of the size and depth of the clandestine grave being searched for, as these factors can have different impacts on the surrounding environment (Gleason 2008). In addition, depending on the size and characteristics of the burial, disruptions in the surrounding environments, such as soil or vegetation disturbances, can indicate the potential location of a grave (Gleason 2008; Powell 2006). The most effective method of examining grave characteristics has been through the study of how the cadaver decomposition process impacts the surrounding environment (Larson et al. 2011). A large body of literature demonstrates changes in both soil and vegetation associated with body decomposition (Anderson et al. 2013; Caccianiga et al. 2012; Carter and Tibbett 2008; Carter et al. 2007; Dent et al. 2004).

The search for clandestine graves usually involves teams of professionals and/or volunteers in areas that are selected based on witness testimony (Gleason 2008). An investigation becomes more focused on areas of greater probability when a multidisciplinary team employs a variety of gravesite detection methods such as eyewitness testimony (Larson et al. 2011), search dogs (Rebmann and David 2000), geophysical methods such as ground-penetrating radar (Ruffell and McKinley 2005), and use of remote sensing data such as aerial photography and satellite imagery (Cheetham 2005; Congram 2008). Remote sensing is defined as the collection of information on the amount of reflected energy by a material at different spatial scales (i.e. *in-situ*, airborne and satellite sensors) (Jones and Vaughan 2010). Remote sensing can be seen as a minimally intrusive method of detecting burials by locating anomalies in the landscape (Gleason 2008). Regardless of the methods used during investigations, the location of a burial site is a time and resource-consuming process as a grave can have various impacts on the surrounding environment depending on the local ecosystem (Cox 2008; Wilson et al. 2007). The development of new methods for detecting changes in the local environment, associated with disturbances caused by mass burials, can potentially reduce search areas, decrease investigation time, and ultimately, bring relief to the families of the victims.

Novel advances in hyperspectral remote sensing have been shown to provide additional tools to detect changes in soil and vegetation characteristics as a result of body decomposition in tropical (Kalacska and Bell 2006; Kalacska et al. 2009) and temperate (Leblanc et al. 2014) environments. Hyperspectral remote sensing is the remote acquisition of information (i.e. *in-situ*, airborne and satellite sensors) on the amount of reflected energy by a material over dozens or hundreds of contiguous spectral bands (Jones and Vaughan 2010). For instance, hyperspectral data provide information on the grain size, abundance and composition of elements (e.g. iron) in minerals at fine spectral resolution (Goetz 2009). Hyperspectral sensors can measure subtle features within spectral signatures that are associated with soil and vegetation properties (Zwiggelaar 1998). A spectral signature is defined as the response of reflected and absorbed electromagnetic radiation at specific wavelengths (Eismann 2012). The release of nutrients into the soil matrix from the decomposition process leads to changes in soil and plant chemistry (Forbes 2008), which may lead to changes in vegetation pigmentation (de Gea 2012; Snirer 2014). Given that a grave manifests differently depending on the local environment, further research is required to better understand and investigate the application of hyperspectral remote sensing in clandestine mass grave detection.

The main objective of this research is to compare differences in spectral reflectance of an experimental mass grave, a reference (i.e. disturbed soil), and a control (i.e. undisturbed soil and vegetation) based on field data (i.e. soil chemistry and vegetation pigmentation), field spectrometry and airborne hyperspectral imagery in a temperate environment. This study aims to answer the following research questions:

1. Are there any significant differences in soil chemistry and vegetation pigmentation between a grave, a reference, and a control?
2. Is the spectral signature of an experimental mass grave distinguishable from those of the reference and control using field spectroscopy and hyperspectral airborne imagery?

The main hypothesis of this research is that the belowground body decomposition process has an impact on the surrounding soil and vegetation resulting in distinguishable features in their spectral signatures. Therefore, potential differences in soil chemistry and vegetation pigmentation could be captured by spectral measurements using field spectroscopy and/or airborne hyperspectral images.

To address these research questions an experimental mass gravesite was constructed at the Flight Research Laboratory – National Research Council Canada (FRL-NRC), Ottawa, Ontario, on June 25th, 2013. Pig carcasses (*Sus Scrofa domesticus)* were used as cadaver proxies. Field data consisting of soil and vegetation samples, field spectrometry and airborne hyperspectral imagery were collected in the first 15 months post-disturbance, over the 2013 and 2014 growing seasons.

The following chapter, Chapter 2, presents a review of the scientific literature related to: mass graves, common burial detection methods, remote sensing application in burial sites detection, and a brief overview of hyperspectral remote sensing and spectral properties of soil and vegetation. Chapter 3 describes the methodological approach carried out to answer both research questions, including the experimental design and data analyses. Chapter 4 reveals the findings for the *in-situ* soils chemistry and vegetation pigments (Q1) as well as on the spectroscopy and airborne analysis for detecting differences on mass grave, reference and control (Q2). Chapter 5 presents a discussion of the results for both primary research questions, noted above, with the goal of temporally integrating the *in-situ* characterization with the remote sensing results between grave, reference and control. This thesis concludes by summarizing the major findings of the current research and provides recommendations for future research within this subject. Overall, this research offers insights on the temporal changes in spectral reflectance of an experimental mass grave and illustrates the utility of hyperspectral remote sensing for the detection of mass burials.

2. Literature Review

2.1. Mass Grave Definition

No agreement has been found in literature on the definition of a mass grave (Table 2.1). The definition of a mass grave varies in terminology from a site containing a minimum of two bodies (Jessee and Skinner 2005) to a site containing at least half a dozen bodies (Skinner 1987). Haglund (2001) defines a mass grave as a site in soil containing an organized or unorganized mass or aggregate of individuals. In the current project, a mass grave is defined as a burial unit in soil containing 20 bodies in close contact with each other. This project focuses on graves involving burials in soil and does not include other scenarios such as burials beneath buildings or under water.

Table 2.1. Summary table of main mass grave definitions reported across the reviewed literature.

Definition	**Reference**
A site containing at least half a dozen individuals.	Skinner (1987)
A site containing two or more bodies in close contact with each other.	Jessee and Skinner (2005)
A site containing a "large quantity or aggregate, usually of considerable size, whether organized or unorganized" in close contact.	Haglund (2001); Haglund et al. (2001a)
Any single burial unit containing "two or more tightly packed, yet indiscriminately placed bodies of victims who have died" as a result of a conflict.	Jessee (2003)
Any site defined as a place of permanent interment from which the bodies are prevented from being moved by natural elements, and which contain two or more bodies.	UN (1994) as cited in Jessee (2003)
A site containing three or more victims of extra-juridical, summary, or arbitrary execution.	UN (1996) as cited in Jessee (2003)
A criminal mass grave is a site containing the remains of a group of individuals who share "some common trait that justified their assassinations in the eyes of the perpetrators".	Schmitt (2001)

By looking at past events investigators can have a better understanding of the characteristics of mass burials that can further help in their detection. An extremely conservative number of victims due to conflicts have been estimate to 200,000 in Guatemala (Stoll 2004), 19,000 in Cambodia (Berkhoff 2004), 800,000 in Rwanda (Dallaire and Beardsley 2005), 33,000 in Babi Yar (Berkhoff 2004), 500,000 in Indonesia (Chalk et al. 1990), and 50,000 of Kurdish (Fischbach 2004) among many other accounts in around the world. Sources in the peer reviewed literature are very limited, with the primary source of information being from reports of organizations such as Amnesty International (AMR), International Commission on Missing Persons (ICMP), Human Rights Watch (HRW), and United Nations (UN). Mass graves have been reported to vary in size and number of victims depending on the location and event leading to its creation. Across the studied literature, the number of found victims in excavated burials can vary from single individuals to more than 2000 victims. Figure 2.1 displays a conservative worldwide representation of the number of victims who were found in mass graves. These examples represent a limited and conservative number of mass graves reported in literature. Details of a few excavated mass graves can be found in Appendix A.

Across the literature, different types of mass graves and mass grave-related sites have been identified. For example, Jessee (2003) makes a distinction between grave types such as execution sites, which can be separated into surface execution and grave execution sites. There are also temporary surface deposition sites, where the victims are deposited until placed in a grave in a different location, and permanent surface deposition sites where human remains are displaced (Cox 2008; Jessee 2003). A distinction between four inhumation sites is also made across the literature. An inhumation site is defined as grave containing multiple individuals who have been executed and buried soon after death and who shared a related cause and manner of death (Jessee and Skinner 2005; Mant 1987; Schmitt 2001; Skinner 1987). There are primary inhumation sites, also called primary mass graves, which are, on occasion, execution sites as well, where there is evidence pointing that all victims have died from a common cause and matter (Jessee and Skinner 2005; Mant 1987; Simmons 2001; Skinner 1987). Another common mass grave is a secondary inhumation site, also called secondary mass grave where the burial shows evidence of being opened and victims being removed (Jessee and Skinner 2005; Sterenberg 2002). Both primary and secondary inhumation sites can also be defined as multiple deposit interment sites where body masses are separated by soil and deposited over time, or looted inhumation ones from which the remains have been removed for the purpose of creating a secondary inhumation site. The method of burial can have an impact on how the presence of the burial site influences the surrounding soil and vegetation and, ultimately, its detection during investigations.

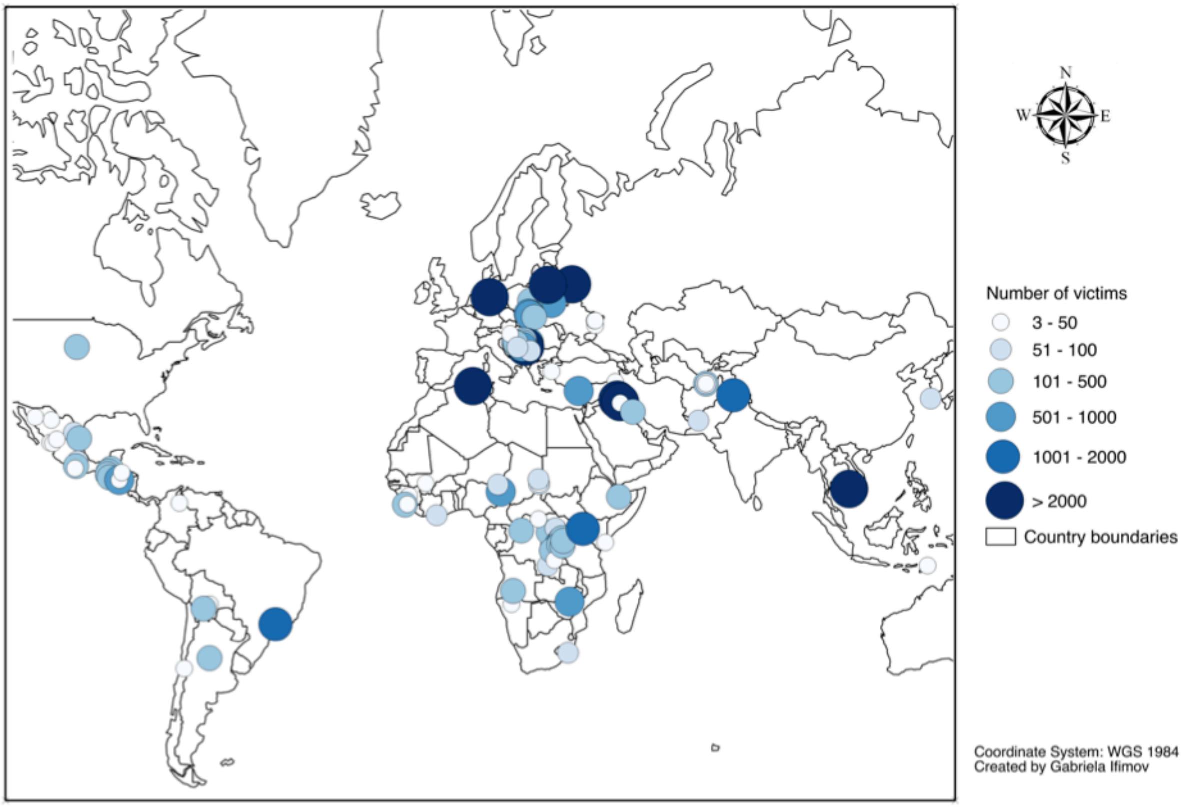

Figure 2.1. Visualization of the number of victims found in a few excavated mass graves around the world. Appendix A contains the details regarding the location, number of victims and source of the illustrated mass graves.

2.2. Decomposition Process

The presence of a buried body has an impact on the surrounding microenvironment as it decomposes (Wilson et al. 2007). A mass grave has been characterized as a unique microenvironment where cadavers decompose at different rates depending on their condition at burial, method of burial, and soil conditions in and around the grave (Mant 1950). In his study, Mant (1950) reveals that cadavers located in the center of a mass grave decompose at a slower rate than those on the outer extent of the grave in a temperate environment, calling it the "feather-edge effect". FizGibbon (1977) reports similar findings in a report on the exhumation of a mass grave from Russia, where various stages of decay with mummification in the upper most layer and sides of the grave have been reported (as cited by Haglund et al. 2001). Multiple studies report a greater preservation at the core of mass graves and a negative correlation between decomposition rate and mass size (Nagy 2010; Wilson et al. 2007). Moreover, Mant (1950) reports a particular case where one female body was remarkably preserved because it was buried immediately after death, at 3 meters depth, well covered with subcutaneous fat, and located towards the center of the mass grave.

Factors such as depth, temperature, moisture, soil type, associated materials, and trauma have an impact on the process of body decomposition (Carter and Tibbett 2008; Carter et al. 2007; Carter et al. 2008a; Dent et al. 2004; Haglund 2001; Mant 1950). The rate of body decomposition can depend primarily on the depth at which the body is buried, as below ground decomposition has been found to have slower decomposition rates than above ground rates (Carter et al. 2007; Haglund 2001; Mant 1950). Temperature has also been noted as an influential factor of decomposition (Carter et al. 2008a; Gill-King 1996; Mant 1950) which is also dependent on the depth of burial (Gordon 2010; Wilson et al. 2007). An increase in temperature has been reported to increase the rate of decomposition due to an increase in microbial activity (Carter and Tibbett 2006). While a slower decomposition rate has been reported at lower temperatures, no initial significant changes in surface grave soil chemistry have been reported in the first 320 days regardless of the season in a pasture field in Northern Nebraska characterized by clay loamy soil (Meyer et al. 2013). The decomposition process of cadavers in a mass burial creates a greater amount of heat during the initial stages in comparison with single buried cadavers in a temperate environment (Jessee 2003). The impacts of soil type and moisture on body decomposition rates have been studied in great detail (Damann et al. 2012; Dekeirsschieter et al. 2009; Dent et al. 2004; Tumer et al. 2013). Soil moisture can affect the metabolism of decomposer microorganisms in different ways (Carter et al. 2010). For example, the lack, or overabundance, of moisture will slow the decomposition process (Carter et al. 2007; Carter et al. 2010). A study conducted by Tumer et al. (2013) on the effects of different soil types on the body decomposition process at a 50 cm depth, reveals that the decomposition rates are faster in loamy and organic soils in comparison with clayey and sandy soils. In addition, it was found that soil moisture could lead to different decomposition rates in the same microenvironment (Wilson et al. 2007). Lastly, the presence of clothing has been found to slow the decomposition process by acting as protection from insects and helps adipocerous formation by keeping the body moist and absorbing water from the soil (Galloway 1996; Gordon 2010; Mant 1950).

The body decomposition process generally has been reported as going thought five main different stages such as the fresh, deflation, decomposition, disintegration, and skeletonization stage (Carter et al. 2007), each of which can have a different effect on the surrounding soil (Langner et al. 2006). A distinctive grave soil and a 'body decomposition island' are formed as nutrients from both soft tissue and bone are leached into the soil matrix (Carter et al. 2007). Several studies have showed that the cadaver decomposition process has an impact on the chemical, physical and biological processes of grave soil (Carter and Tibbett 2008; Forbes 2008; Tibbett and Carter 2009). Table 2.2 shows the different soil chemistry changes caused by the body decomposition process in a temperate environment reported across the literature. According to the decomposition odour analysis database, as many as 478 volatile compounds have been reported to be released during the decomposition process (Vass et al. 2008; Vass et al. 2004) and up to 30 different compounds in the early stages of decomposition (Statheropoulos et al. 2007). Stadler et al. (2012) reports the release of numerous chemicals such as alcohols, sulphides, aromatics, and carboxylic acids compounds (e.g. 1-butanol, 2-and 3-methyl butanoic acid, dimethyl disulfide, dimethyl trisulfide, phenol, and indole) during the decomposition process of pig carcasses in a temperate environment in Ontario, Canada.

Moreover, studies on the body decomposition process revealed increased nutrient concentrations, such as sulfates, sodium, potassium, calcium, magnesium, ammonium, and a higher pH in single grave soil in a temperate environment (Benninger et al. 2008; Carter et al. 2007; Melis et al. 2007; Stokes et al. 2009). The body decomposition process has been shown to represent a significant source of nutrient enrichment, such as inorganic nitrogen, for the surrounding soil and vegetation (Damann et al. 2012; Forbes 2008). While Stokes et al. (2009) reports no significant fluctuation in carbon content between graves and non-graves, a previous study had indicated an increase in carbon concentrations in grave soil beneath pig carcasses (Hopkins et al. 2000). In addition, significant increases in ninhydrin-reactive nitrogen, total nitrogen, and nitrate in grave soil have been found one year postmortem, in comparison with three years postmortem, where there were no significant differences detected between the graves and non-graves (Anderson et al. 2013). A significant positive correlation between ammonium and pH (Pearson's R=0.78) along with a negative correlation between nitrate and pH (Pearson's R=0.88) has also been noted in grave soil (Meyer et al. 2013).

Table 2.2. Summary table of reported soil chemistry changes during the body decomposition process reported across reviewed literature.

Soil chemistry changes	References
Increase in nutrient concentration: carbon, total carbon, calcium, iron, potassium, magnesium, manganese, sodium, nitrogen, total nitrogen, nitrate, ammonium, phosphorus, and available phosphorus	Benninger et al. (2008); Carter and Tibbett (2008); Melis et al. (2007); Stokes et al. (2009); Tibbett and Carter (2009)
Higher soil pH	Anderson et al. (2013); Benninger et al. (2008); Forbes (2008); Tibbett and Carter (2009); Wilson et al. (2007)
Presence of volatile compounds such as: Ethyl benzene, Toluene, tetrachloroethene, 1,4 Dimethyl benzene, Carbon tetrachloride, 1,2 Dimethyl benzene, Naphthalene, Styrene, Benzene, Nonanal, Decanal, Trichloromonofluromethane, Carbon disulfide, Undecane, 1-butanol, 2-and 3-methyl butanoic acid, Dimethyl Disulfide, Dimethyl Trisulfide, Phenol, Indole	Stadler et al. (2012); Statheropoulos et al. (2007); Statheropoulos et al. (2005); Vass et al. (2008); Vass et al. (2004)
Higher levels of Ninhydrin-Reactive Nitrogen	Anderson et al. (2013); Carter et al. (2008b)

Studies on the body decomposition process commonly use animal proxies to human cadaver due to limited availability, as well as ethical and cultural constraints that restrict their use for research purposes (Stokes et al. 2013). Across the literature, various mammalian carcasses have been used for decomposition trials as analogues for human cadavers such as porcine (Forbes et al. 2005; Hopkins et al. 2000; Morton and Lord 2001; Stokes et al. 2009; Wilson et al. 2007), ovine (Carter and Tibbett 2006; Haslam and Tibbett 2009; Tibbett et al. 2004), bovine (Melis et al. 2007), deer (Vass et al. 2008), canine (Reed Jr 1958; Vass et al. 2008), and rabbits (Adlam and Simmons 2007; Bachmann and Simmons 2010; Simmons et al. 2010). When comparing porcine and human decomposition, no differences have been found in terms of the number of insects captured (Anderson and Cervenka 2001; Stokes et al. 2013). Stokes et al.

(2013) found that microbial activity is higher in the decomposition of porcine and bovine tissue in comparison with human cadaver decomposition. Vass et al. (2008) report common volatiles compounds released during the decomposition process for human, deer, dog and pig such as decanal concentration; and benzene and nonanal compounds were detected in human, deer and dog decomposition. Other compounds reported were hexane and diethyl ester for human and deer decomposition, while ethane, 1,1,2-trichloro-1,2,2,-trifluoroethane ($Cl_2FC\text{-}CClF_2$), 1,4-dimethyl benzene, ethyl benzene were revealed for human and dog decomposition. However, the overall patterns of nutrient fluxes and chemical changes have been reported to be similar for ovine, porcine, bovine, and human decompositions (Stokes et al. 2013). Ovine carcasses decomposition has been found to be the most similar to cadaver decomposition in terms of soil pH and nitrate, and porcine in electro-conductivity (Stokes et al. 2013). Based on previous literature, animal carcasses are seen as a good substitute for human proxies but the interpretation must be performed with caution.

2.3. Clandestine Grave Detection

A burial can be characterized as a disturbance within a given environment such as a wooded area or open field and can be created by hand or machinery (Cox 2008; Dupras et al. 2011; Gleason 2008). Haglund et al. (2001b) suggests a depression in the soil is the best indicator of a grave in an area. According to Larson et al. (2011), the most effective method for examining characteristics of a grave is through the understanding of the body decomposition's effects on the surrounding environment. For example, grave soil can potentially be separated from non-grave soil by testing its ninhydrin reactive nitrogen concentration levels (Anderson et al. 2013; Carter et al. 2008b). Another potential means to detect graves is through measuring the flux and soil pore air of gases such as methane (Dalva et al. 2012), nitrous oxide, and carbon dioxide (Dalva et al. 2015). In an experiment looking at methane emissions of a graveyard containing carcasses of zoo animals, in southern Quebec, Canada, Dalva et al. (2012) showed that there are increasing rates of methane production associated with carcass burial that can be used to narrow down the detection of a mature animal burial (15 years). Meanwhile, in a single grave experiment, higher nitrous oxide and carbon dioxide concentrations were found for shallow single graves in comparison with deep single graves and control sites (Dalva et al. 2015). Another method involved the creation of an odor liberation database from human cadavers (Vass et al. 2008; Vass et al. 2004) at Oar Ridge National Laboratory in conjunction with the University of Tennessee's Decay Research Facility for the purpose of developing a sensor package (i.e. LABRADOR – light-weight analyzer for buried remains and decomposition odor recognition) capable of locating clandestine graves (Larson et al. 2011). This chemical-sensitive device is not as sensitive as a canine's nose; however it can be used along with dogs to pinpoint locations where scent is more intense during investigations (Larson et al. 2011).

The body decomposition process potentially can also affect vegetation over top of a grave. According to Damann et al. (2012), the decomposition of animal carcasses acts as a fertilizer for the surrounding vegetation, stimulating biomass production and increasing species spatial heterogeneity and richness. The succession of plant life over time over top of a grave can be inconsistent with the immediate surroundings (Powell 2006). Anderson et al. (2013) denote a gap in vegetation growth during the first year followed by lush vegetation growth by the end of the third year for an above ground experimental burial in a temperate environment. A study, involving the burial of five swine carcasses in Italy at an approximate depth of 80 to 90 cm, reveals that plant species composition and cover were different between the graves and the undisturbed plots (Caccianiga et al. 2012). Disturbed plots showed an increase in ruderal species and a reduction in stress-tolerant ones. Therefore, the characterization of vegetation dynamics can also be included in the detection of clandestine graves as an important component in the investigation process.

Common methods used for grave detection include eyewitness testimony (Larson et al. 2011), search dogs (Rebmann and David 2000), geophysical methods (Ruffell and McKinley 2005; Vaughan 1986), archaeological surveys along with the complementary use of remote sensing data such as aerial photography and satellite imagery (Cheetham 2005; Congram 2008). Search dogs have been found to be an effective method for the search of human remains due to their scent capabilities. Geophysical methods such as ground-penetrating radar, magnetometry, and electrical resistivity are also used to detect changes in the soil structure as anomalies. While ground-penetrating radar detects graves by using the transmission and reflection of electromagnetic energy, centered in the 100 to 500 MHz range, from the ground, magnetometry measures the magnetic values of the surrounding soils and the human-induced magnetic contrast produced by disturbed soil (Larson et al. 2011). Research shows electrical resistivity instruments can be used in burial detection as they can detect natural or induced electrical current in subsurface (Pringle and Jervis 2010).

Geophysical methods have been applied in archaeology to detect ancient burials since 1946 and aerial photography since 1919 (Beazeley 1919) after the First World War, such as the mapping of an old native village in Washington (Huggins 1985). Geophysical methods have been applied for the location of historic graves (Bartel 1982; Brown 1971; Tainter 1978) and criminal burials (Davenport et al. 1990; Davenport et al. 1988). Multiple studies show the successful application of geophysical methods in the detection of clandestine graves using ground penetrating radar, magnetometry and resistivity (Ambos and Larson 2002; Bevan 1983, 1991; Larson and Ambos 1997; Larson et al. 2003; Miller 1996; Nobes 1999). Application of ground penetrating radar is shown in the search of burial sites in U.S.A and Southeast Asia (Miller 1996) and in the search of human remains in New Zealand in a plantation forest (Nobes 2000). Bevan (1983) applied the principles of electromagnetics for mapping buried earth features such as a 18th century French fort in Mississippi River, Illinois, and a Native settlement in northern Oklahoma, USA. Aerial photography, along with ground penetrating radar, was employed to detect historic villages of the Mississippi river valley from 1876 and magnetometry and resistivity to detect ruins in Rapo Nui, Chile (Larson et al. 2003). Bevan (1991) tested the use of ground penetrating radar, resistivity meters, and magnetometers to locate nine unmarked graves. The study reveals that ground-penetrating radar worked best at locating the unmarked burial sites. Nobes (1999) used electro-magnetometers and ground penetrating radar to detect ancient graves in Oaro Urupa, New Zealand. Their study also emphasizes the importance of using several techniques and not relying on one approach in the detection of clandestine burial sites. In another study, magnetometry, ground penetrating radar, and aerial photography were integrated to detect burial sites dating between B.C 400 and A.D. 200 in Navan Fort, Northern Ireland (Larson and Ambos 1997). The use of geophysical methods in burial detection can be limited and not work in all environmental conditions (Buck 2003; Larson et al. 2011). Hansen et al. (2014) highlight that the use of geophysical methods for the detection of unmarked graves depends on the soil type. They found that while both work in sandy and black earth soil, ground-penetrating radar is more optimal in very coarse soil and electrical resistivity in clay-rich soils. Ground penetrating radar can be expensive and natural anomalies are often interpreted as potential graves (Nobes 1999). Low detection of burials in saline environments was reported

(Pringle et al. 2012a), while magnetometry is sensitive to natural and man-made (e.g. trash) anomalies (Larson et al. 2011). Detection methods using electrical resistivity are limited by debris found in search areas and in areas with surface disturbances such as grading and paving (Larson et al. 2011).

2.4. Remote Sensing

2.4.1. Remote Sensing Application in Grave Detection

Remote sensing is the collection of information on the amount of reflected energy by a material at different spatial scales (i.e. *in-situ*, airborne and satellite sensors) (Jones and Vaughan 2010). Comparison of archived materials, such as historical images, with new remote sensing surveys can provide information on areas to search and potential site location during investigations (Cox 2008; Dupras et al. 2011; Harrison and Donnelly 2009; Pringle et al. 2012a; Wright et al. 2005). The inclusion of Geographic Information Systems (GIS) analyses into the search of clandestine graves can aid to locate potential graves (Babic et al. 2000; Congram 2010; Orengo 2006). Harrison and Donnelly (2009) also mention the utility of maps and aerial photography to reduce geographical confinement of the search area.

Remote sensing (such as aerial photography and satellite imagery) has been an important source of data to locate mass graves since the 1970s (Cox 2008) and archived photos for mass grave investigations during the Second World War (Fox 1999). Across the literature, aerial photography (France et al. 1992; France et al. 1996), airborne and space-borne imagery (Berlin et al. 1977), and ground thermal data (Benner and Brodkey 1984; Perisset and Tabbagh 1981) have been used in clandestine burial detection by highlighting sublet changes in soil color and texture (Wynn 1986). An overview of remote sensing methods in forensic investigation of aerial photography and satellite imagery are found across the literature (Brilis et al. 2000; Brilis et al. 2001; Grip et al. 2000; Pringle et al. 2012b; Wilson 1982). Aerial photography can indicate ground disturbance or even physical events (i.e. excavation of a grave), vegetation changes and visible soil disturbances (Cox 2008). A study used aerial photography from 1972, 1982, and 1992 to investigate features that indicated the location of burial sites using change detection of pre and post-burial images and image-enhancement methods that highlighted subtle changes in the soil (Ambos and Larson 2002). France et al. (1996) also applied similar methods on aerial photographs to delineate changes in growth patterns and characteristics of surrounding vegetation, anomalies in surface soil associated with excavation boundaries, and settlement of snow within burial surface depressions of an experimental grave using pig carcasses. Guatame (2010) employed Landsat 5 TM (from 1991) and Landsat 7 ETM+ (from 2001) images to understand the landscape and observe its evolution through time in areas where individual graves have been located in Guatemala. The use of aerial photography to identify unusual features and/or patches of vegetation (France et al. 1992; France et al. 1996; Wright et al. 2005), especially when the sun is at a low sun angle, along with satellite imagery, have been employed to determine potential locations of burials (Ruffell and McKinley 2008); as well to identify access points which are considered prime search locations as heavy objects are rarely carried more than 150 m before being buried (Killam 2004). Raymond et al. (2014) applied a change detection analysis on Quickbird-2 and WorldView-2 satellite imagery to locate potential grave in Abyei, Sudan. More recently, since 2013 a group of researchers have been conducting a study over a period of three years on the application of LiDAR in the detection of clandestine mass graves at the University of Tennessee, Knoxville (Boehnke 2013).

Regardless of the detection method for clandestine graves, there are multiple factors that affect the end result such as length of time since disturbance, changes in soil composition, grave contents, climate, vegetation growth rate, anthropomorphic factors such as disturbances caused by human activities, and post-disturbance plant colonization (Cox 2008; Dupras et al. 2011).

2.4.2. Hyperspectral Remote Sensing

The spectral reflectance of a material is defined as the amount of light reflected and absorbed by the target (Jones and Vaughan 2010). Spectral reflectance can be measured with a spectrometer *in-situ* or remotely with sensors mounted on different platforms such as satellite and airborne. Reflectance spectroscopy is the basis of hyperspectral remote sensing due to the direct relationship between the spectral signature of a material and its inherent structure and compositional characteristics (Eismann 2012; Jones and Vaughan 2010). In terms of imaging sensors (usually airborne or satellite), the spectral signature of the targeted materials is stored in a data cube in dozens or hundreds of contiguous spectral bands (Figure 2.2). A data cube is the result of a third dimensional dataset composed of stacked images, with two spatial dimensions (i.e. across-track and along-track) and one spectral dimension (i.e. wavelength), where each pixel contains a spectrum representative of the measured material/target (Eismann 2012).

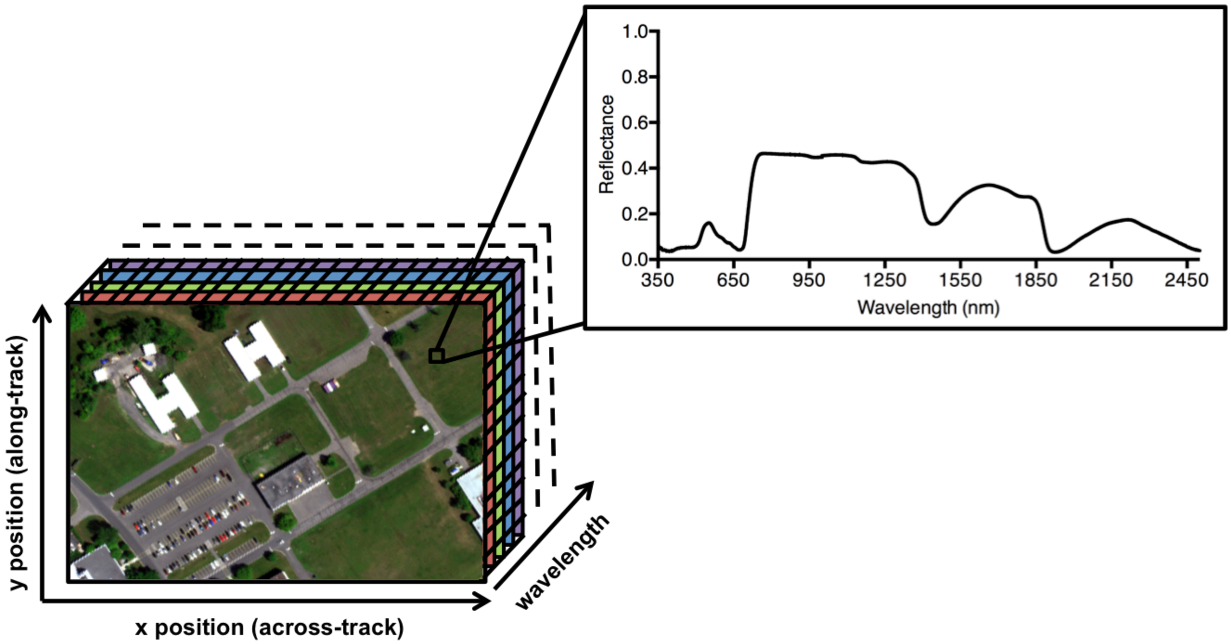

Figure 2.2. Representation of a data cube where multiple images at different wavelengths are stacked up to form a 3D-cube comprised of two spatial dimensions (i.e. across-track and along-track) and a third wavelength dimension. Data is stored in pixels containing spectral information representative of the measured material/target. The displayed spectrum is a representative spectral signature of a grass field collected using ASD FieldSpec 3 spectrometer.

The information stored in a spectrum is the result of the relationship between the spectrum of reflected or emitted light, the vibrational and electronic resonance of molecules composing the material, microscopic surface and volumetric properties (Eismann 2012; Jones and Vaughan 2010). Therefore, the texture, chemical composition, structure, and water content of a specific material influence the amount of radiance that is absorbed, transmitted or reflected at different wavelengths (Jones and Vaughan 2010). This interaction can be used to characterize materials as different ones can have unique absorption features (Eismann 2012). Absorption features in spectral signatures are the result of how light interacts with different material when absorbed light is greater than reflected light (Peñuelas and Filella 1998). Hyperspectral data can be used to detect subtle differences in spectral reflectance between different surfaces and materials (Jones and Vaughan 2010). For instance, vegetation indices such as the normalized difference vegetation index (NDVI) have been developed (Rouse Jr et al. 1974). These spectral indices are used across the literature to study vegetation biochemical properties such as plant chlorophyll and carotenoids content (Huber et al. 2008; Turner et al. 2003), detect vegetation stress (Behmann et al. 2014; Kim and Pyen 2011), identify vegetation health (Solberg et al.

2004; Wulder et al. 2006), as well as, in agriculture to detect weed species (Dammer and Wartenberg 2007; Gibson et al. 2004; Langner et al. 2006), study wheat diseases such as the yellow rust (Huang et al. 2007), and differences between weeds and crops (Yang et al. 2004).

Given the characteristics of hyperspectral data described above, the analyses of these types of data present a novel opportunity for detecting spectral differences between a grave and landscape and other disturbances similar to a grave (i.e. exposed soil, false grave) (Kalacska and Bell 2006; Kalacska et al. 2009; Leblanc et al. 2014). For instance, Kalacska et al. (2009) found that the spectral reflectance of a grave can be separated from the spectral reflectance of other classes (i.e. forest, pasture and empty refilled burial), in a tropical forest environment, after an interval of 16 months using cows as a proxy for human bodies. The study by Kalacska et al. (2009) is one of the first showing the potential utility of applying hyperspectral remote sensing in the detection of experimental graves. The application of hyperspectral data and related techniques has also been investigate in a blind test where the locations of single graves were successfully identified within GPS error using spectral vegetation indices in a temperate environment (Leblanc et al. 2014). Further research in the use of hyperspectral data for forensic studies encompass the detection of single graves (Snirer 2014), mature animal graves (de Gea 2012), and differentiate vegetation grown with animal tissue (liver) from fertilized one with bone meal, blood meal or manure (Herzog 2014). These studies showed promising results, where de Gea (2012) reports spectral differences between a mature grave and a non-grave. Spectral differences were found between single shallow, deep graves, surface burials, and background in a study carried out by Snirer (2014) in a single graves experiment. Herzog (2014) reports changes in leaf structure and soil microbial community and the possibility of distinguishing between plants affected by the decomposition process of animal tissue (liver) from fertilized soils. To fully understand the applications of hyperspectral data in burial experiments and potential detection of mass graves, it is necessary to consider among other variables basic biophysical characteristics of soils and vegetation in function of their reflectance. Below, I briefly describe these characteristics.

Spectral Properties of Soil

Soil stores and supplies nutrients to support the growth of vegetation by providing a medium for roots, transporting air, gases and water and offering physical support (Agren and

Andersson 2012). Soil is composed of minerals, organic matter, water and organisms (Ellis and Mellor 1995). The minerals in soil are from intact rocks of different chemical compositions and originate from different fractions such as rock fragments, gravel, sand, silt and clay. The organic matter is coming from decomposing matter such as vegetation litter (Agren and Andersson 2012; Ben-Dor et al. 1997).

The spectral reflectance of soil is influenced by the physical and chemical properties of its constituents such as amount of organic matter, water, grain size, and its internal structure (Curran 1988). For instance, soil with high organic matter and moisture tends to be darker in colour and therefore is more reflective than soil characterized by lower organic matter composition and moisture (Ben-Dor 2002). Soil composed primarily of organic matter was also mapped using the 500 – 1200 nm (Mathews et al. 1973) and the 900 – 1220 nm wavelength ranges (Beck et al. 1976 as cited in Ben-Dor 2002). The shortwave infrared region of the electromagnetic spectrum has also been used to determine nutrients in soil environments (Barnes et al. 2003; Cambardella et al. 1994; Chang et al. 2001; Curran 1988; Malley et al. 2005; Moore et al. 1993) and quantify soil properties such as carbonates in the 1900 – 2300 nm range, cellulose at 1370 nm, 1735 nm, and 2375 nm, and humus at 1929 nm and 1932 nm (Ben-Dor and Banin 1995; Ben-Dor et al. 1997; Summers et al. 2011) (Table 2.3). The hydroxide group in soil had shown main absorption features in three major spectral regions along the 1300 to 1400 nm, 1800 to 1900 nm, and 2200 to 2500 nm (Ben-Dor 2002). Iron oxides have been generally linked to absorption features at 450 nm and 640 nm (Ben-Dor et al. 1997).

Table 2.3. Main absorption features of soil chemical composition across the electromagnetic spectrum reported in reviewed literature.

Compound	Wavelength (nm)	References
Carbonates	1900 – 2300	Ben-Dor (2002); Ben-Dor and Banin (1995); Ben-Dor et al. (1997); Summers et al. (2011)
Clay	1300 – 1400, 1800 – 1900, 2200 – 2500	
Cellulose	1370, 1725, 2347	
Humus	1929, 1932	
Iron oxides	450, 650	
Soil organic carbon	600 – 900	
Pectin	1320, 1582, 1761, 2111	

Spectral Properties of Vegetation

Plants absorb light in the ultraviolet and visible regions of the electromagnetic spectrum to drive biological processes, such as photosynthesis, that are necessary for growth (Gates et al. 1965). Leaf chlorophylls and carotenoids control light absorption, energy transfer, and electron transport in photosynthesis (Davies 2004; Fassnacht et al. 2015). Carotenoids can absorb incident radiation and transfer energy to chlorophyll B, energy that is then transferred to chlorophyll A (Bartley and Scolnik 1995), which affects the spectral reflectance of leaf in the visible portion of the electromagnetic spectrum.

Leaf reflectance is a function of leaf internal structure, water content, and concentration of biochemical components (Gates et al. 1965; Peñuelas and Filella 1998). The amount of light that is reflected is a function of cell shape and size and the amount of intercellular space found within the leaf in the near-infrared range (Jones and Vaughan 2010; Knipling 1970). The main components of the leaf influencing the reflectance of light over the electromagnetic spectrum are leaf pigmentations in the visible (i.e. 400 to 750 nm), cell structure in the near infrared (i.e. 750 to 1300 nm), and water content, protein lignin and cellulose in the shortwave infrared (i.e. 1300 to 2500 nm) ranges (Figure 2.3). An increase in chlorophyll pigmentation results in a lower absorption at 680 nm, an increase in the green reflectance at 550 nm and a decrease in the infrared at 740 nm (Gates et al. 1965). Main absorption features of leaf components are reported across the literature (Table 2.4). For instance, absorption features of chlorophyll A have been reported in the 670 – 680 nm range, chlorophyll B at 650 nm, and carotenoids in the 420 – 480 nm range.

The main source of nutrients to plants is from the soil matrix through root uptake of nutrients such as nitrogen, potassium, phosphorus, iron, and magnesium (Clemens et al. 2002). The distribution and accumulation of nutrients varies for each element, species of plant, growth season, and the availability of trace elements at the root surface (Kabata-Pendias 2010). The cell structure and pigmentation of a leaf can be influenced by the nutrients, metals, and water absorbed from the soil matrix (Kabata-Pendias and Mukherjee 2007) thereby changes in leaf internal structure, water content, and biochemical components will results in changes in the leaf spectral reflectance (Gates et al. 1965).

The relationship between spectral signature and leaf biochemical properties provides the physical basis for remote detection of vegetation stress through monitoring changes of chlorophyll content (Ren et al. 2008; Zarco-Tejada et al. 2002). Total leaf chlorophyll content and the ratio of chlorophyll A and B decrease when vegetation is under stress (Fang et al. 1998) leading to changes in leaf spectral signature in the 450 – 650 nm range (Gates et al. 1965). Stressed vegetation has been found to show different reflectance features in the green peak and along the red-edge due to changes in pigment levels (Miller et al. 1991; Stylinski et al. 2002).

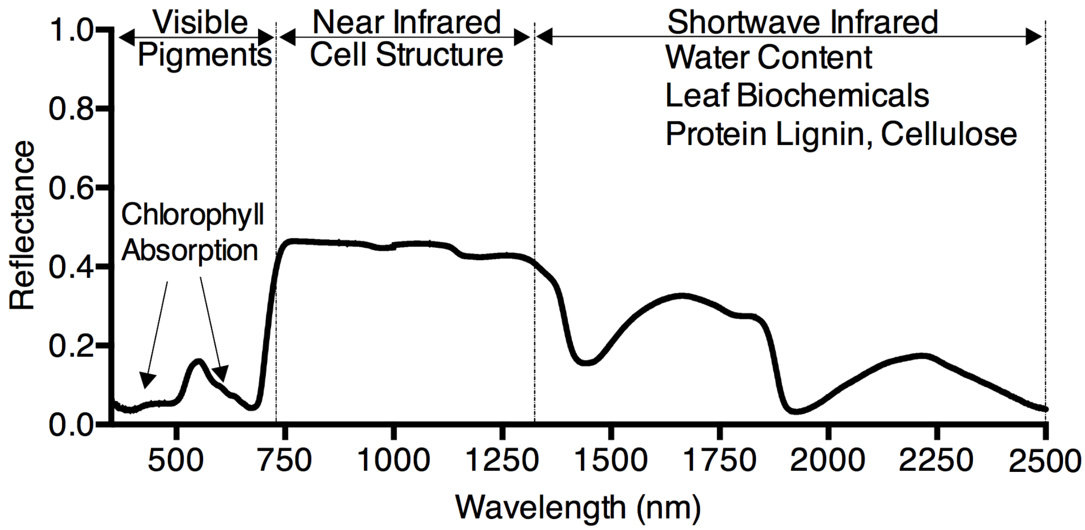

Figure 2.3. Spectral reflectance of a grave leaf sample collected in May 2014 with an ASD FieldSpec 3 spectrometer. Main components of the leaf influencing the reflectance of light over the electromagnetic spectrum between the visible (400 to 750 nm), near infrared (750 to 1300 nm), and shortwave infrared ranges (1300 to 2500 nm).

Table 2.4. Main absorption features of leaf components in the visible, near infrared and shortwave infrared ranges of the electromagnetic spectrum reported in reviewed literature.

Component	Wavelength (nm)	References
Chlorophyll A	435, 670 – 680, 470	Curran (1988);
Chlorophyll B	480, 650	Zwiggelaar (1998)
A-Carotenoid	420, 440, 470	
B-Carotenoid	425, 450, 480	
Anthocyanin	400 – 550	
Water	970, 1200, 1400, 1940	
Lignin	1120, 1420, 1940	
Cellulose	1780	

2.5. Summary

A mass grave can be defined as a burial unit containing two or more victims from events such as war crimes, human rights abuses, and political instability. Great efforts and advances have been made by researchers in the development of detection methods for clandestine mass graves. The advancement of new methods for detecting changes in the local environment, associated with disturbances caused by mass burials, can potentially reduce search areas and decrease investigation time. The release of nutrients from the cadaver decomposition process into the soil matrix can lead to the establishment of an enriched environment for the surrounding vegetation (Carter et al. 2007; Dent et al. 2004; Forbes 2008; Tibbett and Carter 2009) that may improve their capacity of photosynthesis and lead to a higher pigmentation concentration. The spectral reflectance of soil is influenced by the physical and chemical properties of its constituents such as amount of organic matter, water, grain size, and internal structure (Curran 1988). Given that the spectral reflectance of soil is influenced by its physical and chemical components and that the internal structure of vegetation influences the amount of absorbed light across the electromagnetic spectrum, changes in soil chemistry and in pigmentation and cell structure of vegetation can be identified at specific regions of their spectral signatures. Therefore, hyperspectral remote sensing may detect distinct features of a grave due to the effects of the release of nutrients from the cadaver decomposition process on the surrounding soil and vegetation. Furthermore, hyperspectral data can potentially be used to detect early signs of disturbance in soil caused by the emplacement of clandestine burial sites.

3. Methods

3.1. Study Area

The research site is located within the NRC – FRL's campus in close proximity to the MacDonald Cartier International Airport, Ottawa, ON between 45˚19'39.73" - 45˚19'38.5" N and 75˚40'06.42" - 75˚40'05.32" W (Figure 3.1.A). According to Environment Canada (2015), the local climate is characterized as humid continental with fluctuating seasonal temperature and precipitation (Appendix B). Over the study period, mean monthly temperatures fluctuated between -10.8 °C in January and 20.9 °C in July, while the mean monthly precipitation ranged between 20 mm and 140 mm respectively (between 19 and 60 cm of show) (Environment Canada 2015). The soils of the region are characterized as well-drained, sandy loams of the Brunisols series with fragments of granite, gneiss, limestone and dolomite (Schut and Wilson 1987). Prior to disturbance the dominant vegetation consisted of grasses and forbs species with no bare soil or woody vegetation.

3.2. Experiment Description and Setup

Three experiment sites were established on June 25th, 2013: an experimental mass gravesite containing 20 pig carcasses (*Sus Scrofa domesticus*), used as cadaver proxies, a reference site containing only disturbed soil, and an undisturbed control site. Figure 3.1.C shows the location of the study sites (5 x 10 m) at NRC-FRL, Ottawa, ON. Based on the size of the study area, a distance of five meters was chosen between the grave and reference, and seven meters between the reference and control.

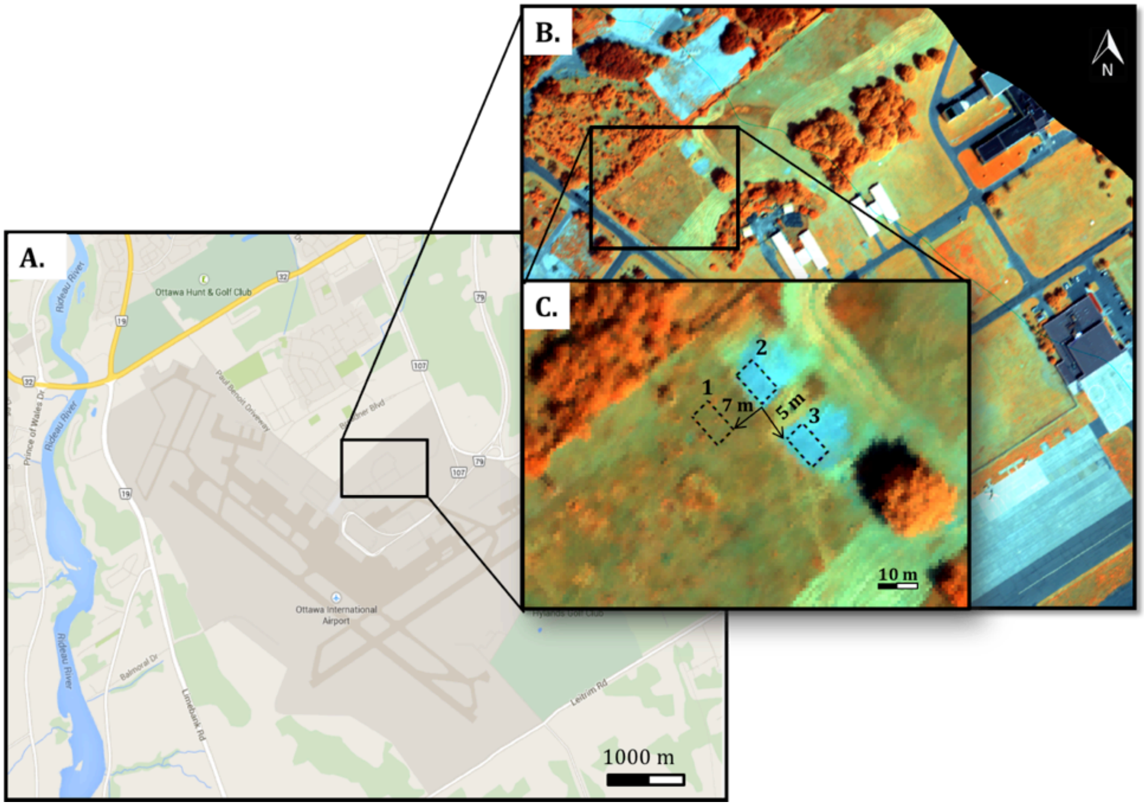

Figure 3.1. Study area located within the NRC – FRL's campus, Ottawa, ON. (A) Research area located in proximity of the MacDonald Cartier International Airport. Map retrieved from Google Maps. (B) Georectified airborne image, 70 cm spatial resolution (R: 1052 nm G: 1624 nm B: 2122 nm), taken on July 12th, 2013. (C) The three established sites are: (1) control (undisturbed soil and vegetation), (2) reference (disturbed soil and no pig carcasses), and (3) experimental mass grave (disturbed soil and 20 pig carcasses). Arrows indicate the distances between sites.

The experimental mass grave, located in the eastern side of the study area, was excavated with a backhoe and has a depth ranging between 0.97 to 1.45 m (Figure 3.2). Twenty food-grade pig carcasses were used as cadaver proxies in the study. The pig carcasses weighted between 89 and 104 kg each and had an average of 99 kg and a total mass of 1977 kg. The carcasses were purchased from a commercial meat processing facility, Desormeaux Meats, Crysler, Ontario. The pigs were inspected and their intestines and stomach contents removed to meet provincial requirements for food grade compliance. Alternatively, with gastro-intestinal tracks intact they would have been classified as non-deadstock and would have had to undergo rigorous environmental assessments. The carcasses were clothed to simulate the burials in mass graves. Ten carcasses were randomly placed on the north and ten on the south side of the site with a gap of 3.70 m in between the two groups (Figure 3.3). Due to the size of the burial pit (i.e. 10 m x 5 m) the pig carcasses were separated into two groups to avoid the cadavers being too spread out.

Throughout data collections, the gap was considered as a separate entity from the two graves. The grave was then refilled with excavated soil back to ground level.

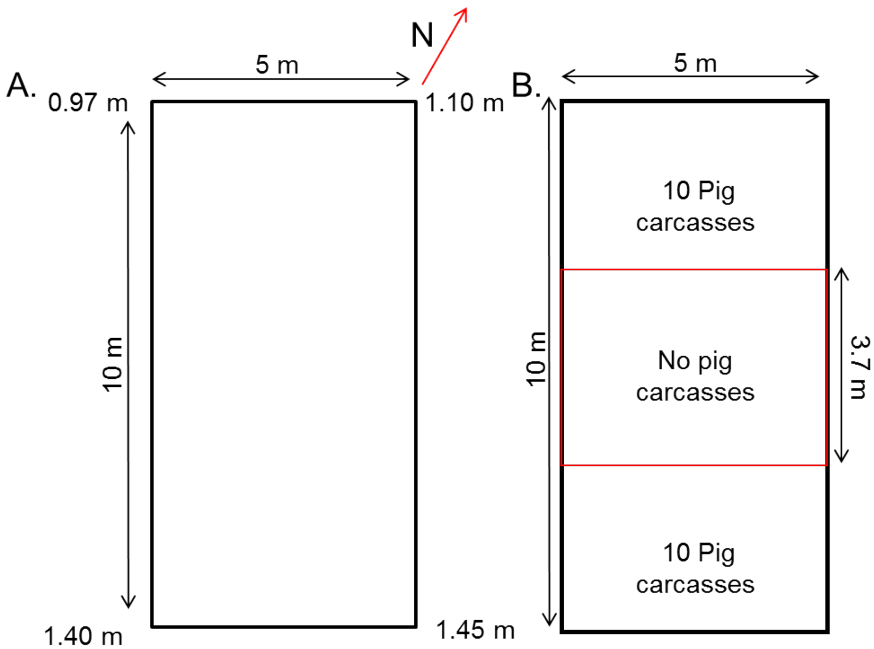

Figure 3.2. Diagrams depicting the measurements of the experimental mass grave. (A) Site dimensions and depth range measured in the North, East, South, and West corners. (B) Pig carcass placement within the burial pit and a 3.70 m gap in-between grave.

Figure 3.3. Placement of clothed pig carcasses inside the burial pit used as cadaver proxies. The pig carcasses were divided into two experiment sites, 10 were placed on each side of the burial pit with a 3.70 m gap between them.

A reference site and a control site were also setup. The reference site was created to investigate the distinction between a grave and a non-grave with the purpose of reducing the number of false positive results. The site, located in the northeast side of the study area, was excavated to a depth ranging between 1.10 m and 1.40 m. The pit was refilled with only the excavated soil. The control site, consisting of undisturbed soil and vegetation, is located west of the reference. The soil and vegetation of the control site were not disturbed throughout the study period. The reference and control sites are characterized by the same dimension of 5 x 10 m. Figure 3.4 shows the grave and reference right after experiment setup.

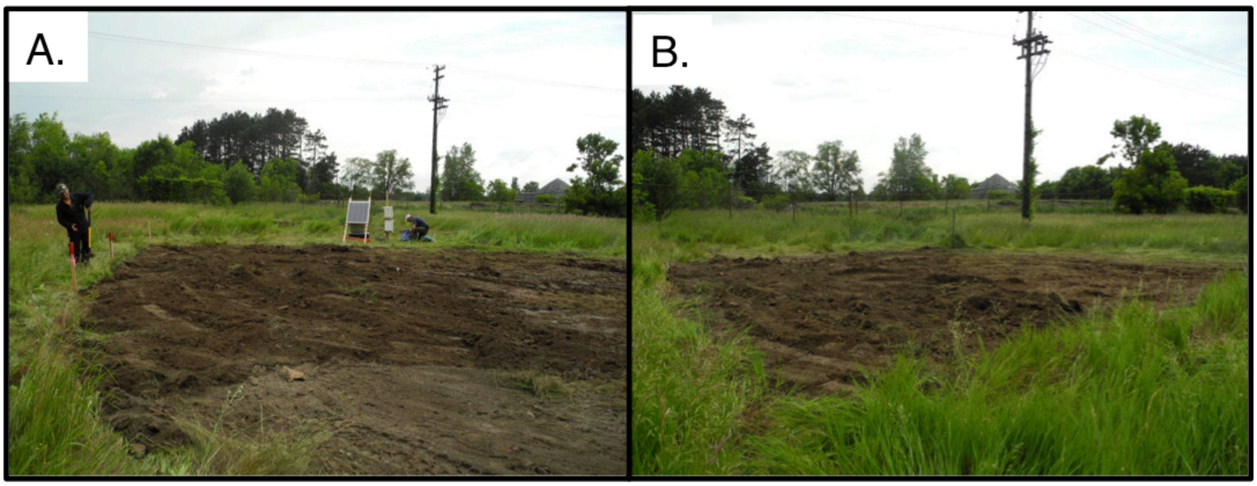

Figure 3.4. Study sites right after experiment setup**:** (A) mass grave, containing 20 pig carcasses and disturbed soil, and (B) reference, characterized by disturbed soil.

3.2.3. Stratigraphic Logs of the Grave and Reference Site

This section is based on Bergen, A. (2013). Stratigraphic Logs for Mass Grave Sites. National Research Council Canada – Flight Research Laboratory. *Unpublished*.

To better understand the sub-surface emplacement environment of the grave and reference, geological cross sections were performed along each side of the sites.

> "The stratigraphic logs show that the first and top layer of the sites can be described by similar layers of a moist, dark-brown soil characterized by medium sized grains (approximately 0.25 mm) intertwined with surface vegetation. Lithic pebble sized clasts (ranging from 5 to 30 mm) are dispersed throughout the layer along both sites. A second orange-brown and poorly sorted soil layer contains well-rounded clasts with diameters ranging between 4 – 6 mm. The second layer from the top of the grave also is

composed of well-rounded pebble sized lithic clasts with a diameter ranging between 10 – 30 mm. Thin beds of flattened clay can also be located along the walls of the grave. The reference site's Northeastern wall shows different clast sizes: cobble sized clasts (diameter ranging between 50 and 100 mm) along with flatted clay and rounded granite, and granule sized lithic clasts with a diameter below 10 mm. While the Northwestern wall, also the bottom layer of the wall, of the reference site is composed of gray clay, the Southwester one consists of large lithic clay boulders of diameters higher than 256 mm.

A third layer is poorly sorted and consists of fine-grained sand containing different sized clasts: granule sized, diameter between 4 – 6 mm, and pebble sized, diameter greater than 6 mm. In this layer clay horizons can also be found with a thickness of between 0.20 – 0.30 m for the grave and between 0.40 – 0.60 m for the reference. A thin secondary layer of fine-grained, moist, white sand is present at various locations across the gravesites. The reference site is composed of coarse granite white sand in this layer. Cobble sized lithic clasts (diameter above 64 mm) can also be located along the walls of both the grave and reference site. Furthermore, the Northeastern and Southeastern walls of the reference are also composed of beds of orange clay. A fourth and fifth layer on the North Eastern wall of the grave is also present being composed of coarse white sand (diameter ranging between 0.5 – 1 mm) and grey clay respectively. The bottom layer of both sites is generally composed of grey clay. The Northeastern and Southeastern walls of the grave also consist of fine-grained moist white sand (diameter ranging between 0.125 – 0.25 mm) and very fine grained sand (0.0625 – 0.125 mm diameter) respectively. The base of both sites is composed of grey clay, which can have an influence on the dispersal of nutrients from the decomposition process (Figure 3.5)."

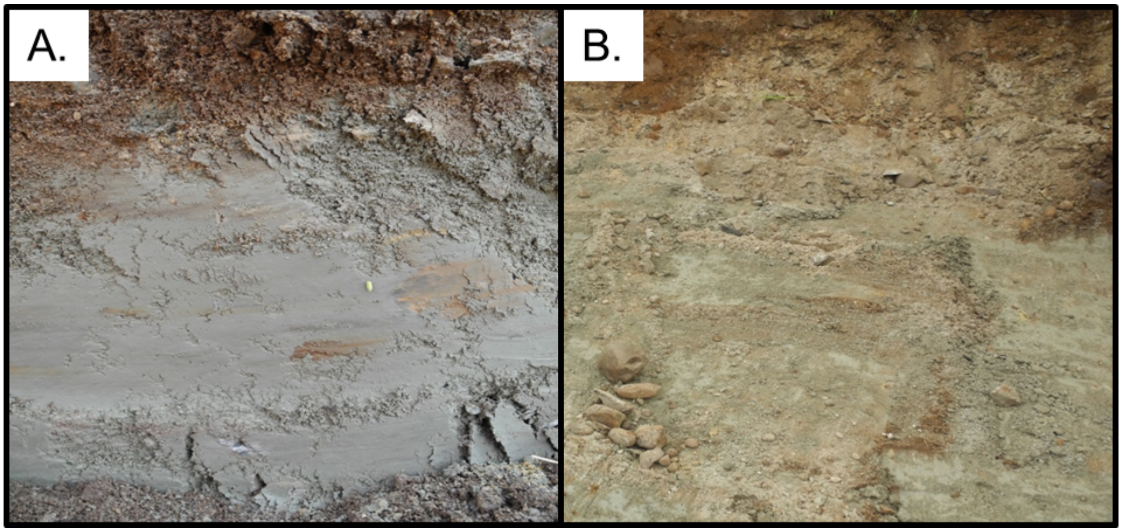

Figure 3.5. Bottom soil layer of the (A) grave and (B) reference composed of clay. Photos of soil layers taken during geological cross section.

3.3. Data Collection

3.3.1. Soil Sampling

In order to identify whether there were significant differences in soil chemistry between the established sites, soil samples were collected over the 2013 and 2014 growing seasons following a stratified sampling methodology. A total number of 15 samples were collected from each site adding up to 45 soil samples per collection date (Figure 3.6.A). Each sample weighing approximately 15 g and was collected from the top 15 cm of the respective section. After the samples were collected they were placed in individual paper bags and labeled. The samples from 2013 were then dried in an oven for 24 hours at a temperature of 80°C, while the samples from 2014 were air dried for 48 hours. All soil samples were then sieved with a 200 mesh (i.e. 0.074 mm size). They were stored in individual labeled plastic bags until further analysis. Soil samples were collected in November 2013 and monthly between May and November 2014.

Soil Chemistry Analyses

Soil samples collected in November 2013 were sent for analysis to Acme Laboratory (Vancouver, BC). An Aqua Regia digestion ICP – ES analysis was performed to extract 33 elements via inductively coupled plasma mass spectroscopy. For the purpose of this study, elements that were found to be present in grave soil in previous studies such as calcium (Ca), iron (Fe), potassium (K), magnesium (Mg), manganese (Mn), sodium (Na), and phosphorus (P) were investigated.

Soil samples collected over the 2014-growing season were sent to the Nutrient and Trace Analysis Laboratory, McGill University, for available phosphorus (P), ammonium (NH_4) and nitrate (NO_3) extraction. Available P was extracted using the Mehlich III solution following the Tran and Simard (1993) methodology. Mehlich III solution is a mixture of acetic acid, ammonium nitrate, ammonium fluoride, nitric acid and EDTA (Tran and Simard 1993). Available P concentration was determined using a colorimetric technique (Lachat Instruments, Milwaukee, USA) where its concentration was measured at 880 nm following a complexion with ammonium molybdate and an ascorbic reducing solution. Standards were prepared in extraction solution (Lalande pers. comm.). Extractable NH_4 and NO_3 from the soil samples were performed using a 2 M potassium chloride extraction and a ratio of 1:10 soil-to-solution (Maynard and Kalra 1993). A multi-channel Lachat auto-analyzer was used to analyze the filtrate by colorimetry for the determination of N as NH_4 and N as NO_3 (Lachat Instruments, Milwaukee, USA). The N–NH_4 and N–NO_3 solutions were measured colorimetrically at 660 nm and 520 nm, respectively, on a Lachat flow injection instrument (Lalande pers. comm.). The N–NH_4 and N–NO_3 concentrations were then converted to NH_4 and NO_3 content.

3.3.2. Vegetation Sampling

Vegetation pigment content (i.e. chlorophyll A, B and total, and carotenoids) and spectral reflectance were collected to investigate the potential temporal differences in vegetation between the three experimental sites. Leaf samples of *Agropyron repens (L.) Beauv*, a grass species with narrow blade-shaped leaves, were collected monthly from the grave, reference, and control sites over the 2013 and 2014 growing seasons. A number of 45 leaf samples per site were collected for a total of 135 samples per collection date. Similarly to the soil sampling, the study sites were divided based on the three sections of the experimental mass grave (Figure 3.6.B). Within each section the leaf samples were collected across three transects with five leaves per each. The same sampling method was applied to collect leaves from the reference and control sites. Once vegetation started to grow and mature on top of the disturbed sites, leaf samples were collected monthly between August and November in 2013, and between May and November in 2014.

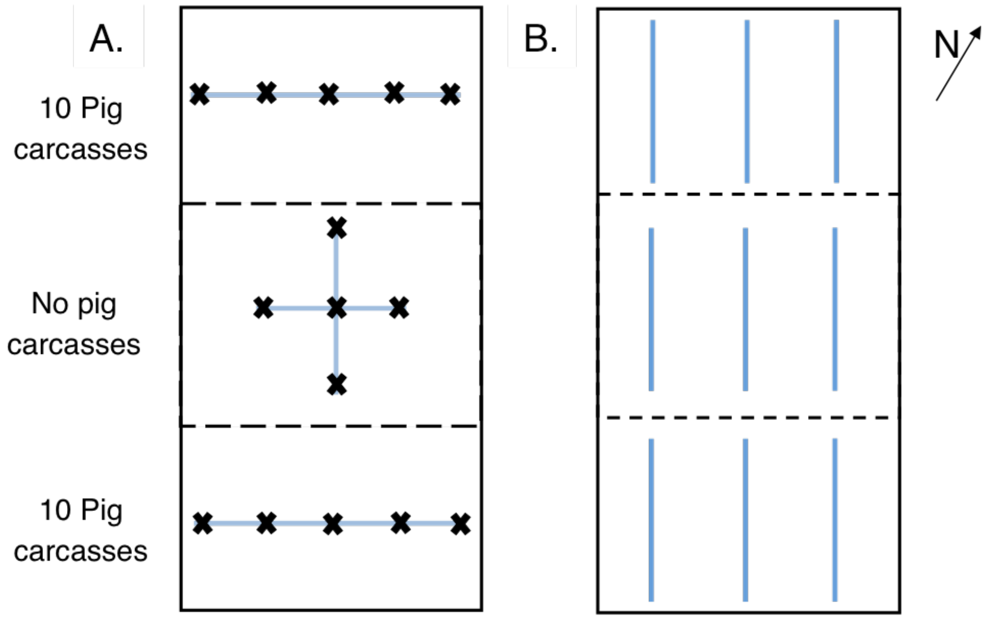

Figure 3.6. (A) Diagram of soil sampling design collected from the experiment sites. The soil samples were collected along transects in the (x) marked locations. Sampling was designed based on the experimental setup of the mass grave. (B) Transects (blue lines) along which the leaf samples were collected from the experimental mass grave, the reference and control sites.

Leaf Level Spectral Reflectance Collection

An ASD FieldSpec 3 Spectrometer (Analytical Spectral Devices Inc., Boulder, Colorado) was used to collect the spectral reflectance of the vegetation samples. The instrument, with a spectral range of 350 to 2500 nm, has a spectral resolution of 3 nm Full Width at Half Maximum (FWHM) at 700 nm and 10 nm FWHM at 1400 nm and 2100 nm, which are resampled to 1 nm. A plant probe and a leaf clip were connected to the instrument to collect the spectrum of each leaf sample (Figure 3.7). The leaf clip holds the leaf in place and excludes background light. It also has an embedded 99% reflective white panel for white reference measurements. During the collection, the upper side of the leaf was sampled, as it is the side exposed to the sunlight. White reference measurements were taken every five minutes using the white reference disk attached to the leaf clip. A total of 45 leaf spectra per site were collected. After the spectral signatures were collected, each leaf was individually wrapped in aluminum foil, for preservation reason, and labeled. The samples were frozen until further analyses consisting of chlorophyll A, chlorophyll B, total chlorophyll, and carotenoids content extraction.

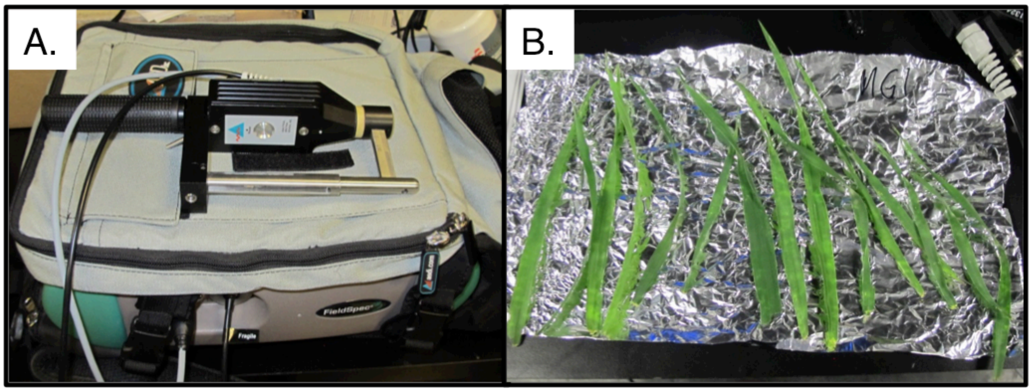

Figure 3.7. Leaf spectral reflectance collection. (A) ASD FieldSpec3 with plant probe and leaf clip attached. (B) Example of leaf samples from grave collected on May 29th, 2014.

Leaf Pigment Extraction

To extract the pigment concentrations, the collected leaves were cut to a standard size (i.e. 1 cm^2) and mixed with 10 ml of Dimethyl Sulfoxide (DMSO) in a centrifuge tube. The tubes were then placed in a 65°C water bath for a period of 35 minutes. Next, the tubes were left to cool down, after which, each sample was mixed and immediately transferred to a disposable 1 cm path length cuvette using a disposable plastic pipette. The samples were then placed in a Genesis 10 UV Spectrophotometer where their absorbance was measured at 470 nm, 650 nm, and 666 nm. The methodology for the chlorophyll extraction follows that of Hiscox and Israelstam (1979). The peak absorbance features of leaf pigments were established by measuring the absorbance of chlorophyll A, chlorophyll B, and beta-carotene standards across the 460 to 480 nm, 640 to 660 nm, and 656 to 676 nm wavelength ranges. The results indicated that chlorophyll A has an absorbance peak at 666 nm, chlorophyll B at 650 nm, and carotenoids at 470 nm for the utilized spectrophotometer. The uncertainty for each of the pigment concentrations for this specific spectroradiometer was also tested during this experiment by measuring the absorbance of DMSO solution at the 470 nm, 650 nm, and 666 nm wavelengths. The results indicate an uncertainty below ± 0.001 g L^{-1} for all the tested vegetation pigments.

The chlorophyll concentrations, in g L^{-1} units, for each leaf were then calculated using Arnon's equations (Arnon 1949), which were then converted in mg cm^{-2} based on the leaf's sample size (Table 3.1). The carotenoid concentration was calculated using Lichtenthaler's equations (Lichtenthaler 1987) and then converted to mg cm^{-2} based on the sample size (Table 3.1).

Table 3.1. Equations used to estimate the concentration of chlorophyll A, chlorophyll B, total chlorophyll, and carotenoids using the three absorbance (Abs) peaks at 470 nm, 650nm, and 666 nm and their calculated uncertainty.

Pigmentation ($g\ L^{-1}$)	Equation	Reference	Uncertainty ($mg\ cm^{-2}$)
Chlorophyll A	(0.0127 ×Abs 666)-(0.00269 ×Abs 650)	Arnon (1949)	± 0.00010
Chlorophyll B	(0.0229 ×Abs 650)-(0.00468 ×Abs 666)	Arnon (1949)	± 0.00018
Total Chlorophyll	(0.0202 ×Abs 650)-(0.00802 ×Abs 666)	Arnon (1949)	± 0.00028
Carotenoids	((1000 ×Abs 470)-(1.82 ×Chl A)- (85.02 ×Chl B)/198)÷1000	Lichtenthaler (1987)	± 0.00002

3.3.3. *In-situ* Field Spectrometry

Prior to field measurements, a non-systematic characterization of the sites was carried out by taking perpendicular photos of the grave, reference and control. The photos were taken facing the northwest direction using a Nikon Powershot G12. Since vegetation characterization plot were not established the photos helped to have a general idea of the vegetation growing patterns throughout the duration of the experiment.

In order to investigate potential measurable differences in spectral reflectance of the experimental mass grave at the site spatial scale, *in-situ* data were collected over the 2013 and 2014 growing seasons. The same ASD FieldSpec3 portable spectroradiometer as employed for the leaf spectra collection, measuring the 350 – 2500 nm wavelength range, was used with a pistol grip. To minimize interference from non-target induced spectra (i.e. surrounding area) a foreoptics lens of 8˚ was utilized to decrease the field of view (FOV) from the built-in 25˚. A 99% reflective spectralon panel that has near Lambertian (diffuse) reflectance properties was used for white reference collection. Photos of the collected sample and sky conditions were taken during data collections using a Nikon Powershot G12 and a Canon EOS 60D with a hemispherical lens respectively (Figure 3.8.A and B). Photographs of the measured target and the sky were taken simultaneous with the spectral acquisition to better understand the target and atmospheric conditions during data collections for subsequent analysis. A four channels Microtops II sunphotometer, which measures the solar irradiance at different wavelengths (i.e.

380 nm, 500 nm, 870 nm, 936 nm, and 1020 nm), was also utilized to calculate atmospheric visibility during data collections.

Experimental Design

To minimize site disturbance during data collections the ASD pistol grip with attached foreoptics was placed on a 3 m long pole and set-up on a tripod. The side with the foreoptics was set-up at a height of 1 m above the surface (Figure 3.8.C). The pole had a length of approximately 2.5 m from the tripod's axis. The pistol grip with the fiber optic cable and the target camera were placed on the field side of the pole, while the hemispherical camera was attached at the opposite end. During data collections, white reference samples were collected using a 99% reflective spectralon panel every five to ten minutes depending on atmospheric conditions. The spectralon panel, dimensions of 0.53 x 0.53 m, was set upon a tripod at a height of 0.50 m making sure that the 8° hemisphere FOV was entirely on the panel. Prior to data collections the tripods were leveled and the foreoptics was setup perpendicular to the spectralon panel.

To minimize disturbance during data collections, the experimental sites were divided based on the grave's characteristics into eight sections measuring 2.5 x 2.5 m (Figure 3.8.D). The following naming convention was established: MG1 to MG8 for the grave, R1 to R8 for the reference and C1 to C8 for the control site. The gap section covers the MG3 to MG6 sections. Site and off-site (i.e. surrounding area) samples were collected over each section starting with the spectralon panel located outside the site area. Spectral measurements were taken for each section resulting in seven site measurements, six off-site and two white reference (i.e. spectralon panel) ones. In total, 28 site and 24 off-site (i.e. surrounding area) spectral samples were collected. A tripod set at a height of one meter along with the use of an 8˚ FOV lens resulted in a target diameter of 14 cm on the ground and a total measurement area of 0.43 m^2 per site. Prior to data collections, the instrument is calibrated using a spectralon white reference. During the optimization process the spectrometer automatically sets the integration time for the VNIR detector, the gains and offsets of the two SWIR detectors, and collects dark current. The integration time is the time the detectors of the spectrometer capture light reflected from samples. It was adjusted automatically to maximize the signal without saturating the detectors.

The dark current calibration subtracts the small electronic noise present in all photosensitive devices from the data.

Factors taken into consideration during spectral measurements were solar position, atmospheric conditions, such as cloud cover and wind effects, instrument FOV and tripod height, sampling, and illumination geometry. When necessary the spectroradiometer underwent optimization for changes in light conditions and temperature. The spectroradiometer was optimized every five minutes and/or when moved to a new location (i.e. site section). The spectral average sampling was set to 25 scans and data were collected in units of reflectance. The described sampling strategy was applied to all data collections and experiment sites for consistency and comparison.

In-situ spectral reflectance was collected monthly over the study period. Over the 2013-growing season, four *in-situ* data collections were performed between the months of July and October. Over the 2014-growing season, seven *in-situ* data collections were conducted between May and September.

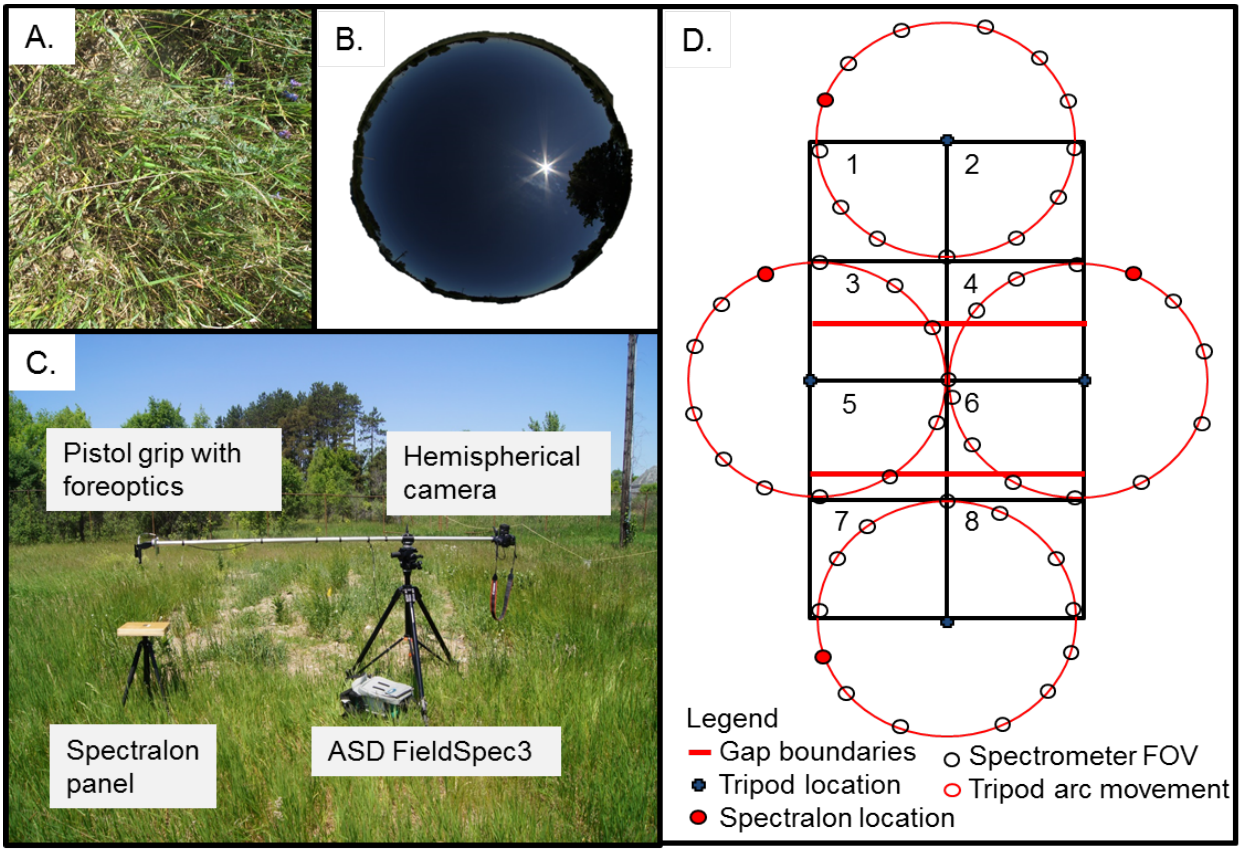

Figure 3.8. (A) Example of *in-situ* collected sample. (B) Sky photos collected using a hemispherical lens. Displayed target and sky photos were acquired on June 20th, 2014. (C) Photo showing the placement of the different instrumentations used during *in-situ* spectral sampling. The photo was taken during spectral acquisition of the reference site on June 20th, 2014. (D) Experimental design of *in-situ* spectral collection based on the mass grave setup where the site was divided into eight sections (i.e. 1 to 8). The red circles represent the starting measurement point where the spectralon panel was placed.

3.3.4. Airborne Hyperspectral Imagery

Airborne hyperspectral imagery was collected over the study area using Compact Airborne Spectrographic Imager 1500 (CASI-1500) and Shortwave Infrared Airborne Spectrographic Imager (SASI-644) sensors installed aboard the NRC-FRL's Twin Otter aircraft. The CASI sensor, covering the 376 – 1048 nm wavelength range, is a push-broom style Hyper Spectral Imager (HSI) and was configured to collect 199 spectral channels. The system covers a FOV of 39.9° and acquires 1500 (1493 used) spatial pixels across the flight line. The SASI system, also a push-broom style HSI, covers the 870 – 2524 nm range and is composed of 160 contiguous spectral channels. It acquires 644 (640 used) spatial pixels across the flight line with a FOV of 39.7°. To maintain a consistent across-track pixel resolution a constant ground speed and altitude in meters above ground level (AGL) were held during image acquisition at 41 m/s and 643 m respectively. The constant across-track pixel resolution is of 0.30 m for the CASI and 0.70 m for the SASI imagery. Along-track spacing and resolution depends on recorded altitude and ground speed during image acquisition.

Airborne imagery using the CASI and SASI sensors were collected over the sites and surrounding area throughout the study period. In 2013, three airborne images were acquired between the months of June and September using the SASI sensor. Over the 2014-growing season, monthly airborne hyperspectral imagery was collected between May and August using both sensors, CASI and SASI. Table 3.2 shows the parameters of the imagery acquired with both sensors during the study period.

Table 3.2. Parameters of the airborne imagery acquired over the study area between June 2013 and August 2014 using the CASI and SASI sensors.

Date	**Sensor**	**Acquisition Time (GMT)**	**Pixel Resolution**		**Altitude (m AGL)**	**Ground Speed (m/s)**
			Across Track	**Along Track**		
2013-06-20	SASI	17:48:06	0.71	0.72	643	44.80
2013-07-12	SASI	15:28:10	0.71	0.62	643	38.60
2013-09-18	SASI	16:09:11	0.71	0.64	643	40.06
2014-05-08	CASI	15:28:22	0.33	1.45	643	46.30
	SASI	15:28:25	0.71	0.71	643	45.80
2014-06-17	CASI	14:42:38	0.33	1.18	643	37.60
	SASI	14:46:02	0.71	0.75	643	46.80
2014-07-10	CASI	15:05:17	0.33	1.40	643	44.80
	SASI	15:04:47	0.71	0.72	643	44.80
2014-08-08	CASI	15:52:04	0.33	1.06	674	34.00
	SASI	15:40:06	0.71	0.58	643	36.42

3.4. Data Pre-processing

3.4.1. Field Spectrometry

Prior to data analyses, the *in-situ* data (i.e. plot level) were organized and resampled to the CASI and SASI's spectral response in ENVI 5.1 (Exelis Visual Information Solutions, Boulder, Colorado). The *in-situ* data were also adjusted to the R(8°:h) to R(0°:45°) viewing and illumination geometry factors of the spectralon. To avoid noise, the 350 – 400 nm and 2400 – 2500 nm wavelength ranges were not used in the analyses. The 1325 – 1488 nm and 1765 – 2100 nm ranges, which are affected by atmospheric water, were also removed from the spectral data and not used in the analyses. No analyses were performed on the collected off-site (i.e. surrounding area) spectral signatures.

3.4.2. Airborne Hyperspectral Imagery

The CASI and SASI images were converted from raw digital numbers to radiance in $\mu Wcm^{-2}\ sr^{-1}\ nm^{-1}$ units via in-lab generated radiometric correction coefficients by NRC-FRL. The imagery was subsequently atmospherically and vicariously corrected (VC) (Secker et al. 2001). The atmospheric correction of the radiance imagery was performed with the Fast Line-of-Sight Atmospheric Analysis of Spectral Hypercube (FLAASH) tool in ENVI 5.1. Based on the location of the sites, the Mid-Latitude Summer Atmospheric Model and the Rural Aerosol Model were run to remove the influence of the atmosphere. A water absorption feature of 820 nm for the CASI imagery and one of 1135 nm for the SASI imagery was used. The specific sensor altitude of the flight line and a ground elevation of 111 m were used for the atmospheric correction. The CO_2 mixing ratio was retrieved from the National Oceanic and Atmospheric Administration (NOAA)'s database (Tans and NOAA/ESRL 2015)(Table 3.3). Initial visibility was calculated using the aerosol optical depth (AOD) at 550 nm that was collected with the sunphotometer during image acquisition. The visibility was calculated by the following equation:

$$V = \frac{3.912}{\beta} \qquad \textbf{(Equation 1)}$$

where β is the horizontal optical depth per km and can be calculated by dividing the AOD at 550 nm by the effective aerosol thickness layer, typically around 2 km (Koschmieder (1926) as referenced in Pueschel and Noll (1967)). The AOD at 550 nm was calculated by a linear interpolation of the AOD at 500 nm and 870 nm collected during imagery acquisition. Table 3.3 shows the calculated visibilities for the respective airborne acquisition dates.

Table 3.3. Initial visibility (km) and CO_2 mixing ratio (ppm) used in the atmoshperic correction process of the acquired airborne imagery.

Date	Initial Visibility (km)	CO_2 Mixing Ratio (ppm)*
2013-06-20	52.70	415.97
2013-07-12	12.90	417.23
2013-09-18	70.03	393.51
2014-05-08	26.62	398.60
2014-06-17	52.72	398.80
2014-07-10	76.30	398.50
2014-08-08	54.70	398.73

* CO_2 mixing ratio was retrieved from the NOAA database (Tans and NOAA/ESRL 2015)

The final pre-processing step involved the VC process (Secker et al. 2001) where the CASI and SASI imagery were further calibrated using simultaneously collected ground data of a homogenous target (e.g. concrete surface) within the flight line. The FieldSpec3 spectrometer was used to collect the ground data for the vicarious calibration process. The ratios between the ground and the airborne spectra, in reflectance, of the same concrete target was calculated and applied as a gain factor to the airborne imagery in ENVI 5.1. Figure 3.9 shows an example of both the uncorrected and corrected spectral signatures of the same target collected using the ASD, CASI and SASI systems.

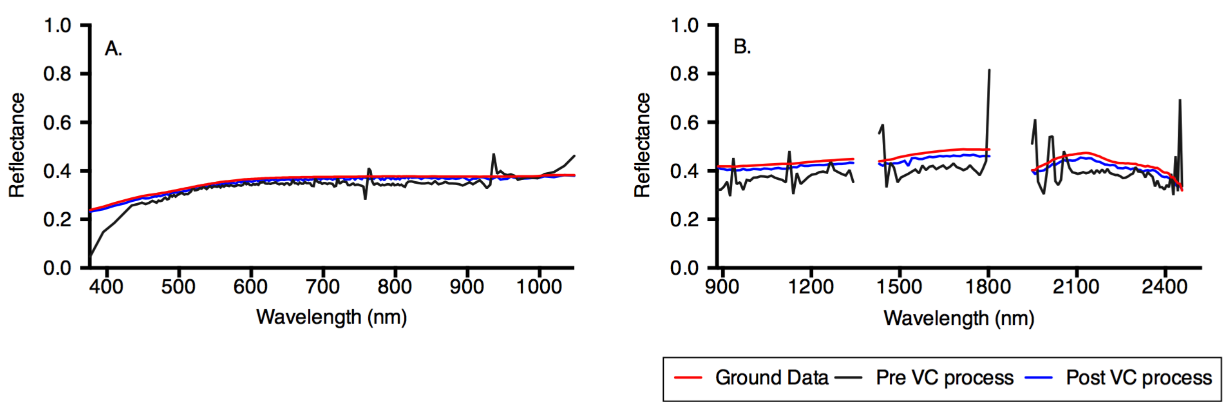

Figure 3.9. Comparison of the U-61 cement target spectral signature collected using the (A) CASI collected on May 8th, 2014, and (B) SASI sensors collected on September 18th, 2013, of the atmospherically corrected airborne (pre vicarious calibration (VC) process), ground, and vicariously calibrated airborne spectral reflectance (post VC process).

Following the VC process, the airborne images were ready for analysis. All spectral analyses were performed on non-geocorrected data to avoid the potential introduction of errors caused from the geocorrection process (Allux and Leblanc 2010). Regions of interest (ROIs) were selected to investigate the spectral differences between all sites. Pure site pixels were selected in order to avoid the introduction of mixed pixels containing information of both site pixels and surrounding area. Figure 3.10 illustrates the ROI location of each site for the airborne imagery and the number of pixels per site. The same number of pixels was attempted per site ROI for all acquired images for consistency and comparison.

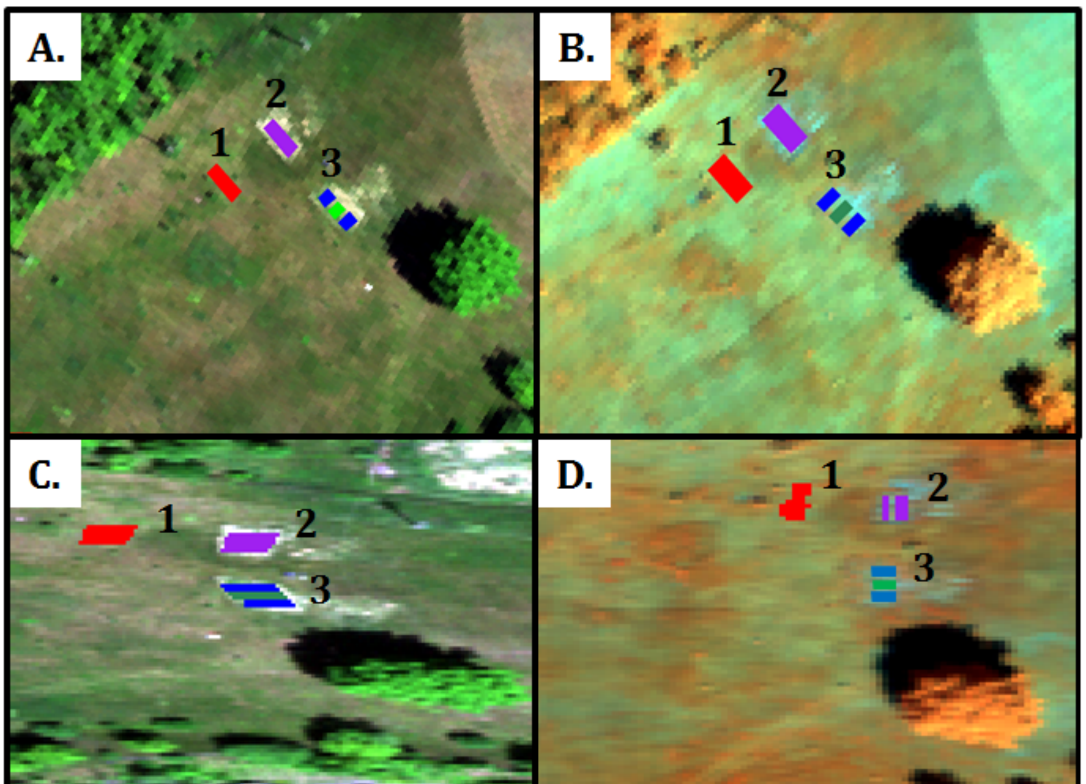

Legend	No. of ROI pixels	No. of ROI pixels
(1) Control	65	50
(2) Reference	65	50
(3) Graves	50	40
(3) Gap	15	10

Figure 3.10. Georectified (A) CASI (R: 739 nm G: 698 nm B: 553 nm) and (B) SASI (R: 1052 nm G: 1624 nm B: 2122 nm) and non-georectified (C) CASI (R: 739 nm G: 698 nm B: 553 nm) and (D) SASI (R: 1052 nm G: 1624 nm B: 2122 nm) collected on June 17th, 2014, illustrating the selected site region of interest (ROI): (1) Control (red), (2) Reference (purple), (3) Graves (blue), and Gap (green).

3.5. Data Analyses

3.5.1. Soil Chemistry and Vegetation Pigmentation Statistical Analyses

To investigate whether there are significant differences between all study sites in terms of soil chemistry and vegetation pigmentation statistical analyses were performed. The datasets were tested for normality with the Kolmogorov-Smirnov test, where the null hypothesis is that the datasets follow a normal distribution. One-way Analysis of Variance (ANOVA) followed by Tukey's multiple comparisons test was performed for the normally distributed datasets to test significant differences in spectral reflectance between all sites. The non-parametric Wilcoxon rank sum test or Kruskal – Wallis test were performed on the non-normally distributed datasets.

The statistical hypothesis testing was performed using Matlab R2014a. The null hypothesis was that there are no significant differences in means between the study sites, while the alternative hypothesis was that such differences exist between the sites. A robust nominal mixture clustering analysis was performed to test the separability between sites based on their soil chemical composition for the 2013 and 2014 growing seasons. A robust nominal mixture is an unsupervised statistical method that predicts the proportion of each value to each cluster using a maximum likelihood with respect to a mixture of Hubarized normal distribution that is a class of modified normal distribution that is more resistant to outliers (McLachlan and Peel 1998). The robust nominal mixture clustering analysis was performed using JMP 10 (SAS Institute Inc., Cary, NC).

3.5.2. Site Spectral Reflectance

The first step towards examining the temporal changes and differences in spectral reflectance between sites was to compute the mean spectral reflectance and variability (± one standard deviation from the mean) of each site per collection date. Overall differences in spectral signatures are investigated for the leaf, *in-situ* (i.e. ground) and airborne data collected during the 2013 and 2014 growing seasons. Furthermore, leaf and *in-situ* differences in spectral reflectance were computed using Price's equations of amplitude (D) and shape (θ) (Price 1994):

$$D = \left[\frac{1}{\lambda_b - \lambda_a} \int_{\lambda_a}^{\lambda_b} [S_1(\lambda) - S_2(\lambda)]^2 d\lambda\right]^{1/2}$$ **(Equation 2)**

$$\theta = \cos^{-1}\left[\frac{\int S_1(\lambda) S_2(\lambda) d\lambda}{[\int S_1(\lambda) d\lambda]^{\frac{1}{2}} [\int S_2(\lambda) d\lambda]^{\frac{1}{2}}}\right]$$ **(Equation 3)**

where S1 and S2 are pairs of spectra over a wavelength region (λa – λb). Different wavelength regions were used for the leaf and *in-situ* data: 400 – 2400 nm range (i.e. a= 400 and b=2400) for the leaf spectra, and 400 – 912 nm, 917 – 1317 nm, 1500 – 1771 nm, and 2047 – 2404 nm for the *in-situ* spectra.

The metrics determine the differences in amplitude (D) and shape (θ) of a spectral signature in comparison with a base spectrum, where the greater the differences the more dissimilar the spectral signatures (Price 1994). Spectral differences of within grave, within reference and between grave and reference were investigated by computing both metrics within the 400 – 2400 nm range. Analyses of the spectral amplitude (D) and shape (θ) for vegetation was computed for within site (i.e. within grave and within reference) to investigate the within site variability at the leaf spatial scale. For all data collections, the spectrum that was found to be the median at 550 nm was chosen as the base spectral signature. Next, the differences in spectral amplitude (D) and shape (θ) were computed between all grave spectra in comparison to the base reference spectrum per collection date. The reference spectral signature that was found as the median at 550 nm was chosen as the base sample and compared to each grave spectrum.

In the case of the *in-situ* data, spectral differences were tested over four separate intervals due to the data being resampled to match the airborne imagery (i.e. CASI and SASI ranges) and to not include water absorption bands in the analysis: 400 – 912 nm (i.e. CASI range), 917 – 1317 nm, 1500 – 1771 nm, and 2047 – 2404 nm. Analyses of within site spectral D and θ variability were computed between spectra over the four spectral ranges. To investigate between sites spectral differences in D and θ, the reference spectra were compared against the grave spectra over the four spectral ranges and all data collections. For each of the data collections significant differences between the within site and between-sites spectral differences were investigated for both the leaf and *in-situ* spectral reflectance using the Wilcoxon rank sum sites ($\alpha<0.05$).

The forward feature selection (featself) algorithm, using the nearest neighbour criterion and part of the PRTools for Matlab R2014a, was applied to to (1) find the optimal number of best separable bands and (2) determined which bands are frequently found to give the best distinction between the grave and reference based on their spectral reflectance at the leaf, *in-situ*, and airborne spatial scales. The algorithm was run as a two-class problem (i.e. grave versus reference) where each site was considered as one class. The criterion of separation between sites ranges between 0 and 1, where 1 represents a complete separation between sites in theory. The number of optimal bands was selected based on the criteria of separation in spectral reflectance between the two sites.

3.5.3. Vegetation indices

A series of vegetation indices were computed on the leaf, *in-situ* and airborne data to explore site spectral separation. Table 3.4 illustrates the pertinent information required to calculate and interpret vegetation indices. These indices are designed to highlight particular properties of a spectral signature and measure pigment concentration and vegetation stress (Peñuelas and Filella 1998). The vegetation index values for the collected spectra were calculated in Matlab R2014a for the leaf and *in-situ* data and in ENVI 5.1 for the airborne imagery. The results were tested for normality and then tested to investigate significant differences in vegetation indices between sites (α=0.05). For the airborne imagery, the forward feature selection algorithm was also applied to depict which indices show the greatest differences between the grave, gap section, reference, and control.

Table 3.4. Computed vegetation indices on the leaf, *in-situ* and airborne data collected of the study sites over the study period. μ = mean and ρ = reflectance.

Index	Acronym	Description	Equation	Index range	Reference
Normalized Difference Pigment Index	NDPI	Chlorophyll and carotenoids content	$(\rho680 - \rho430)/(\rho680 + \rho430)$	-1 to 1	Peñuelas and Filella (1998)
Normalized Difference Vegetation Index 1	NDVI 1	Greenness	$(\rho750 - \rho680)/(\rho750 + \rho680)$	-1 to 1	Rouse Jr et al. (1974)
Normalized Difference Vegetation Index 2	NDVI 2	Greenness	$(\rho860 - \rho660)/(\rho860 + \rho660)$	-1 to 1	Tucker (1979)
Plant Senescence Reflectance Index	PSRI	Senescence and carotenoids content	$(\rho680 - \rho500)/\rho750$	-1 to 1	Merzlyak et al. (1999)
Red Edge NDVI	RENDVI	Greenness and vegetation stress detection	$(\rho752 - \rho701)/(\rho752 + \rho701)$	-1 to 1	Gitelson and Merzlyak (1994)
Red-edge Position Index	REP	Chlorophyll content	$(\rho670 - \rho780)/2$	-0.5 to 0.5	Curran et al. (1995)
Red-Edge Vegetation Stress Index	RVSI	Vegetation stress	$((\rho714 + \rho752)/2) - \rho733$	-0.5 to 0.5	Merton and Huntington (1999)
Sum Green Index	SGI	Greenness	$\mu\,(\rho500{:}\ \rho600)$	0 to 50	Lobell and Asner (2003)
Structure Insensitive Pigment Index	SIPI	Chlorophyll and carotenoids content	$(\rho800 - \rho445)/(\rho800 - \rho680)$	0 to 2	Penuelas et al. (1995)
Vogelmann Red Edge Index 1	VOG1	Chlorophyll Content	$\rho740 / \rho720$	0 to 20	Vogelmann et al. (1993)
Vogelmann Red Edge Index 2	VOG2	Chlorophyll Content	$(\rho734 - \rho747)/(\rho715 + \rho726)$	0 to 20	Vogelmann et al. (1993)

4. Results

4.1. Soil Chemistry

4.1.1. 2013 Soil Chemistry

The differences in soil chemistry, such as Ca, Fe, K, Mg, Mn, Na, and P, of soil samples collected five months post-disturbance, in November 2013, were tested. The Kolmogorov-Smirnov test shows that the November 2013 concentrations are normally distributed ($p<0.05$), with the exception of the Na concentration ($p>0.05$). A one-way ANOVA multiple comparisons (i.e. Tukey's multiple comparisons test, $\alpha=0.05$) was computed to test the differences between sites for the normally distributed datasets; meanwhile, the Kruskal Wallis test was computed for the Na concentration dataset ($\alpha=0.05$). No significant differences were found between sites in K, Na, and total P concentrations (Table 4.1). A significant difference in Ca and Mg concentrations is shown between the control and disturbed sites (i.e. grave, gap, and reference) ($p<0.01$) (Table 4.2). The control is significantly different in Fe and Mn content from the grave ($p=0.01$ and $p=0.02$ respectively) and in Fe concentration from the gap ($p=0.04$). Moreover, a significant difference is revealed between the grave and reference for Ca ($p=0.004$) and Mn ($p=0.02$) concentrations. Table 4.3 shows the mean and standard deviations of the investigated elements. The grave records a higher Mn concentration, at 1147 ppm, in comparison with the reference at 905 ppm. In contrast, the reference shows a higher percentage of Ca, at 1.91, than the grave at a percentage of 1.37. Lower concentrations are observed for the control site in Ca at 0.72 %, Fe at 1.78 %, Mg at 0.56 %, and higher in P concentration at 0.10 %.

Table 4.1. One-way ANOVA ($\alpha=0.05$) of potassium (K) and total phosphorus (P) concentrations between study sites (i.e. control, grave, gap, and reference) of soil samples collected in November 2013 (n=9 per site).

Element	ANOVA table	SS	DF	MS	F (DFn, DFd)	P-value
K	Between sites	0.0048	3	0.001604	F (3, 23) = 0.4017	0.7531
	Within site	0.0918	23	0.003994		
	Total	0.0966	26			
P	Between sites	0.0001	3	0.00003449	F (3, 23) = 0.6280	0.6043
	Within site	0.0012	23	0.00005492		
	Total	0.0013	26			

Table 4.2. One-way ANOVA multiple comparisons (Tukey's multiple comparisons test, alpha of 0.05) between control (C), grave (G), gap, and reference (R) of soil sampled collected November 2013.

Element		**C vs. G**	**C vs. Gap**	**C vs. R**	**G vs. Gap**	**G vs. R**	**Gap vs. R**
Mn	P-value	0.0259*	0.3969	0.9984	0.8636	0.0186*	0.3375
	F	4.343	2.266	0.2313	1.1	4.55	2.43
	DF	23	23	23	23	23	23
Fe	P-value	0.0102*	0.0405	0.4239	0.9995	0.1866	0.3137
	F	4.918	4.053	2.196	0.1558	2.954	2.5
	DF	23	23	23	23	23	23
Ca	P-value	0.0007*	< 0.0001*	< 0.0001*	0.2928	0.0042*	0.6777
	F	6.45	7.82	13.31	2.564	5.455	1.592
	DF	23	23	23	23	23	23
Mg	P-value	0.002*	0.0005*	< 0.0001*	0.5507	0.3907	0.999
	F	5.895	6.664	9.143	1.889	2.283	0.1983
	DF	23	23	23	23	23	23

* Significant differences between sites (α=0.05

Table 4.3. Mean (μ) and standard deviation (σ) of investigated soil element concentrations of study sites (control, grave, gap, and reference) of soil samples collected in November 2013 (n=9 per site).

Element		**Control**	**Grave**	**Gap**	**Reference**
Ca (%)	μ	0.724¶	1.365*	1.707	1.907*
	σ	0.326	0.222	0.235	0.231
Fe (%)	μ	1.784¶	2.177	2.193	1.941
	σ	0.293	0.217	0.081	0.122
K (%)	μ	0.246	0.232	0.257	0.219
	σ	0.095	0.037	0.049	0.031
Mg (%)	μ	0.597¶	0.988	1.157	1.140
	σ	0.263	0.139	0.035	0.098
Mn (ppm)	μ	916.20	1147.00*	1069.00	905.20*
	σ	122.20	185.90	160.50	124.80
Na (%)	μ	0.027	0.022	0.027	0.018
	σ	0.008	0.004	0.006	0.004
P (%)	μ	0.101	0.098	0.095	0.097
	σ	0.010	0.008	0.004	0.004

¶Significant differences between control and all other sites (α=0.05)
*Significant differences between grave and reference (α=0.05)

4.1.2. 2014 Soil Chemistry

Over the 2014-growing season, differences in available P, NH_4, and NO_3 concentrations were tested between grave and non-grave soil samples. Significant differences in available P concentration were found between the control and disturbed sites (Table 4.4). A significant difference in available P concentration is seen between the grave and reference in November 2014 ($p<0.0001$). No significant differences in available P are recorded between the gap and the other disturbed sites (i.e. graves and reference), with the exception of against the reference in November 2014 ($p=0.001$). Between May and October 2014, the control records a higher available P concentration than the disturbed sites (Figure 4.1). A seasonal fluctuation in available P is observed for the control with the highest concentration being recorded in October 2014 at 58.62 mg kg^{-1}. A gradual increase in available P concentration of samples collected from the grave is also revealed from 18.66 mg kg^{-1}, in May, to 29.51 mg kg^{-1} in November. The gap section records the highest concentration of available P at the start and end of the collection period in May, at 23.52 mg kg^{-1}, and November, at 31.10 mg kg^{-1} respectively.

Table 4.4. P-values of statistical analyses computed to test the differences between control (C), grave (G), gap, and reference (R) based on available phosphorus (P) concentration (mg kg^{-1}) of soil samples collected over the 2014-growing season.

Month	C vs. MG	C vs. Gap	C vs. R	G vs. Gap	G vs. R	Gap vs. R
[1]May	< 0.0001*	< 0.0001*	< 0.0001*	0.6784	0.8082	0.2459
[1]June	< 0.0001*	< 0.0001*	< 0.0001*	0.9981	> 0.9999	0.9957
[1]July	< 0.0001*	0.0012*	< 0.0001*	0.8777	0.9995	0.8154
[1]August	< 0.0001*	0.0005*	< 0.0001*	0.9816	0.9973	0.9418
[2]September	0.0148*	0.0142*	0.0003*	> 0.9999	> 0.9999	> 0.9999
[2]October	0.0042*	0.0322*	< 0.0001*	> 0.9999	> 0.9999	> 0.9999
[2]November	0.008*	0.4703	0.5111	> 0.9999	< 0.0001*	0.0010*

[1]One-way ANOVA multiple comparisons (Tukey's multiple comparisons test, $\alpha=0.05$)
[2]Kruskal Wallis multiple comparisons ($\alpha=0.05$)
*Statistically significant ($\alpha=0.05$)

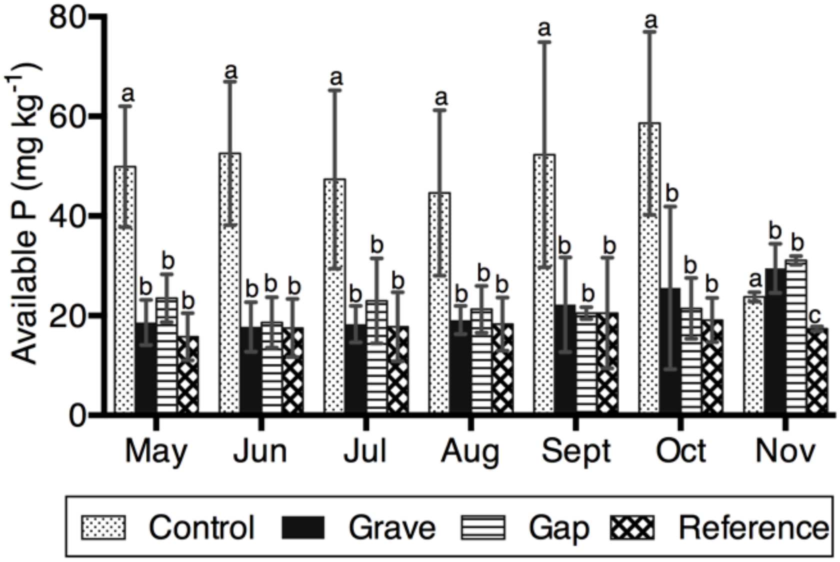

Figure 4.1. Available phosphorus (P) concentration (mg kg^{-1}) of soil samples collected over the 2014-growing season (control: n= 15, grave: n= 10, gap: n= 5, reference: n= 15). The different letters indicate significant differences between sites (α=0.05). Error bars indicate 1 standard deviation from the mean. Note: In November 2014, 10 samples were collected from the control and reference, 10 from the grave and 5 from the gap section.

A seasonal pattern in NH_4 concentration is also revealed, where the control shows the highest values, between 4.14 and 5.95 mg kg^{-1}, over the study period (Figure 4.2). The NH_4 concentration of the grave is fluctuating over the study period reaching a high of 3.64 mg kg^{-1} in October. Significant differences are seen between the grave and reference in NH_4 concentration in August ($p<0.0001$) and November ($p=0.0018$) (Table 4.5). Figure 4.3 illustrates the NO_3 concentrations extracted from the soil samples collected over the 2014-growing season. Between May 2014 and July 2014, low NO_3 concentrations are recorded at values below 33 mg kg^{-1} for the control and below 10 mg kg^{-1} for the disturbed sites. The NO_3 concentrations were below detectable levels of 1 mg kg^{-1} for the grave in June and for the gap in June and July. The NO_3 concentrations are peaking for all sites in August, between 58.36 and 119.40 mg kg^{-1}, and decreasing by the end of the growing season, in November, between 4.58 and 9.32 mg kg^{-1}. The results indicate significant differences in NO_3 concentrations between the control and disturbed sites in August 2014 (Table 4.6). A significant difference is also shown in NO_3 concentration between the grave and reference in October 2014 ($p=0.0113$) and November 2014 ($p=0.0045$). Starting with September the grave records the highest NO_3 concentrations in comparison with the other sites.

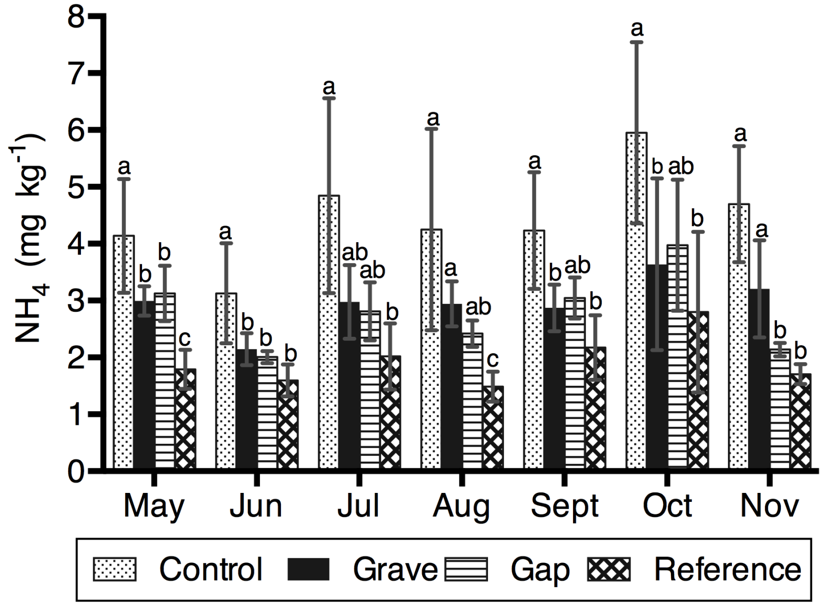

Figure 4.2. Ammonium (NH_4) concentration (mg kg^{-1}) of soil samples collected over the 2014-growing season (control: n= 15, grave: n= 10, gap: n= 5, reference: n= 15). The different letters indicate significant differences between sites (α=0.05). Error bars indicate 1 standard deviation from the mean. Note: In November 2014, 10 samples were collected from the control and references, 10 from the grave and 5 from the gap section.

Table 4.5. P-values of statistical analyses computed to test the differences between control (C), grave (G), gap, and reference (R) based on ammonium (NH_4) concentration (mg kg^{-1}) of soil samples collected over the 2014-growing season.

Month	C vs. MG	C vs. Gap	C vs. R	G vs. Gap	G vs. R	Gap vs. R
[1,2]May	0.0027*	0.0396*	<0.0001*	0.9452	0.0259*	0.0400*
[1,2]June	0.0006*	0.0839	<0.0001*	>0.999	0.0675	0.5739
[2]July	0.1587	0.0193	<0.0001*	>0.999	0.0787	0.5919
[1,2]August	0.6643	0.0700	<0.0001*	0.0127*	<0.0001*	<0.0001*
[1]September	0.0159*	0.3587	<0.0001*	0.4425	0.3452	0.2760
[2]October	0.0023*	0.0608	<0.0001*	0.9755	0.5107	0.4225
[1,2]November	0.6326	<0.0001*	<0.0001*	0.7021	0.0018*	0.4232

[1]One-way ANOVA multiple comparisons (Tukey's multiple comparisons test, α=0.05)
[2]Kruskal Wallis multiple comparisons (α=0.05)
*Statistically significant (α=0.05)

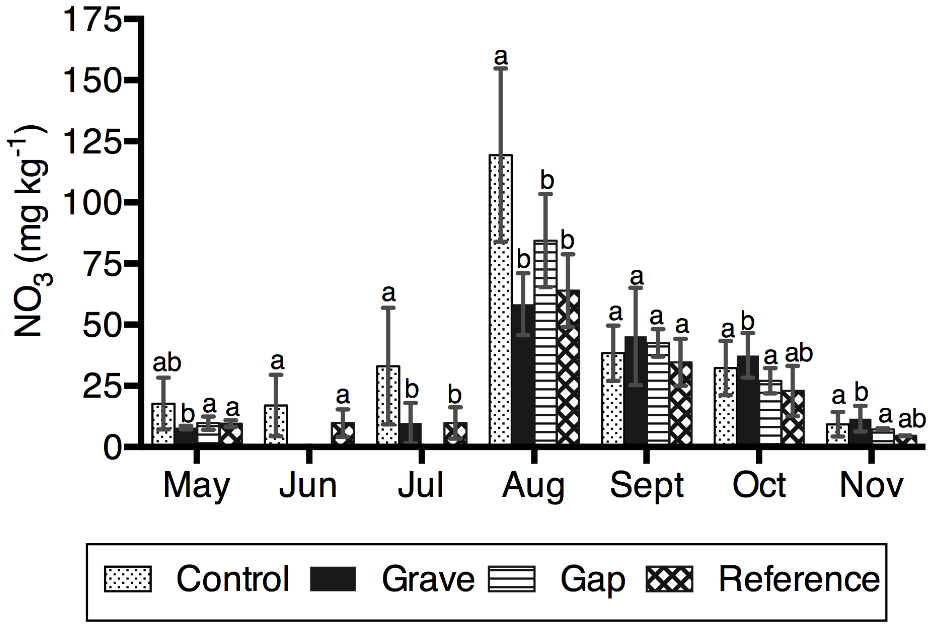

Figure 4.3. Nitrate (NO_3) concentration (mg kg^{-1}) of soil samples collected over the 2014-growing season (control: n= 15, grave: n= 10, gap: n= 5, reference: n= 15). The different letters indicate significant differences between sites (α=0.05). The error bars indicate 1 standard deviation from the mean. Note: NO_3 concentrations were below detection levels (i.e. 1 mg kg^{-1}) for soil samples collected from the grave and gap in June 2014, and for soil samples collected from the gap in July 2014.

Table 4.6. P-values of statistical analyses computed to test the differences between control (C), grave (G), gap, and reference (R) based on nitrate (NO_3) concentration (mg kg^{-1}) of soil samples collected over the 2014-growing season.

Month	C vs. MG	C vs. Gap	C vs. R	G vs. Gap	G vs. R	Gap vs. R
[1,2]May	0.0337*	0.3076	0.1258	>0.999	0.9772	>0.999
[2]June	N/A	N/A	0.1024	N/A	N/A	N/A
[1]July	0.1143	N/A	0.0894	N/A	>0.999	N/A
[1]August	<0.0001*	0.0350*	<0.0001*	0.2121	0.9413	0.3618
[1]September	0.5676	0.9209	0.8587	0.9820	0.2020	0.6358
[1,2]October	0.4061	0.5661	0.2903	0.1470	0.0113*	>0.999
[1]November	0.6551	0.8111	0.1139	0.2156	0.0045*	0.6225

[1]One-way ANOVA multiple comparisons (Tukey's multiple comparisons test, α=0.05)
[2]Kruskal Wallis multiple comparisons (α=0.05)
*Statistically significant (α=0.05)

4.1.3. Cluster Analysis

A robust nominal mixture cluster analysis was performed to test the separability between sites based on the significantly differences in soil chemistry found between the grave and reference. A cluster analysis was performed based on Ca, Fe, and Mg concentrations of samples collected in November 2013 (Figure 4.4). A separation between the reference and control soil samples is revealed. Only three of the grave soil samples are separated from the reference based on the Ca, Fe, and Mg concentrations. A k-means cluster analysis was also computed based on the available P, NH_4, and NO_3 concentrations to investigate the separation between all sites in August and November 2014 (Figure 4.5). In August 2014, an overall separation can be seen between the control and disturbed sites. No separation is observed between the disturbed sites (i.e. grave, gap, and reference) in terms of available P, NH_4, and NO_3 concentrations. In comparison, a separation is revealed between the grave and reference in November 2014. The results show clusters based on available P, NH_4, and NO_3 concentrations where the reference is separable from the other sites. Clusters divide the control and gap samples; meanwhile the grave is divided between two clusters with three samples closer to the mean of the gap cluster and five to the mean of the control one.

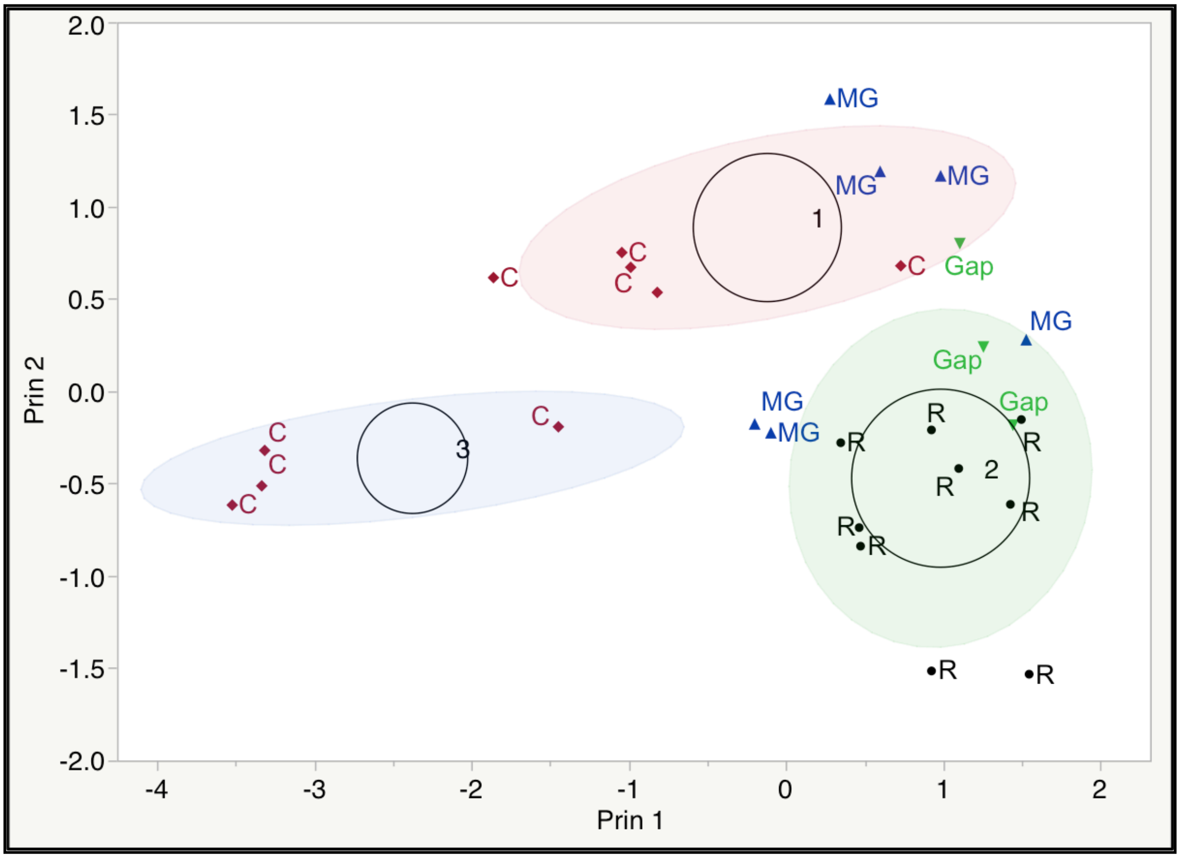

Figure 4.4. Robust normal mixture cluster analysis of elements showing significant differences between sites based on calcium, iron, and magnesium concentrations that were found to be significantly different between the control and disturbed sites (i.e. grave, gap, and reference) ($p<0.05$) in November 2013 ($n=27$). Legend: Control (C), grave (MG), gap, reference (R). The size of the circles is proportional to the count inside the cluster representing 90% density contour around the mean.

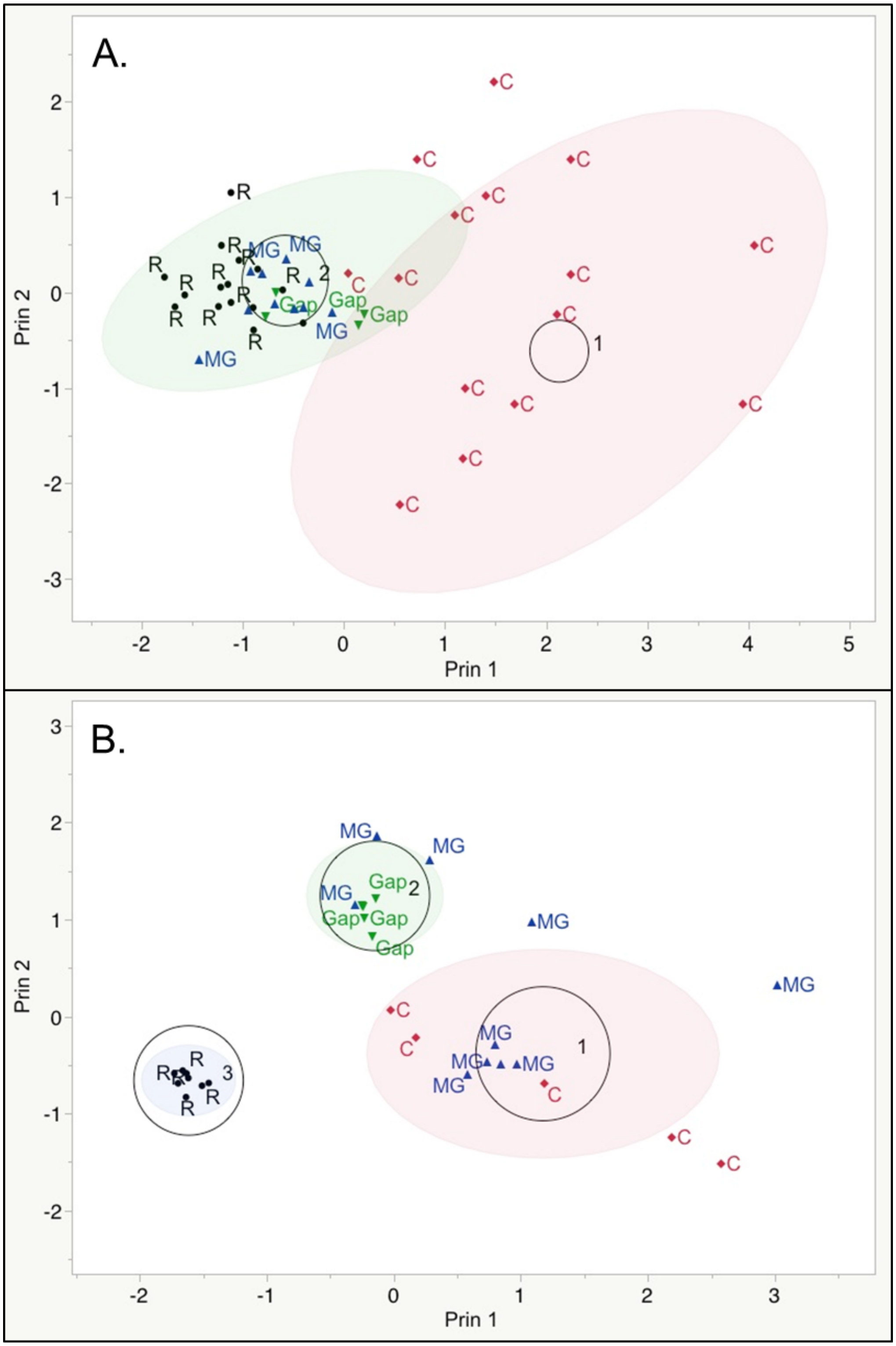

Figure 4.5. Robust normal mixture cluster analysis of elements showing significant differences in available phosphorus, ammonium, and nitrate concentrations between sites in (A) August 2014 (n=45) and (B) November 2014 (n=35). Legend: Control (C), grave (MG), gap, reference (R). The size of the circles is proportional to the count inside the cluster representing 90% density contour around the mean.

4.2. Leaf Pigmentation

Vegetation pigmentation, such as carotenoids, chlorophyll A, B and total were extracted from the collected leaf samples to test significant differences between sites during the first 15 months post-disturbance. The Kolmogorov-Smirnov test shows that the vegetation pigmentation results are not normally distributed for all data collections ($p>0.05$). The Kruskal Wallis non-parametric test was computed to test the differences in vegetation pigmentation between sites ($\alpha=0.05$). This section relates the results of the vegetation pigmentation concentration extracted from samples collected over the study period.

4.2.1. Carotenoids

Figure 4.6 shows the distribution of carotenoid concentration of leaf samples collected over the study period. Significant differences are found between the control and disturbed sites in carotenoid concentration, with the exception of September and October 2014. The results also indicate significant differences in carotenoid concentration between the grave and reference site for July ($p=0.0164$) and August ($p<0.0001$) 2014. In July 2014, the grave has a higher concentration of carotenoids, at 5.43 μg cm^{-2}, than the reference, at 4.61 μg cm^{-2}. Overall, a seasonal pattern is observed in carotenoid concentration peaking between 4.00 and 7.00 μg cm^{-2} between the months of May 2014 and June 2014 ($p>0.05$).

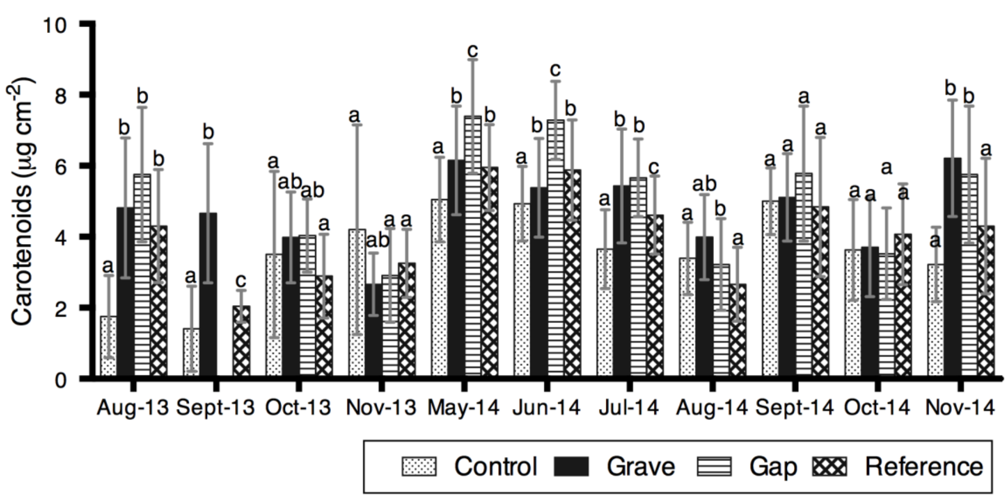

Figure 4.6. Carotenoid concentration of leaf samples collected over the 2013 and 2014 growing seasons (control: n=45; graves: n=30; gap: n=15; reference: n=45). The different letters indicate significant differences between sites (Kruskal Wallis, $\alpha=0.05$). The error bars represent 1 standard deviation from the mean.

4.2.2. Chlorophyll A

The results of the chlorophyll A concentration show a significant difference between the control and disturbed sites over the 2013 and 2014 growing seasons (Figure 4.7). The disturbed sites show a higher concentration of chlorophyll A, ranging between 35.76 and 40.00 μg cm^{-2}, in comparison with the control, between 7.74 and 25.06 μg cm^{-2}. In 2013, a significant difference in chlorophyll A between the grave and reference is observed ($p<0.0001$) where the reference shows a higher concentration at approximately 20.00 μg cm^{-2}. A significant difference in chlorophyll A is revealed between the grave and reference from July 2014, 13 months post-disturbance, at a difference of 10.00 μg cm^{-2}, to September 2014, at 31.76 μg cm^{-2} for the grave and 25.28 μg cm^{-2} for the reference ($p<0.001$). Furthermore, the grave shows a higher concentration of chlorophyll A, peaking in July 2014 at 40.00 μg cm^{-2}, over these months. A significant difference is also shown between the grave and gap in July 2014 ($p=0.0204$), at 40.00 μg cm^{-2} and 34.17 μg cm^{-2}, and August 2014 ($p=0.0039$) at 33.70 μg cm^{-2} and 30.52 μg cm^{-2} respectively. No significant differences are found in chlorophyll A concentration between the disturbed sites for October and November 2014 ($p>0.05$).

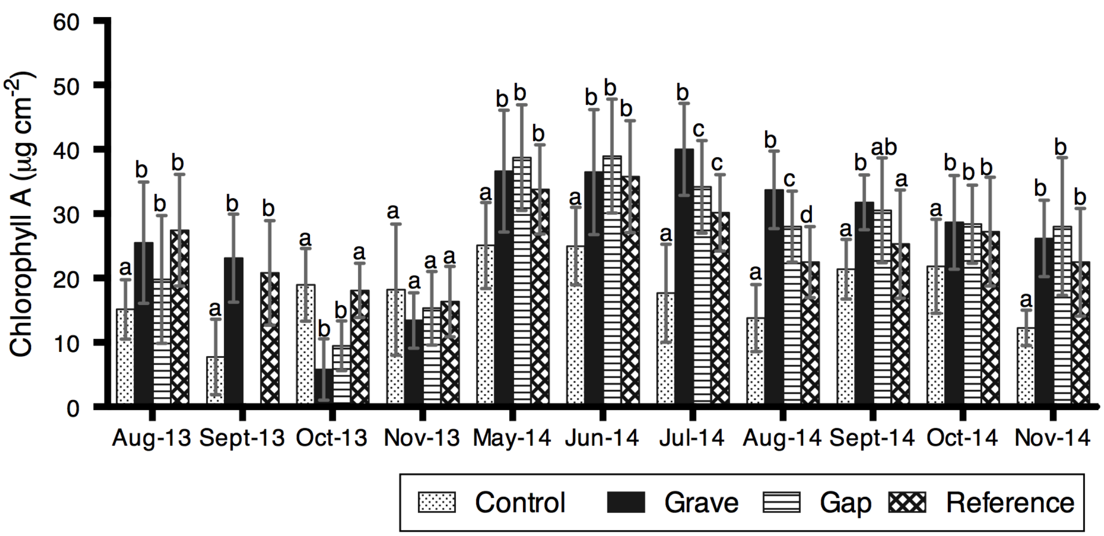

Figure 4.7. Chlorophyll A concentration of leaf samples collected over the 2013 and 2014 growing seasons (control: n=45; graves: n=30; gap: n=15; reference: n=45). The different letters indicate significant differences between sites (Kruskal Wallis, $\alpha=0.05$). The error bars represent 1 standard deviation from the mean.

4.2.3. Chlorophyll B

Figure 4.8 illustrates the chlorophyll B concentration of the leaf samples collected over the study period. The results show that the grave has an overall higher concentration of chlorophyll B in comparison with the control and reference, except in October 2013 where the reference shows a higher concentration at 6.37 µg cm^{-2}. The highest chlorophyll B concentrations for the grave are recorded in June and July 2014 at approximately 14.00 µg cm^{-2}. Significant differences are seen in chlorophyll B between the grave and reference from July, at 14.16 µg cm^{-2} and 11.43 µg cm^{-2}, to September 2014, at 10.27 µg cm^{-2} and 8.54 µg cm^{-2} respectively ($p<0.001$). Significant differences are also revealed between the control and disturbed sites over the 2013 and 2014 growing seasons ($p>0.05$), where the control shows the highest concentration at 9.20 µg cm^{-2} and the disturbed sites at 12.94 µg cm^{-2} respectively. In October and November 2014, no significant differences ($p>0.05$) are observed between the disturbed sites (i.e. grave, gap, and reference).

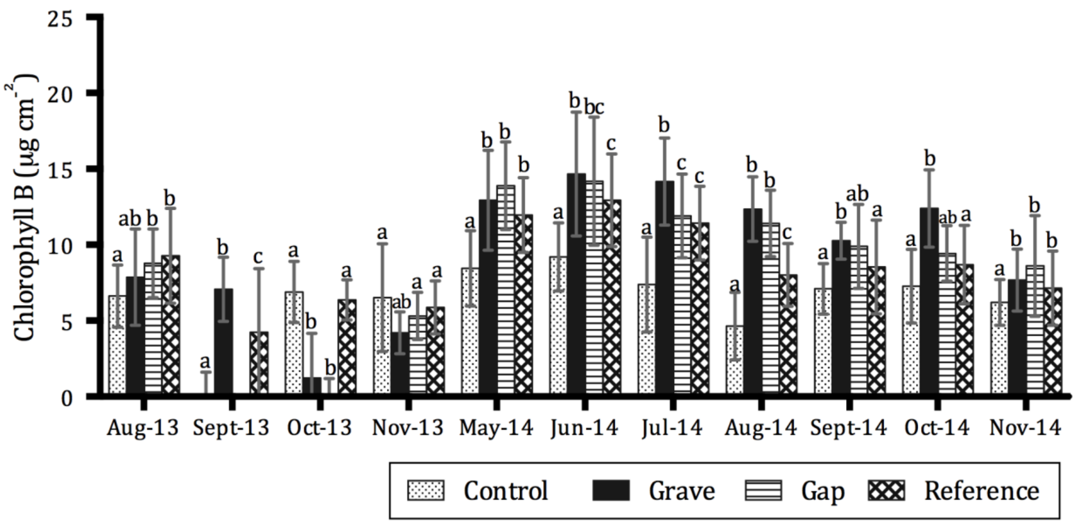

Figure 4.8. Chlorophyll B concentration of leaf samples collected over the 2013 and 2014 growing seasons (control: n=45; graves: n=30; gap: n=15; reference: n=45). The different letters indicate significant differences between sites (Kruskal Wallis, α=0.05). The error bars represent 1 standard deviation from the mean.

4.2.4. Total Chlorophyll

The total chlorophyll concentration results show similar trends where the control is significantly different ($p>0.05$) from the disturbed sites over the study period (Figure 4.9). In the first 12 months post-disturbance, no significant differences are seen between the disturbed sites in total chlorophyll ($p>0.05$). A significant difference is seen in October 2013 between the grave and reference ($p=0.002$), where similarly to chlorophyll A and B concentrations the reference site shows a higher concentration of total chlorophyll at 24.44 μg cm^{-2} in comparison with the grave at 11.61 μg cm^{-2}. However, starting with the 13th month disturbance point, July 2014, significant differences are seen between the grave and reference, at 54.15 μg cm^{-2} and 41.56 μg cm^{-2}, up to the 15th month post-disturbance, September 2014 ($p<0.001$), at 42.01 μg cm^{-2} and 33.80 mg cm^{-2} respectively. Starting with July 2014, the grave also shows the highest concentration trends in total chlorophyll, peaking at 54.15 μg cm^{-2}, in comparison with the other sites. No significant differences are seen between the disturbed sites towards the end of the 2014-growing season in October and November ($p>0.05$).

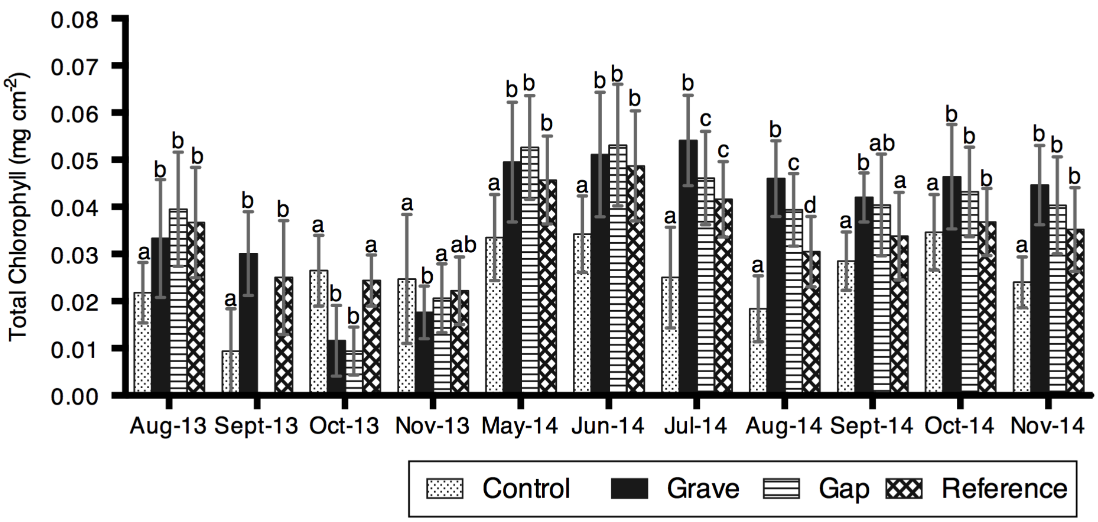

Figure 4.9. Total chlorophyll concentration in leaf samples collected over the 2013 and 2014 growing seasons (control: n=45; graves: n=30; gap: n=15; reference: n=45). The different letters indicate significant differences between sites (Kruskal Wallis, $\alpha=0.05$). The error bars represent 1 standard deviation from the mean.

4.3. Vegetation Spectral Reflectance

4.3.1. Leaf Spectral Reflectance

Figure 4.10 shows the average spectral signatures of leaf samples collected over the 2013-growing season. The greatest differences are observed between the control and disturbed sites where the control shows lower amplitude in comparison with the disturbed sites (i.e. grave, gap, and reference) over the 450 – 2500 nm range. A difference is seen between the grave and reference in the 800 – 1300 nm range in August and September 2013 where the reference shows a higher reflectance of approximately 0.05 (i.e. 5%) (Figure 4.10.A and B). A difference in leaf average spectral reflectance between the grave and reference is also observed in September 2013 over the 1600 – 1800 nm and 2100 – 2400 nm ranges where the reference shows a higher reflectance, at approximately 0.40 and 0.20, in comparison with the grave at approximately 0.30 and 0.10. Similar trends in average spectral reflectance are observed for October and November 2013 (Figure 4.10.C and D). Among the disturbed sites, the greatest differences in spectral signatures can be observed in the 800 – 1300 nm range where the reference has the highest reflectance, at approximately 0.50, while the grave shows the lowest reflectance at 0.40. A small difference is also seen in the 1600 – 1800 nm range where the reference shows a higher reflectance peaking at 0.35 in comparison with the grave and gap at 0.30 in the 1600s nm range. A difference in reflectance of 0.05 is also observed between the control and disturbed sites in the 550 – 680 nm range. Average leaf spectral reflectance shows similar pattern at the beginning of the 2014-growing season with the greatest differences revealed in the 800 – 1300 range (Figure 4.11). In 2014, small differences are observed in average spectral signatures of the study sites.

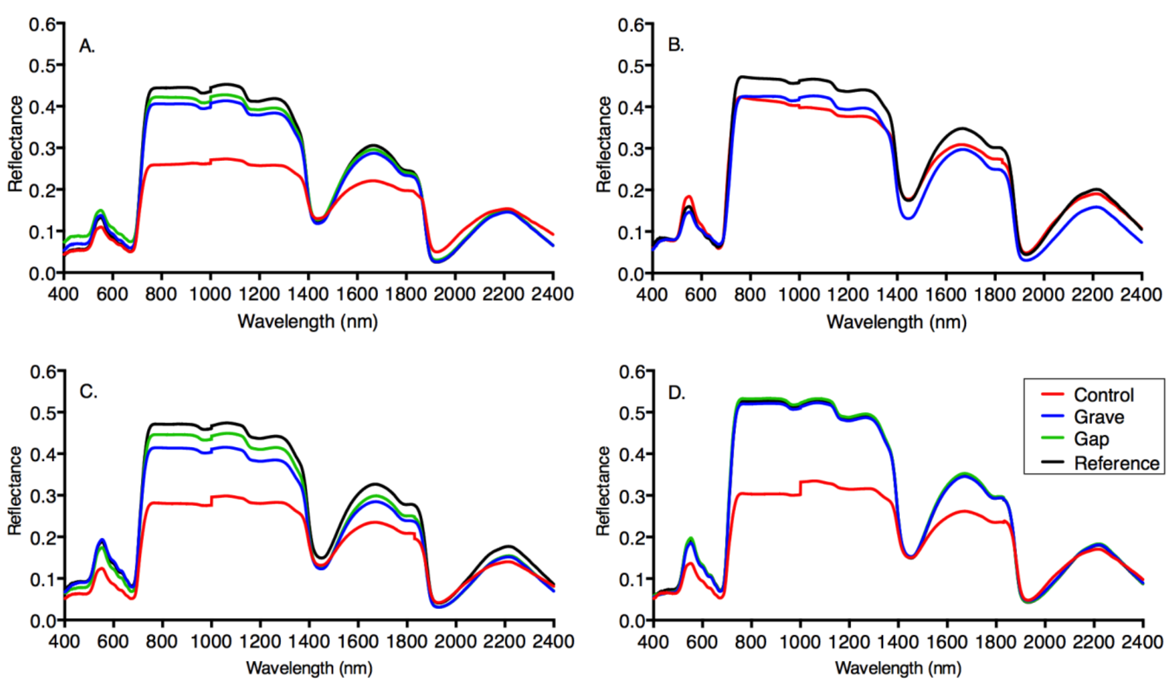

Figure 4.10. Average spectral reflectance of leaf samples collected from the (red) control, (blue) grave, (green) gap, and (black) reference over the 2013-growing season on: (A) August 13th, (B) September 13th, (C) October 18th, and (D) November 8th. Due to the high standard deviation (not shown) there are no differences between the sites.

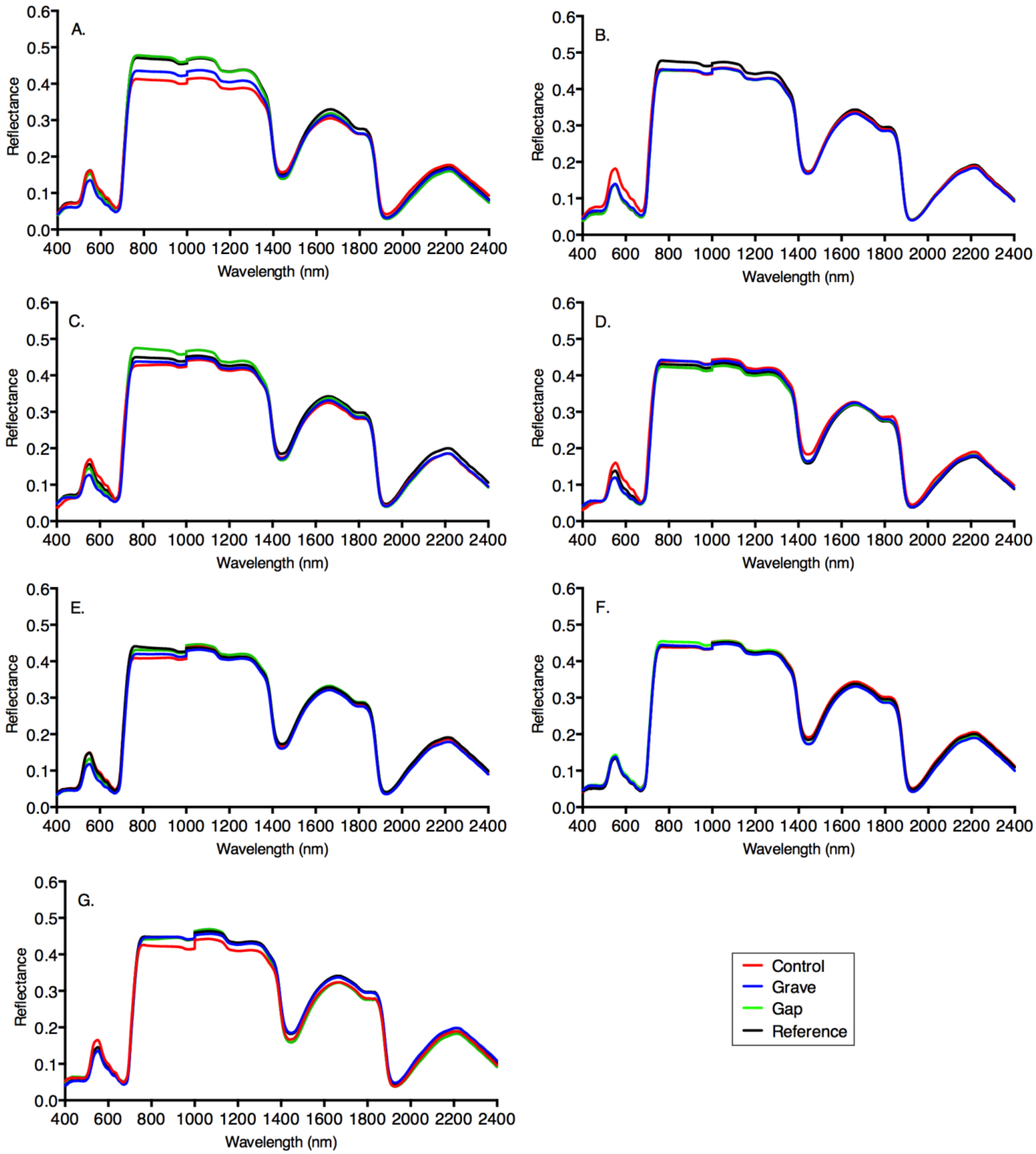

Figure 4.11. Average spectral reflectance of leaf samples collected from the (red) control, (blue) grave, (green) gap, and (black) reference sites over the 2014-growing season on: (A) May 29th, (B) June 19th, (C) July 25th, (D) August 21st, (E) September 25th, (F) October 24th, and (G) November 17th, 2014. Due to the high standard deviation (not shown) there are no differences between the sites.

Table 4.7 shows the differences in amplitude (D) between the grave and reference site over the 2013 and 2014 growing season. Significant differences in D between-sites and within grave spectra were found in September, at 0.041 and 0.012, and October 2013, 0.045 and 0.016 respectively ($p<0.0001$). Significant differences between-sites and within reference spectra in 2013 were also observed in September, at 0.041 and 0.016, and November, 0.061 and 0.030 respectively ($p<0.0001$). Overall significant differences in D are revealed between-sites over the 2014-growing season, against grave between July and September ($p<0.01$) with values ranging from 0.014 to 0.018 for the grave and 0.021 to 0.028 for the between-sites. A significant difference between-sites, at 0.037, and within reference, at 0.014, is observed in June 2014 ($p=0.008$). No other significant differences in amplitude are revealed between-sites in October 2014, differences between 0.020 and 0.022, and November 2014 between 0.030 and 0.034 ($p>0.05$).

The results indicate significant differences in shape (θ) between-sites and within grave spectral reflectance over the 2013 and 2014 growing seasons (Table 4.8). Over the 2013-growing season significant differences are seen against the grave in September, at 0.032 for the within grave and 0.061 for between-sites, and October at 0.044 and 0.068 respectively ($p<0.001$). The reference site θ difference, at 0.024, is also significantly different from between-sites in September 2013 ($p<0.0001$). In 2014, significant differences are seen against grave in July ($p=0.0315$), at 0.030, August ($p=0.004$) at 0.035, and September ($p=0.001$), at 0.027; while significant differences are observed against the reference in June ($p=0.001$), at 0.028, and July at 0.031 ($p=0.037$). No significant differences in spectral shape are observed between sites in October and November 2014 ($p>0.05$) with values ranging between 0.040 and 0.056 and a standard deviation of 0.025.

Table 4.7. Average (μ) and standard deviation (σ) of differences in spectral amplitude (D) of within grave, within reference, and between sites (i.e. each of the reference spectra compared against each spectrum of the grave) of the leaf spectral signatures (400 – 2400 nm range) collected over the 2013 and 2014 growing seasons.

Date		Grave		Reference		Reference vs. Grave	
		μ	σ	μ	σ	μ	σ
2013	Aug	0.024	0.023	0.040	0.036	0.033	0.030
	Sept	0.012*	0.006	0.016*	0.008	0.041	0.008
	Oct	0.016*	0.009	0.045	0.027	0.045	0.011
	Nov	0.057	0.037	0.030*	0.042	0.061	0.052
2014	May	0.022	0.024	0.015*	0.007	0.030	0.030
	Jun	0.027	0.024	0.014*	0.006	0.037	0.031
	Jul	0.018*	0.017	0.019	0.013	0.024	0.020
	Aug	0.014*	0.008	0.028	0.015	0.024	0.014
	Sep	0.014*	0.011	0.021	0.011	0.021	0.008
	Oct	0.021	0.014	0.020	0.016	0.022	0.014
	Nov	0.030	0.019	0.035	0.024	0.034	0.020

*Significant differences between sites (reference vs. grave) (Wilcoxon rank sum, α=0.05)

Table 4.8. Average (μ) and standard deviation (σ) of differences in spectral shape (θ) of within grave, within reference, and between sites (i.e. each of the reference spectra compared against each spectrum of the grave) of the leaf spectral signatures (400 – 2400 nm range) collected over the 2013 and 2014 growing seasons.

Date		Grave		Reference		Reference vs. Grave	
		μ	σ	μ	σ	μ	σ
2013	Aug	0.042	0.032	0.065	0.056	0.061	0.040
	Sept	0.032*	0.016	0.024*	0.010	0.061	0.022
	Oct	0.044*	0.031	0.063	0.032	0.068	0.033
	Nov	0.070	0.038	0.057	0.045	0.089	0.069
2014	May	0.026	0.015	0.035	0.021	0.032	0.012
	Jun	0.035	0.018	0.028*	0.013	0.042	0.022
	Jul	0.030*	0.016	0.031*	0.015	0.038	0.016
	Aug	0.035*	0.025	0.057	0.029	0.051	0.025
	Sept	0.027*	0.021	0.041	0.023	0.043	0.023
	Oct	0.040	0.030	0.030	0.013	0.043	0.028
	Nov	0.040	0.025	0.056	0.028	0.057	0.025

*Significant differences between sites (reference vs. grave) (Wilcoxon rank sum, α=0.05)

4.3.2. Spectral Separability

The forward feature selection (featself) algorithm, using the nearest neighbour criterion, was applied to select the optimal minimal number of bands and the specific wavelength required to separate between the grave and reference based on their spectral reflectance. The algorithm was run as a two-class problem (i.e. grave versus reference) where each site was considered as one class. Figure 4.12 shows the criteria of separability between the grave and reference spectra over 15 bands over the study period. The number of bands for the separation was chosen based on the number of bands showing the highest criteria of separation between the two. Depending on the disturbance stage and time in the growing season, the number of optimal bands varies between data collections from 5 bands in September 2014 to 15 bands in November 2013. The highest separation between sites is seen between September 2013 and November 2013, and in September 2014 at a criterion of 1.00. The lowest criterion of separation is recorded in November 2014 at 0.71 with a minimal number of 10 bands. In July 2014, 13 months post-disturbance, a minimal use of 11 best bands shows a criterion of separation at 0.88, meaning that the grave spectra can be separated from the reference spectra at 88% percent using those specific wavelengths.

Figure 4.13 illustrates the distribution of best separable wavelengths between grave and reference based on leaf spectral reflectance. The results show a cluster along the 400 to 800 nm and 1400 – 1600 nm ranges, along with a smaller cluster in the 2100 – 2300 nm range. Over the 2013-growing season, a separation between the grave and reference can be made using bands in the 400s nm wavelength range. Depending on the stage in the growing season and in the disturbance, a separation between grave and reference is revealed in the 500s nm and 700s nm ranges for May 2014, 500s nm range for July 2014, and 1400 – 1600 nm range for August 2014. At the end of 2014, between September and November, the grave is separable from the reference in the 600 – 700 nm wavelength range.

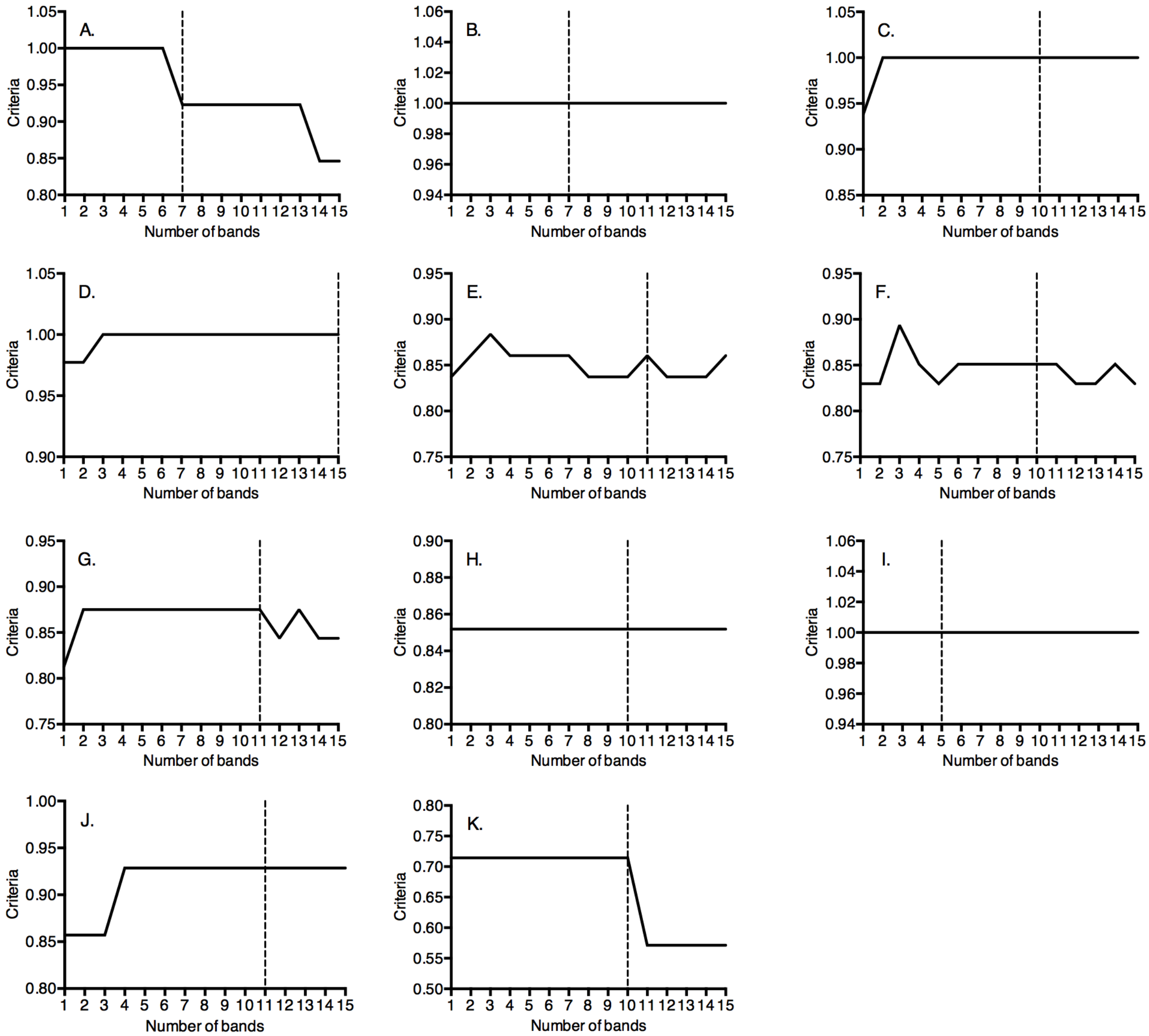

Figure 4.12. Criteria of separation of leaf spectral reflectance between grave and reference following the forward featured selection algorithm using 15 bands for (A) August 2013, (B) September 2013, (C) October 2013, (D) November 2013, (E) May 2014, (F) June 2014, (G) July 2014, (H) August 2014, (I) September 2014, (J) October, 2014 and (K) November 2014. The dashed vertical line represents the number of bands showing the highest separability between grave and reference. Theoretically the values range between 0 and 1, where 1 represents 100 percent separation between sites.

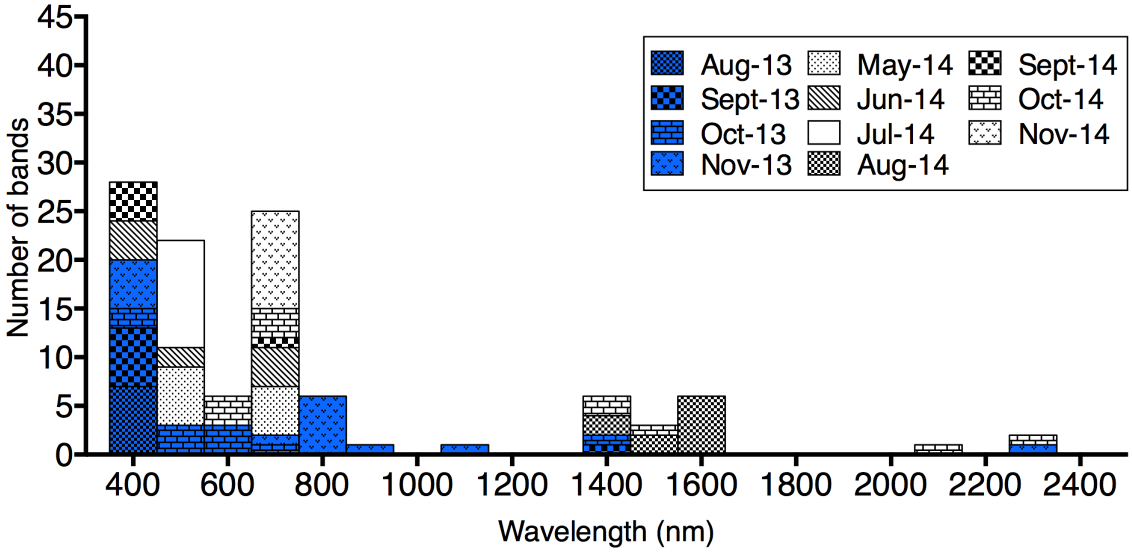

Figure 4.13. Distribution of separable wavelengths between grave and reference following the forward feature selection algorithm for the leaf spectra collected over the (blue) 2013 and (clear) 2014 growing seasons. The patterns represent different data collections. The results reveal a clustering in the 400 – 800 nm range.

4.3.3. Vegetation Indices

Various vegetation indices were computed to investigate differences between sites over the 2013 and 2014 growing seasons. The Wilcoxon rank sum was computed to test significant differences in vegetation indices between sites (α=0.05). Appendix C contains the results of the computed indices of data collected over the study period. Overall, a distinction between the control and disturbed sites can be made throughout the study period ($p<0.05$). The grave shows higher NDVI1, 0.65 to 0.83, and RENDVI, 0.39 to 0.57, in comparison with the control with a NDVI1 between 0.66 and 0.78 and a RENDVI between 0.39 and 0.52. For examples, in July 2014 the grave shows a leaf RENDVI of 0.39 in comparison with the control at 0.56.

Looking at the statistical test, the separation in leaf spectral reflectance between grave and reference based on vegetation indices depends on the disturbance stage and time of collection in the growing season. Overall, the indices showing significant differences between the grave and reference over the study period are NDPI, NDVI, RENDVI, SGI, SIPI and VOG ($p<0.05$). For instance, the grave records the highest NDVI1 values in July 2014, at 0.78, August and September 2014 at 0.80. The NDPI index shows significant differences between the grave, at -0.06, and reference, at -0.02 and -0.11, in the first three months post-disturbance, between

August ($p=0.011$) and September 2013 ($p<0.001$). The SGI index shows significant difference between the grave and reference in May 2014 ($p=0.0005$), values of 0.11 and 0.13, August 2014 ($p=0.019$), at 0.09 and 0.11, and September 2014 ($p<0.001$), at 0.09 and 0.11 respectively.

4.4. Field Spectrometry

4.4.1. General Site Changes

Over the study period, the control site was cover by undisturbed vegetation specific of the study area consisting of grasses and forbs species with no bare soil or woody vegetation (Figure 4.14). Lower variability in control site vegetation cover changes were observed during collection times. Figure 4.15 shows the vegetation cover of the grave and reference over the 2013 – growing season. Based on visual observations, at the beginning of the collection period, in July 2013, the grave and reference were covered by soil with no vegetation. In September 2013, a partial growth in vegetation is observed on top of the two sites (Figure 4.15.B and C). The grave shows more vegetation growth on the northwest side of the site, while patches of vegetation are seen overall the reference site. By October 2013, patches of vegetation growth are observed for the grave and reference. Figure 4.16 shows the vegetation cover of the grave and the reference over the 2014 – growing season. At the beginning of the growing season, May 2014, the grave and reference are covered by soil with small patches of vegetation observed for the reference site. By July 2014, visual observations show an increase in vegetation cover for both the grave and reference with various soil patches. At the end of the collection period, in September 2014, the grave and reference are predominately covered by vegetation. Based on observations, the vegetation growth on the northeastern side of the grave was much slower than the rest of the site.

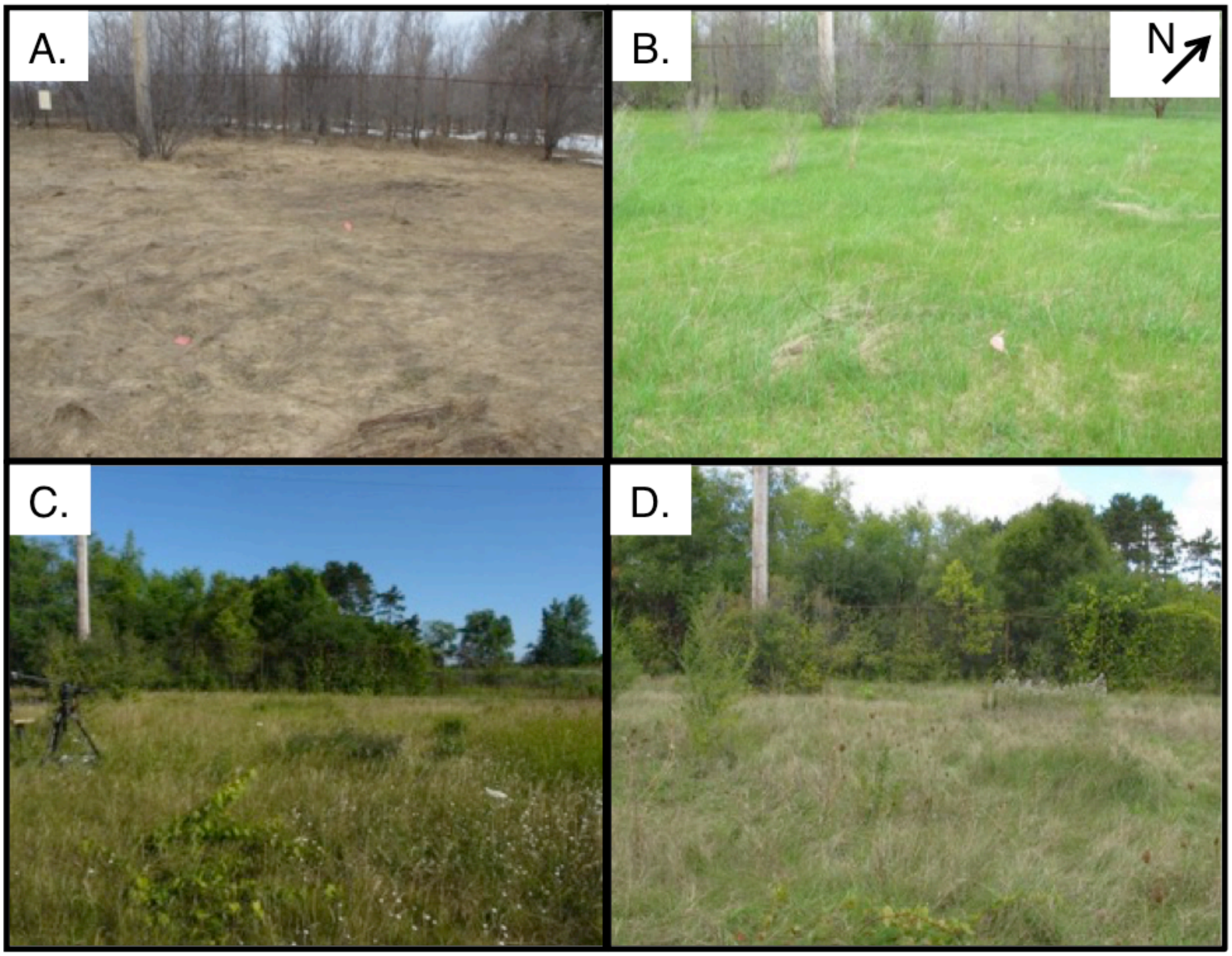

Figure 4.14. Vegetation cover on top of the control site during the 2014-growing season on: (A) April 27th, (B) May 7th, (C) July 11th, and (D) September 18th. The control site shows undisturbed homogenous vegetation cover over the study period.

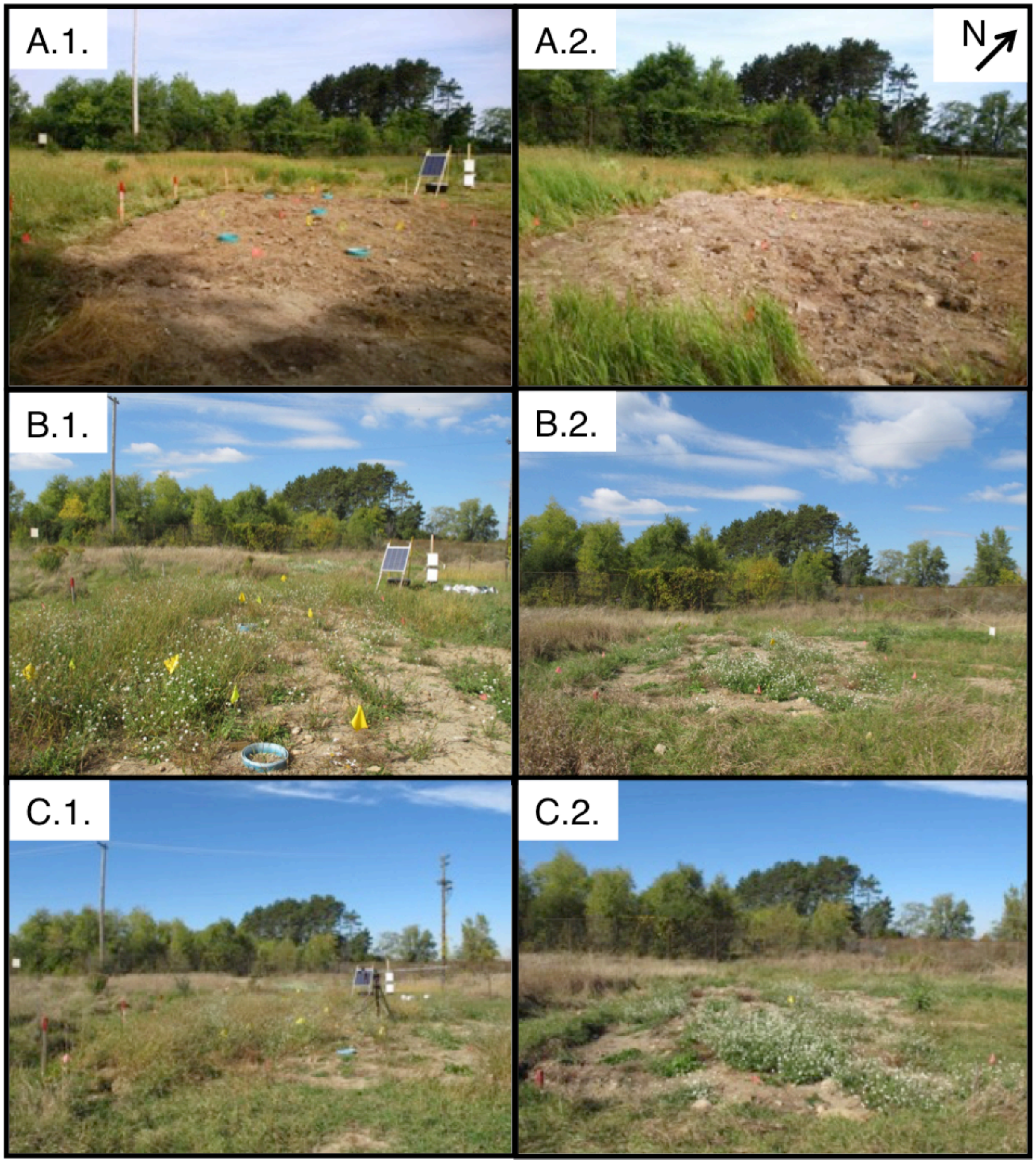

Figure 4.15. Vegetation cover on top of the (1) grave and (2) reference during the 2013-growing season on: (A) July 22[th], (B) September 27[th] and (C) October 11[th], 2013. The disturbed sites show a transition from soil cover to a mix of soil and vegetation in the first four months post-disturbance.

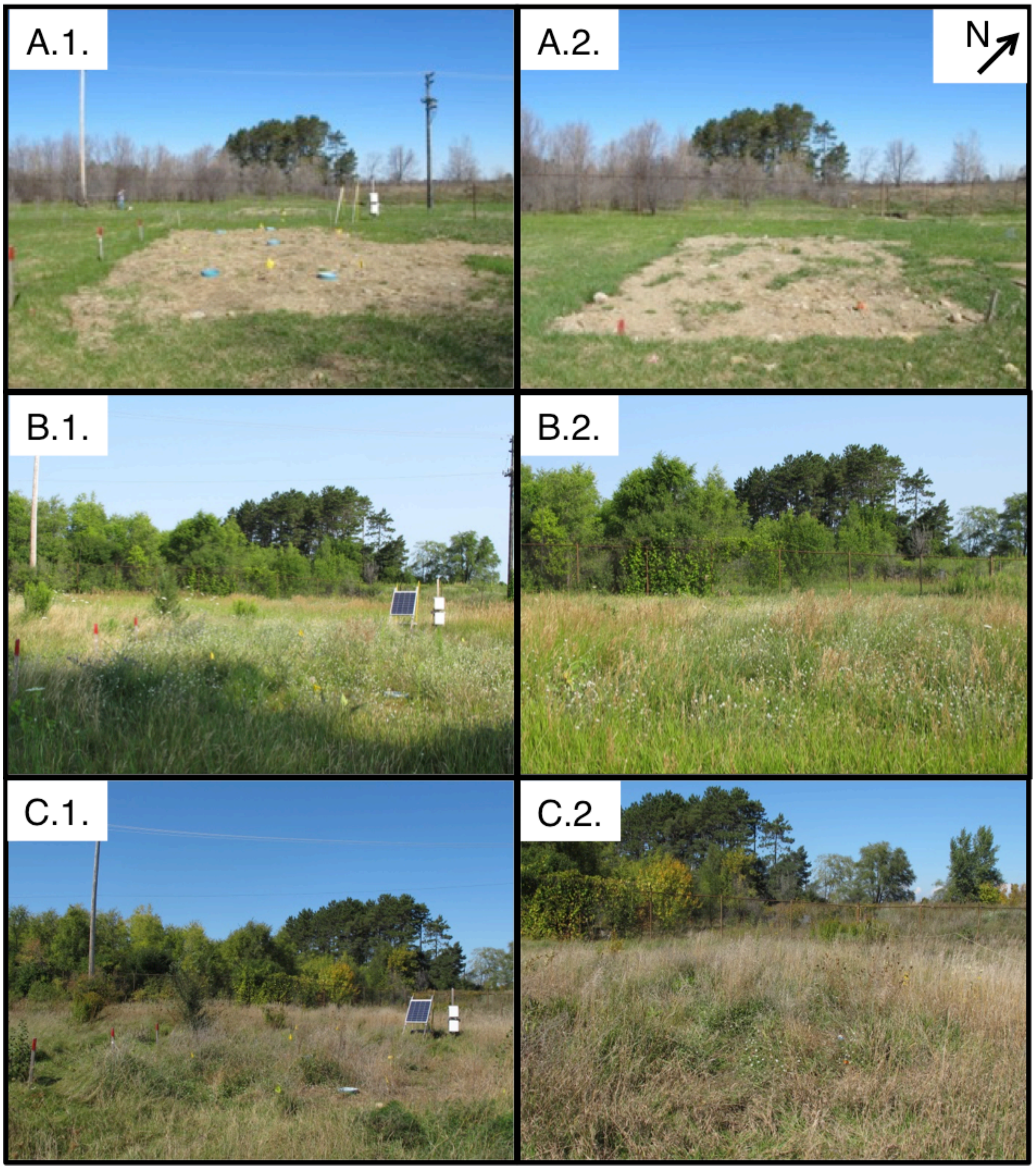

Figure 4.16. Vegetation cover on top of the (1) grave and (2) reference during the 2014-growing season on: (A) May 7th, (B) July 11th and (C) September 18th. The disturbed sites show a transition from predominant soil cover to more predominant vegetation cover by the 15th month since disturbance.

4.4.1. *In-situ* Spectral Reflectance

A difference in average spectral reflectance is observed between the control and disturbed sites over the 2013-growing season (Figure 4.17). In July 2013, the disturbed sites display a spectral signature characteristic of soil. The greatest differences between the disturbed sites are revealed along the 900 – 1300 nm and 1500 – 1800 nm ranges at this time (Figure 4.17.A). The average spectral signature of the reference has the highest reflectance at a magnitude of 0.05 (i.e. 5%) among the disturbed sites two weeks post-disturbance. By August 2013, the average spectra of the disturbed sites are changing to that characteristic of mix of soil and vegetation (Figure 4.17.B). Differences are observed between all sites across the 400 – 2400 nm range at this stage in the disturbance. The control has the lowest *in-situ* average reflectance, at 0.30, while the highest reflectance is seen for the gap, at 0.40 along the 800 - 1300 nm range, and the reference at 0.30 along the 1600 – 2400 nm range. In Figure 4.17.C, a difference in site average spectral reflectance, between 0.05 and 0.1, is seen along the 800 – 1300 nm range in September and October 2013. In September 2013, three months post-disturbance, the reference shows a difference in average spectral reflectance from the other sites in the 1500 – 1800 nm range. Small differences, at a magnitude of 0.05, are observed between the sites in the 450 – 680 nm range in October 2013 (Figure 4.17.D).

At the beginning of the 2014 – growing season, the disturbed sites average spectra follow those of a mix of vegetation and soil signatures (Figure 4.18). The gap shows a more reflective signature around 0.30 in comparison with the grave and reference at 0.20 in the 800 – 1100 nm range. The average *in-situ* spectral signature of the grave displays a higher reflectance, at approximately 0.35, than the reference in the 1100 – 1300 nm, 1500 – 1700 nm, and 2100 – 2400 nm ranges (Figure 4.18.A). Differences in average spectral reflectance are observed in June 2014 between the grave, at 0.05, and reference, at 0.10, in the 600 – 700 nm range (Figure 4.18.B). The grave also shows a higher reflectance, at 0.40, in the 750 – 1100 nm at this stage. By July 2014, small differences in average spectral signatures are displayed between the disturbed sites (Figure 4.18.C). The greatest differences between the grave and reference are found along the 750 – 1300 nm range where the grave shows an average reflectance of 0.40 in comparison with the reference at 0.30. A month later, August 2014, the average *in-situ* spectral reflectance shows similar differences between the sites (Figure 4.18.D). A small difference is shown between the grave and reference along the 1500 – 1800 nm, at 0.20 and 0.25, and 2100 – 2400 nm ranges, at

0.10 and 0.15 respectively. In September 2014, the greatest differences are observed between the control and disturbed sites where the control shows a higher reflectance, ranging between 0.40 and 0.50, in the 800 – 1300 nm range (Figure 4.18.E). Similarly to August 2014, a difference in average spectral signatures is shown between the reference and grave in the 1500 – 1800 nm and 2100 – 2400 nm ranges where the reference site shows a higher reflectance at 0.25 and 0.20 respectively. The average *in-situ* spectral signature of the grave also displays difference from the reference in the 1100 – 1300 nm range at approximately 0.30 (i.e. 30% reflectance).

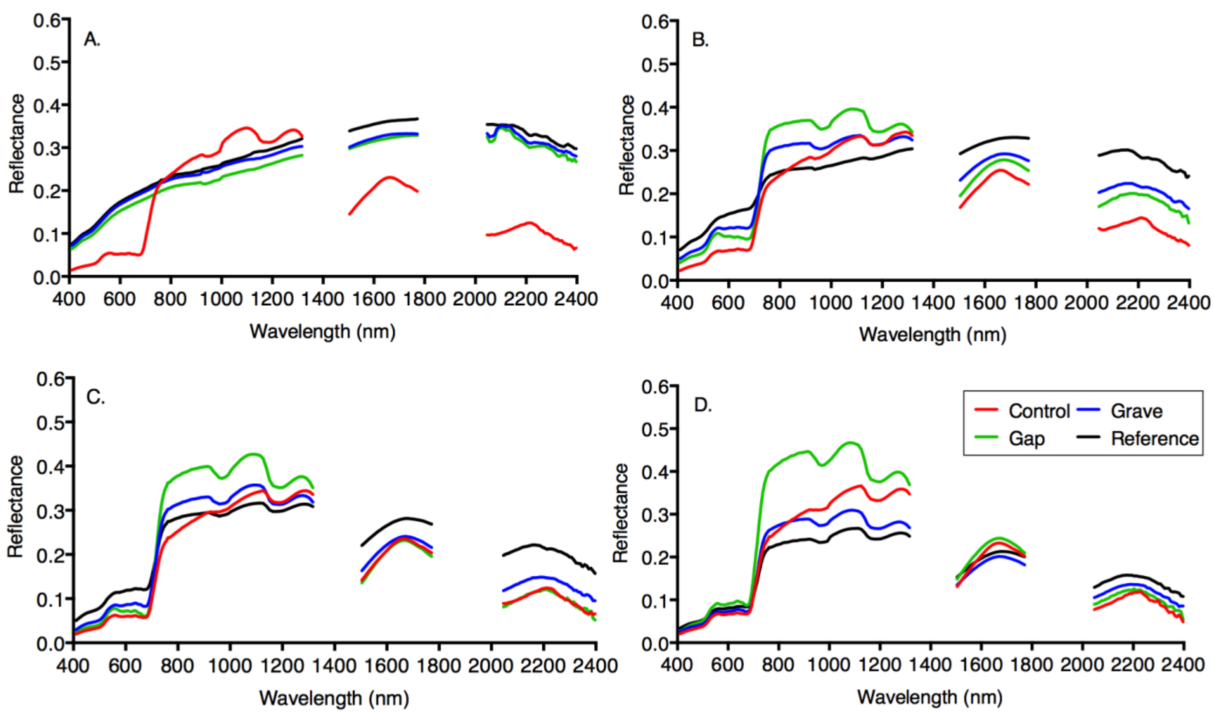

Figure 4.17. Average *in-situ* spectral reflectance of (red) control, (blue) grave, (green) gap, and (black) reference collected on (A) July 12th, 2013 and (B) August 19th, 2013, (C) September 27th, 2013 and (D) October 11th, 2013 (control: n=28; grave: n=22; gap: n=6; reference: n=28). The gaps in spectral reflectance represent the removed water absorption wavelengths. Due to the high standard deviation (not shown) there are no differences between the sites.

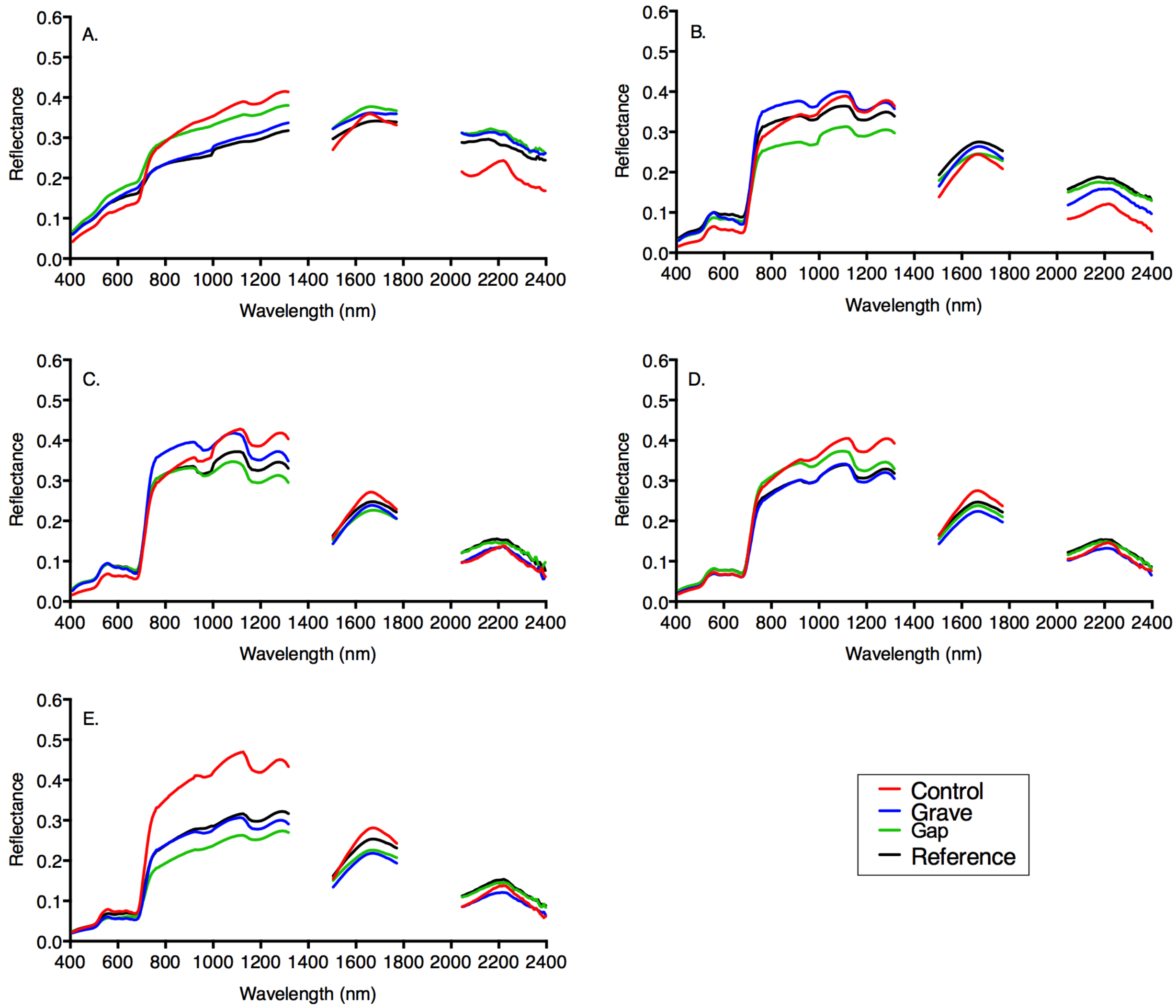

Figure 4.18. Average *in-situ* spectral reflectance of (red) control, (blue) grave, (green) gap, and (black) reference collected on (A) May 7th, 2014 and (B) June 20th, 2014, (C) July 11th, 2014, (D) August 6th, 2014, and (E) September 18th, 2014 (control: n=28; grave: n=22; gap: n=6; reference: n=28). The gaps in spectral reflectance represent the removed water absorption wavelengths. Due to the high standard deviation (not shown) are no differences between the sites.

To investigate the differences in spectral signatures between the grave and reference, the amplitude (D, Equation 2) and shape (θ, Equation 3) metrics were computed on the collected *in-situ* spectra - as was done for the leaf spectra in section 4.4.2. Based on the Kolmogorov – Smirnov test of normality, the D and θ *in-situ* spectral differences are not normally distributed ($p>0.05$). The non-parametric Wilcoxon rank sum ($\alpha=0.05$) was applied to test the significant differences between within-site and between-sites (i.e. each spectrum of the reference site was compared to each spectrum of the grave). Differences were computed on the *in-situ* spectral reflectance resampled to the CASI and SASI spectral bands.

Table 4.8 displays the differences in amplitude between the grave and reference of the *in-situ* spectral reflectance collected over the 2013 and 2014 growing seasons. In 2013, the only significant difference along the 410 – 917 nm range between-sites, at 0.049, is observed in August from the grave at 0.040 ($p=0.03$) and reference at 0.027 ($p<0.001$). In the first three months post-disturbance, significant differences are seen between-sites and within grave over the 925 – 2404 nm range in July and September 2013 ($p<0.02$). The within grave amplitude differences show values between 0.019 and 0.025, while between-sites amplitude differences are ranging between 0.021 and 0.032. At the end of the 2013-growing season, significant differences are observed against the grave over the 1500 – 1771 nm and 2047 – 2404 nm ranges ($p<0.001$). Significant differences between-sites and within reference are revealed in July 2013 along the 925 – 1317 nm range ($p=0.0254$), 410 – 2404 nm range ($p<0.001$) in August 2013, 1500 – 1771 nm ($p=0.005$) and 2047 – 2404 nm ranges ($p=0.004$) in September 2013, and along the 1500 – 1771 nm range in October 2013 ($p=0.028$). The within reference differences in amplitude range between 0.015 and 0.029, while the between-sites ones range between 0.021 and0.049 over the 2013-growing season.

At the beginning of the growing season, in May 2014, significant differences in amplitude are seen against within reference over the 925 – 1317 nm range ($p=0.0105$) and against both within reference and grave over the 2047 – 2404 nm range ($p<0.001$ for within grave and $p=0.028$ for within reference). Significant differences against the within grave are observed over the 410 – 925 nm range in June 2014 ($p<0.001$) and against within reference in August ($p=0.003$). Both the within grave and reference show significant difference along the 925 – 2404 nm range in June 2014 ($p<0.02$), while only the within reference shows significant differences in August 2014 ($p<0.01$) from the between-sites amplitudes. In July 2014, the between-sites amplitude displays a significant difference against the reference along the 925 – 1317 nm range ($p<0.001$) and against the grave along 2047 – 2404 nm ($p=0.001$). At the end of the 2014-growing season, significant differences in amplitude are seen against the reference over the 410 – 917 nm ($p=0.002$) and 925 – 1317 nm ranges ($p<0.001$), and against the grave along 1500 – 1771 nm ($p=0.001$) and 2047 – 2404 nm ($p<0.001$).

Table 4.9. Average (μ) and standard deviation (σ) of differences in spectral amplitude (D) of within grave (G) and reference (R) and between-sites (i.e. each of the reference spectra compared against each spectrum of the grave) of the *in-situ* spectra resampled to CASI range (410 – 912 nm) and SASI range (925 – 1317 nm, 1500 – 1771 nm, and 2047 – 2400 nm ranges) collected over the 2013 and 2014 growing seasons.

Site		2013 Jul	2013 Aug	2013 Sept	2013 Oct	2014 May	2014 Jun	2014 Jul	2014 Aug	2014 Sept
410 to 917 nm range										
G	**μ**	0.016	0.040*	0.037	0.037	0.016	0.034*	0.043	0.037	0.047
	σ	0.011	0.023	0.023	0.025	0.010	0.023	0.027	0.025	0.033
R	**μ**	0.017	0.027*	0.035	0.038	0.020	0.047	0.033	0.027*	0.030*
	σ	0.011	0.025	0.021	0.021	0.015	0.026	0.018	0.019	0.018
G vs. R	**μ**	0.017	0.049	0.039	0.040	0.017	0.050	0.037	0.033	0.041
	σ	0.012	0.027	0.021	0.019	0.009	0.024	0.024	0.016	0.024
925 to 1317 nm range										
G	**μ**	0.011*	0.023*	0.025*	0.025	0.011	0.021*	0.027	0.029	0.037
	σ	0.009	0.018	0.018	0.019	0.008	0.014	0.020	0.021	0.028
R	**μ**	0.012*	0.015*	0.023*	0.024	0.010*	0.031*	0.020*	0.021*	0.026*
	σ	0.008	0.014	0.015	0.016	0.007	0.022	0.013	0.017	0.018
G vs. R	**μ**	0.012	0.024	0.026	0.026	0.011	0.028	0.027	0.026	0.033
	σ	0.009	0.015	0.017	0.018	0.007	0.019	0.018	0.018	0.022
1500 to 1771 nm range										
G	**μ**	0.012*	0.031	0.019*	0.016*	0.016	0.014*	0.019	0.014*	0.018*
	σ	0.009	0.023	0.014	0.011	0.011	0.010	0.015	0.011	0.013
R	**μ**	0.018	0.020*	0.020*	0.025*	0.017	0.026*	0.019	0.013*	0.026
	σ	0.013	0.016	0.015	0.018	0.014	0.018	0.015	0.012	0.020
G vs. R	**μ**	0.018	0.029	0.021	0.022	0.018	0.022	0.020	0.016	0.023
	σ	0.013	0.021	0.014	0.015	0.013	0.015	0.015	0.011	0.018
2047 to 2404 nm range										
G	**μ**	0.017*	0.039	0.024*	0.023*	0.016*	0.018*	0.021*	0.013*	0.016*
	σ	0.015	0.028	0.018	0.017	0.012	0.014	0.016	0.008	0.014
R	**μ**	0.021	0.028*	0.029*	0.033	0.027*	0.033*	0.026	0.016	0.024
	σ	0.015	0.021	0.021	0.024	0.022	0.025	0.018	0.012	0.022
G vs. R	**μ**	0.021	0.041	0.032	0.030	0.023	0.029	0.025	0.017	0.021
	σ	0.014	0.028	0.020	0.022	0.019	0.022	0.017	0.011	0.020

* Significant differences from the between sites (G vs. R) (Wilcoxon rank sum, α=0.05).

In terms of spectral shape (θ), the results show overall significant difference between sites over the study period (Table 4.9). The between-sites shape differences are significantly different from both within grave ($p=0.02$) and reference ($p<0.001$) in July 2013 and from the reference in August 2013 ($p<0.001$). The shape metric also shows an increase in differences between the months of July and August 2013 from 0.031 to 0.216 for the within grave. The within reference and between-sites spectral shape also show increasing differences at this time from 0.047 to 0.142 and from 0.026 to 0.239 respectively. Over the SASI ranges, the within reference is significantly different along 925 – 1317 nm and 2047 – 2404 nm in July 2013 and along 925 – 2404 nm in August 2013 ($p<0.001$). In comparison, the within grave shape differences are significant along 1500 – 1771 nm ($p<0.001$) in July 2013 and over 2047 – 2404 nm in August 2013 ($p=0.002$). Three months post-burial, September 2013, significant differences are seen between-sites and within site over the 925 – 1771 nm range ($p<0.01$) and only against the within reference over the 2047 – 2404 nm range ($p<0.001$). At the end of the 2013-growing season, significant difference are revealed against the within grave over the 925 – 2404 nm range ($p<0.01$), while no significant differences are found against the reference ($p>0.05$). The within grave shape difference shows a value of 0.158 while the between sites is at a value of 0.174.

Over the 2014-growing season, the within grave is found to be significantly different in spectral shape during the months of May and July, while the within reference during the months of August and September ($p<0.05$). The within grave is significantly different over all investigated ranges (i.e. 410 – 2404 nm) between May and July 2014 ($p<0.03$). Similar to 2013, between May and June 2014 the differences in shape increase from 0.069 to 0.123 for the within grave and from 0.090 to 0.273 for between-sites along the 410 – 917 nm range. In August 2014, the within reference is found to be significant different in spectral shape along all ranges ($p<0.03$), while the within grave along 410 – 917 nm ($p=0.029$) and 2047 – 2404 nm ($p=0.027$). At the end of the collection date, in September 2014, the only differences are observed between-sites and reference over the 410 – 1771 nm range ($p<0.001$).

Table 4.10. Average (μ) and standard deviation (σ) of differences in spectral shape (θ) of within grave (G) and reference (R) and between sites (i.e. each of the reference spectra compared against each spectrum of the graves) of the field spectral reflectance resampled to CASI range (410 – 912 nm) and SASI range (925 – 1317 nm, 1500 – 1771 nm, and 2047 – 2400 nm ranges) collected over the 2013 and 2014 growing seasons.

Site		2013 Jul	2013 Aug	2013 Sept	2013 Oct	2014 May	2014 Jun	2014 Jul	2014 Aug	2014 Sept
410 to 917 nm										
G	**μ**	0.031*	0.216	0.160	0.198	0.069*	0.123*	0.134*	0.123*	0.174
	σ	0.022	0.151	0.116	0.148	0.071	0.091	0.094	0.090	0.126
R	**μ**	0.047*	0.142*	0.206	0.238	0.149*	0.225*	0.160*	0.130*	0.128*
	σ	0.035	0.133	0.146	0.169	0.139	0.168	0.112	0.090	0.089
G vs. R	**μ**	0.026	0.239	0.183	0.237	0.090	0.273	0.104	0.157	0.184
	σ	0.017	0.162	0.101	0.160	0.068	0.112	0.072	0.089	0.123
925 to 1317 nm range										
G	**μ**	0.035	0.069	0.052*	0.080*	0.029*	0.055	0.046*	0.041	0.070
	σ	0.024	0.043	0.033	0.044	0.018	0.033	0.028	0.024	0.049
R	**μ**	0.026*	0.048*	0.057*	0.095	0.040	0.057	0.053*	0.041*	0.047*
	σ	0.016	0.039	0.043	0.061	0.026	0.036	0.033	0.027	0.029
G vs. R	**μ**	0.032	0.072	0.060	0.097	0.036	0.060	0.062	0.044	0.063
	σ	0.019	0.042	0.037	0.049	0.022	0.033	0.037	0.024	0.039
1500 to 1771 nm range										
G	**μ**	0.013*	0.050	0.049*	0.051*	0.013*	0.042*	0.041*	0.043	0.046
	σ	0.020	0.035	0.035	0.035	0.008	0.031	0.029	0.035	0.032
R	**μ**	0.011	0.021*	0.051*	0.060	0.031*	0.056	0.042	0.035*	0.034*
	σ	0.006	0.023	0.040	0.043	0.030	0.041	0.029	0.028	0.023
G vs. R	**μ**	0.013	0.051	0.058	0.059	0.024	0.055	0.046	0.044	0.043
	σ	0.016	0.038	0.037	0.038	0.023	0.038	0.031	0.029	0.025
2047 to 2404 nm range										
G	**μ**	0.047	0.100*	0.119	0.158*	0.035*	0.099*	0.261*	0.135*	0.116
	σ	0.023	0.064	0.047	0.084	0.014	0.041	0.262	0.066	0.045
R	**μ**	0.038*	0.061*	0.123*	0.172	0.049*	0.106	0.219	0.141*	0.114
	σ	0.013	0.048	0.098	0.109	0.039	0.050	0.108	0.148	0.044
G vs. R	**μ**	0.047	0.090	0.130	0.174	0.046	0.113	0.250	0.145	0.119
	σ	0.018	0.061	0.069	0.088	0.027	0.044	0.198	0.110	0.038

* Significant differences from the between sites (G vs. R) (Wilcoxon rank sum, α=0.05)

4.4.2. Spectral Separability

Similarly to the leaf spectra, the forward feature selection (featself) algorithm, using the nearest neighbour criterion, was applied to select the minimum number of bands and the specific wavelength required to separate between the grave and reference based on their *in-situ* spectral reflectance. The optimal number of best bands was selected based on the criteria of separation for the 2013 and 2014 *in-situ* spectra (Figure 4.19). The number of optimal wavelengths depends on the date of collection. The criterion of separability between sites increases over time from 0.71, in the first month post-disturbance, to 81 percent, the 15th month since disturbance. The separability between grave and reference spectra peaks at 0.91 in August 2013 with a minimum of 17 bands and in May 2014 with a minimum of seven bands.

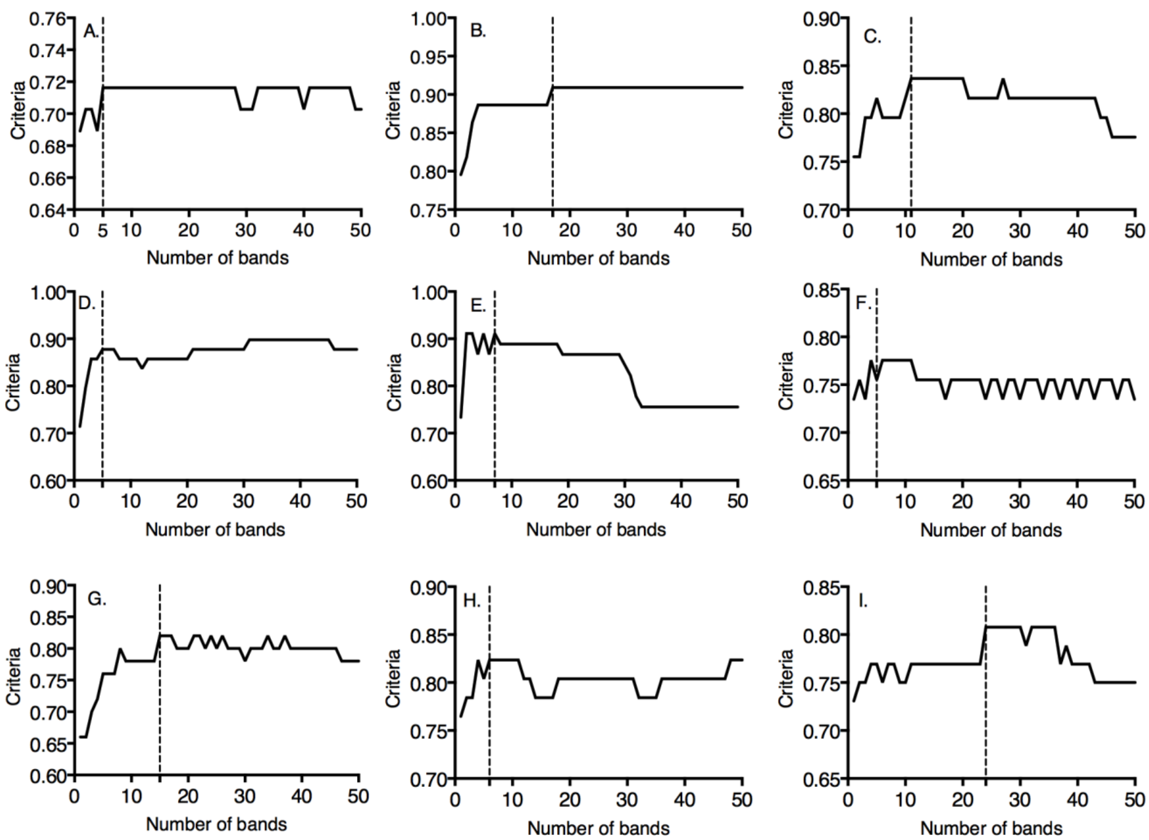

Figure 4.19. Criteria of separation of *in-situ* spectral separability between grave and reference following the forward featured selection algorithm using 50 bands for (A) July 2013, (B) August 2013, (C) September 2013, (D) October 2013, (E) May 2014, (F) June 2014, (G) July 2014, (H) August 2014, and (I) September 2014. The dashed vertical line represents the number of bands showing the highest separability between grave and reference. Theoretically values range between 0 and 1, where 1 represents 100 percent separation between sites.

Figure 4.20 illustrates the distribution of separable wavelengths between the grave and reference over the study period. The range of wavelengths, where there is separation between the grave and reference, depends on the stage of disturbance and time in the growing season. Overall, a differentiation between the two sites can be made along the 400 – 1000 nm range. Over the 2013-growing season, the grave is separable from the reference in the 400 – 700 nm range. A cluster is also observed in the 1300s nm range in August 2013, in the 1500s nm and the 2100 – 2400 nm ranges in September 2013. Over the 2014-growing season, the grave can be separated from the reference in the 400 – 500 nm and 700 – 1000 nm wavelength ranges. In July 2014, best separable bands are clustering along the 700 – 1000 nm range.

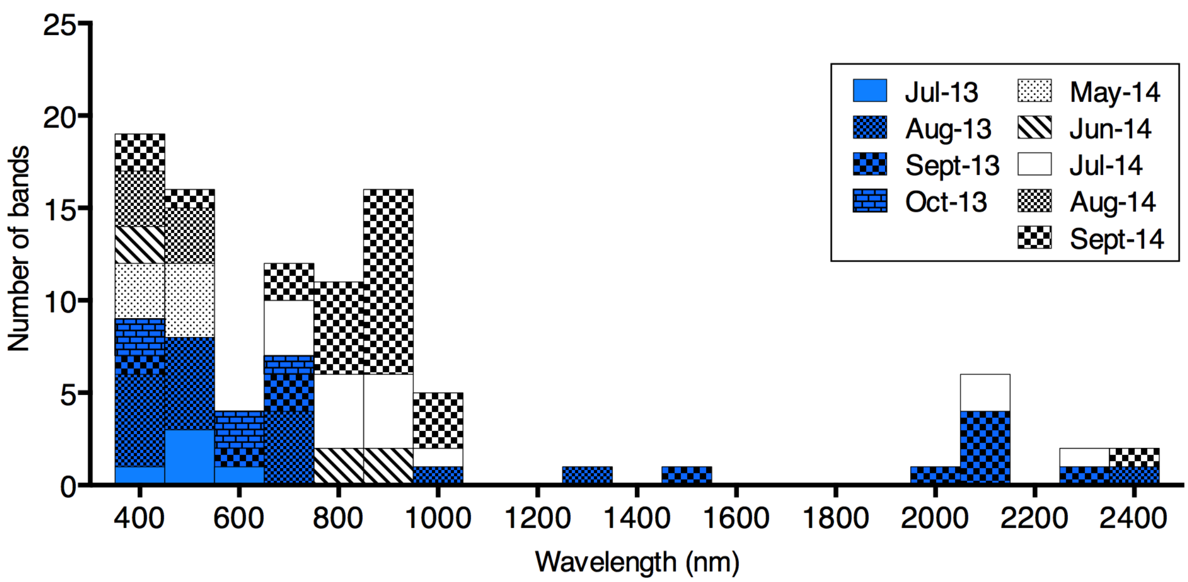

Figure 4.20. Distribution of separable wavelengths between grave and reference following the forward feature selection algorithm for the *in-situ* spectral reflectance collected over the (blue) 2013 and 2014 growing seasons. The patterns represent different data collections. The results reveal a clustering in the 400 – 1000 nm range.

4.4.3. Vegetation Indices

Various vegetation indices were computed to investigate spectral differences at the *in-situ* spatial scale between sites over the 2013 and 2014 growing seasons. The Kolmogorov – Smirnov test of normality shows that the computed vegetation indices are not normally distributed ($p>0.05$). The non-parametric Wilcoxon rank sum test ($\alpha=0.05$) was applied to investigate significant differences in vegetation indices between sites. Appendix D contains the mean vegetation indices computed for the *in-situ* data collected between July 2013 and September

2014. Overall, significant differences are found between the control and disturbed sites (i.e. grave, gap, and reference) over the study period ($p>0.05$). For instance, the greatest differences between the control and disturbed sites are seen early in the disturbance, July 2013, and in the growing season, May 2014. The control site shows a NDVI1 value of 0.60 in July 2013 and 0.31 in May 2014, while the grave is at 0.05 and at 0.12 respectively. Similar to the leaf vegetation indices, the results show a high variability between data points. Therefore, any significant differences found between the grave and reference show a low confidence due to their high standard deviation.

No significant differences were found between the grave and reference early in the disturbance stage in July 2013, towards the end of the growing season in October 2013, and after 12 months post-disturbance in June 2014 ($p>0.05$). Vegetation indices showing a significant difference between grave and reference in the early stages of disturbance, August and September 2013, are NDVI ($p<0.01$), RENDVI ($p\leq0.01$), SGI ($p<0.01$), SIPI ($p=0.03$), and VOG ($p<0.02$). Another vegetation index show significant differences at certain times in the disturbance is PSRI in August 2013 ($p=0.015$), at 0.16 for the grave and 0.26 for the reference, and in May 2014 at 0.33 and 0.28 respectively ($p<0.01$). The NDPI also indicates a significant difference between the grave, at 0.36, and reference, at 0.31, in May 2014 ($p<0.01$). In the later stages of the disturbance, a significant difference between the grave and reference is shown by SGI in August 2014 ($p=0.003$). The grave has an SGI of 0.06, while the reference has a value of 0.07. Overall, no significant differences are revealed between the grave and gap over the study period ($p>0.05$).

4.5. Airborne Hyperspectral Imagery

4.5.1. Airborne Spectral Reflectance

The spectral signatures of the SASI airborne imagery collected pre-disturbance, June 2013, show small differences of less than 0.05 (i.e. 5% reflectance) between sites across the 870 – 2400 nm range (Figure 4.21.A). In comparison, two weeks post-disturbance, July 2013, differences in spectra are seen between the control and disturbed sites (Figure 4.21.B). For instance, the control has a reflectance above 0.30 along the 870 – 1300 nm range, while the disturbed sites show a reflectance below 0.30 over the same wavelength range. In September 2013, there are visible differences between all sites, of approximately 0.05, with the exception between grave and gap along the 1500 – 1800 nm range (Figure 4.21.C). The reference also shows a higher reflectance, at approximately 0.25, from the other sites along the 2100 – 2400 nm range. At the beginning of the 2014-growing season, the main differences in average spectral signatures are observed between the control and disturbed sites across both the CASI and SASI ranges (Figure 4.22). The control is more characteristic of a vegetation spectrum, while the grave and reference that of a mix of soil and vegetation spectral signatures. Most revealing differences in spectra between sites are seen in June (Figure 4.22.B) and July 2014 (Figure 4.22.C) along the 750 to 1800 nm range. Smaller differences are observed between the grave and reference in August 2014 over the 600 – 700 nm range where the grave shows a higher reflectance at 0.30 (Figure 4.22.D).

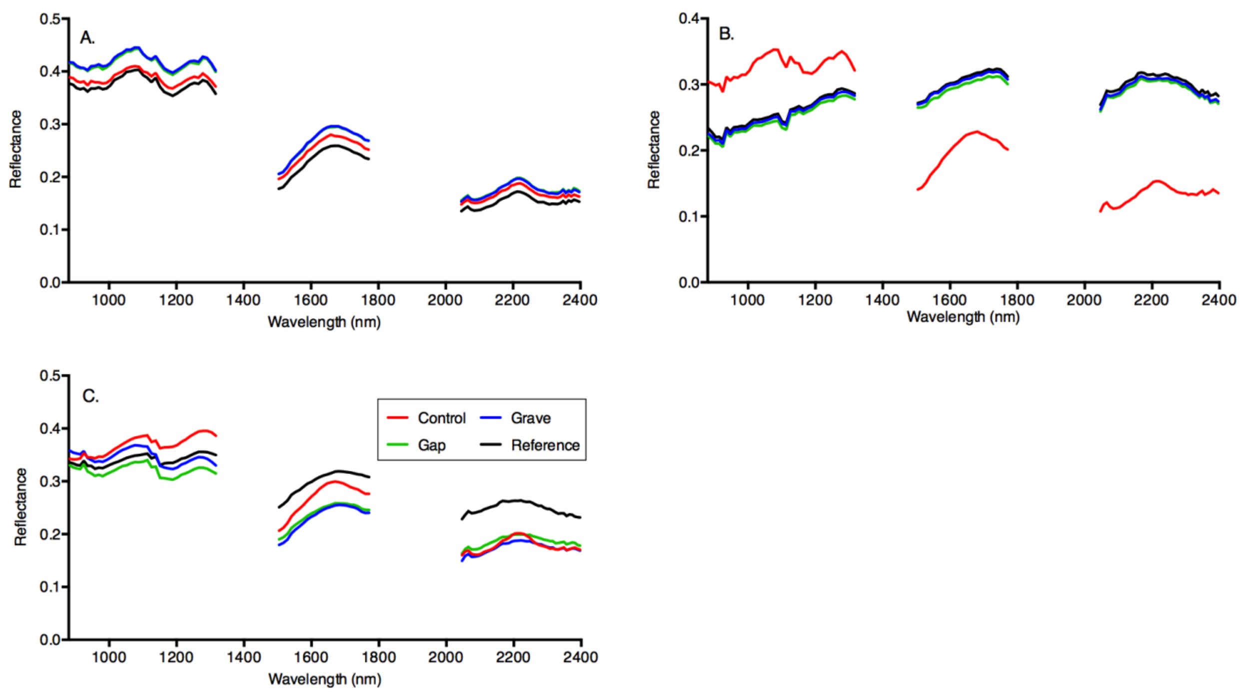

Figure 4.21. Site average spectral reflectance of (red) control, (blue) grave, (green) gap, and (black) reference collected on (A) June 20th, 2013, (B) July 12th, 2013, and (C) September 18th, 2013 using the SASI sensor. The gap in the spectral signatures represents removed noise from data collections. Due to the high standard deviation (not shown) there are no differences between the sites.

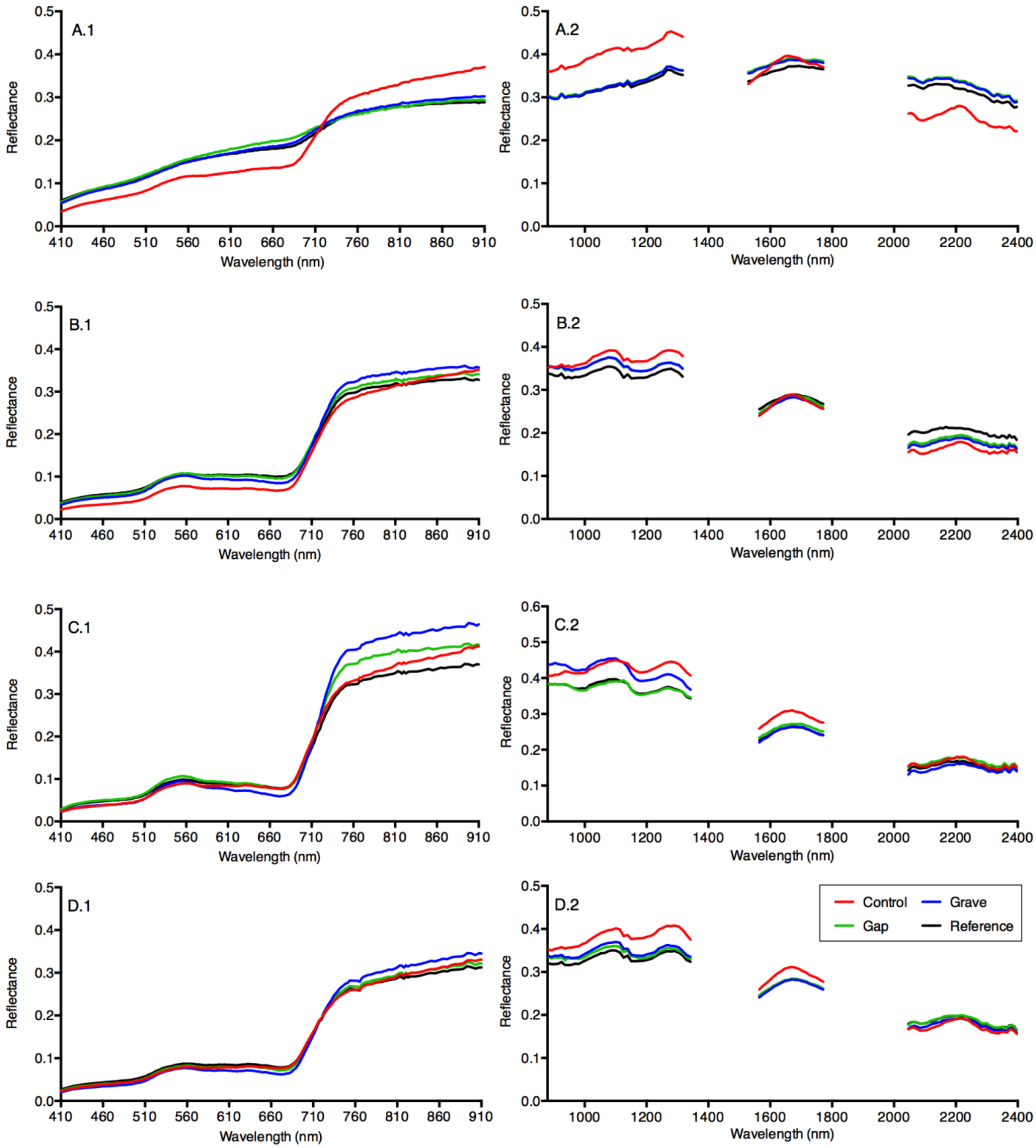

Figure 4.22. Site average spectral reflectance of (red) control, (blue) grave, (green) gap, and (black) reference collected using the (1) CASI and (2) SASI sensors on (A) May 8th 2014, (B) June 17th, 2014, (C) July 10th, 2014, and (D) August 8th, 2014. The gap in the spectral signatures represents removed noise from data collections. Due to the high standard deviation (not shown) there are no differences between the sites.

4.5.2. Spectral Separability

Similarly to the leaf and *in-situ* spectra, the forward feature selection was applied to retrieve best airborne bands that show the highest separation between grave and reference. The optimal number of separable bands depends on the disturbance stage and time of collection in the growing season (Figure 4.23). Over the 2013-growing season the separation between grave and reference is between 0.95 and 9.98 with number of 15 to 23 bands. In 2014, the highest criterion of separation is shown in May for both CASI and SASI at 0.97 and 0.93 respectively. Figure 4.24 shows the distribution of separable wavelengths across the 400 – 2400 nm range. Prior to site setup, the best separable wavelengths are distributed across the 900 to 2300 nm range. Two weeks post-disturbance, July 2013, the wavelengths showing the greatest separation between the grave and reference are concentrated in the 900 – 1100 nm and 2000 – 2400 nm ranges. Three months post-disturbance, September 2013, the grave can be spectrally separated from the reference in the 900 – 1200 nm range. Early in the 2014-growing season (i.e. May 2014, 11 months post-disturbance) a separation between the grave and reference is revealed in the 400 – 700 nm and 2100 – 2400 nm ranges. The wavelengths at which the grave can be differentiated from the reference are clustering in the 400 - 800 nm range by August 2014. The greatest separation between sites is seen in the 400s nm and 900s nm ranges in the first 14 months post-disturbance.

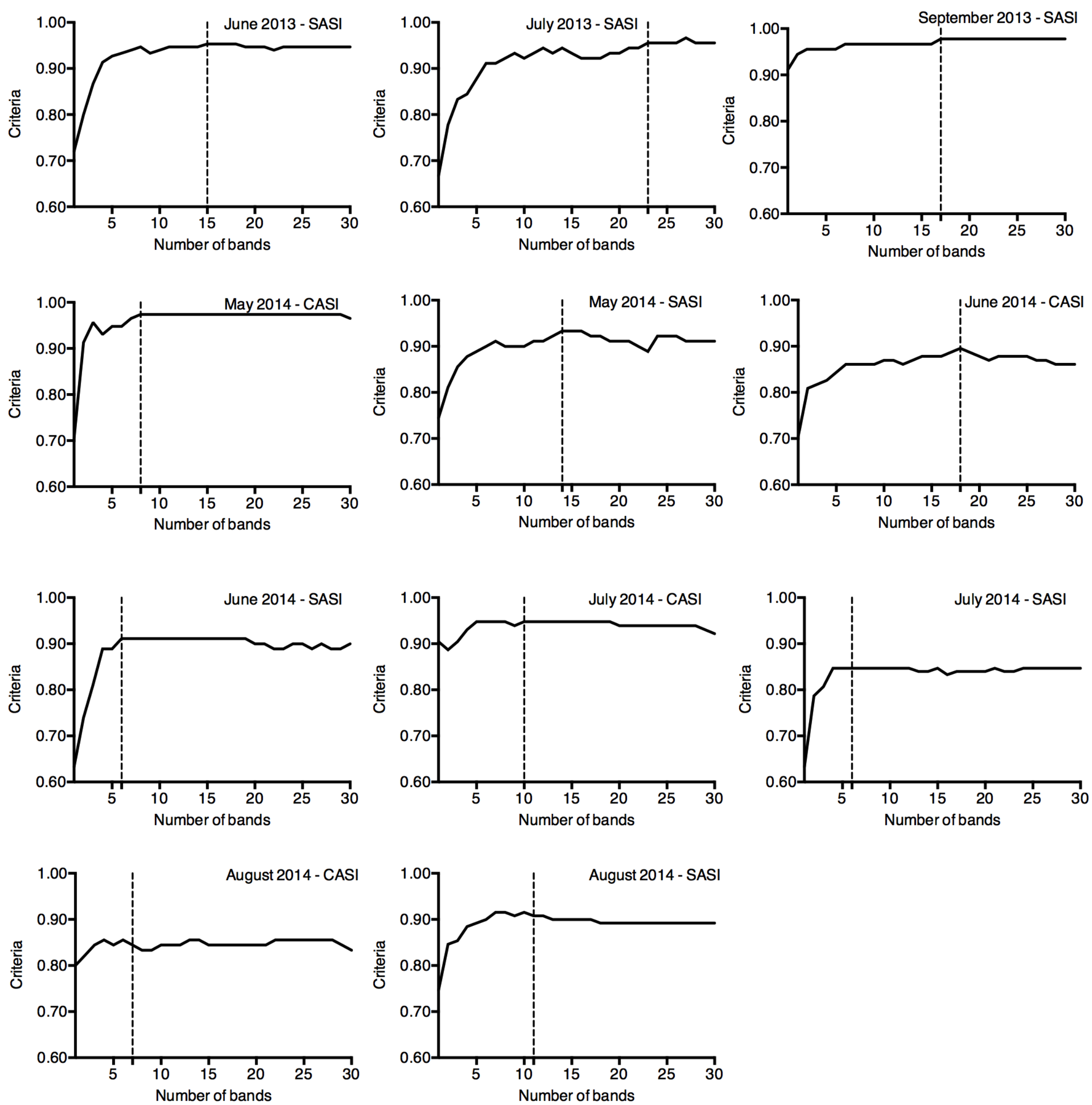

Figure 4.23. Criteria of airborne spectral reflectance separability between sites (i.e. graves vs. reference) collected following the forward featured selection over a minimum of 30 bands for data collected with the SASI and CASI sensors. The dashed vertical line represents the number of bands showing the highest separability between grave and reference. Theoretically values range between 0 and 1, where 1 represents 100 percent separation between sites.

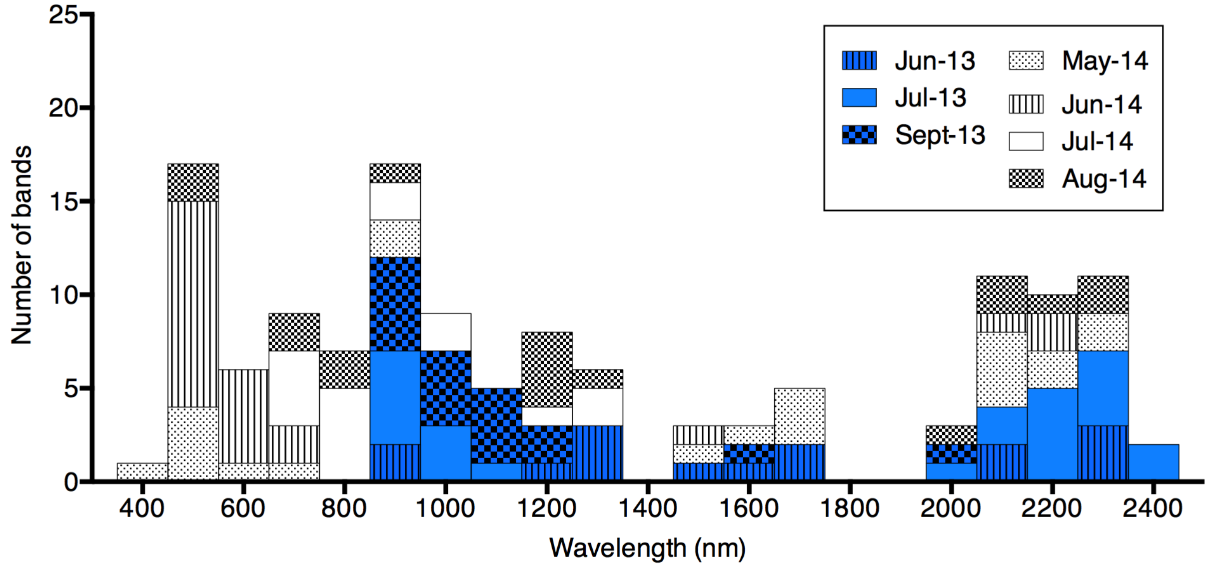

Figure 4.24. Distribution of separable wavelengths between grave and reference following the forward feature selection algorithm collected on the airborne imagery collected using the CASI and SASI sensors over the (blue) 2013 and (clear) 2014 growing seasons. The patterns represent different data collections.

4.5.3. Hydroxyl Distribution

An indicator in the detection of potential grave locations in a temperate climate is to compute the relative distribution of hydroxyl (OH^-) that has been found to have an absorption feature at 2200 nm (Ben-Dor 2002). Hydroxyl is often an indicator of clay presence, which is important because the activity of grave excavation is expected to leave traces of clay on the surface (Leblanc et al. 2014). Between July 2013 and May 2014, there are significant differences between the sites in OH^- ($p<0.01$), except between the grave and gap ($p>0.05$). The highest reflectance of the 2200 nm band is recorded early in the growing season, May 2014, at a value of 28% for the control, and between 32 – 34% for the disturbed sites (Table 4.10). In June 2014, the reference is significantly difference from the other sites and shows the highest reflectance at 26% ($p<0.01$). In July 2014, significant differences are seen between all sites ($p<0.05$), with the exception of between the gap and control. A change occurs in August 2014 where only the reference, at 19.80%, is significantly different from the grave at 19.72% ($p=0.034$) and control at 19.09% ($p<0.0001$).

Table 4.11. Mean (μ) and standard deviation (σ) in percentage of reflectance of the hydroxyl (OH^-) distribution band at the 2203.5 nm wavelength of the study sites over the 2013 and 2014 growing seasons. The reflectance was scaled to percentage.

Date		Control		Grave		Gap		Reference	
		μ	**σ**	**μ**	**σ**	**μ**	**σ**	**μ**	**σ**
2013	**Jun**	18.50	0.83	19.47	0.55	19.51	0.14	17.03	0.72
	Jul	15.22*	0.52	30.83	0.93	30.48	0.89	31.56*	0.89
	Sept	20.10*	0.66	18.73	2.81	19.94	2.86	26.33*	3.04
2014	**May**	27.89*	0.71	33.65	1.15	33.91	0.75	32.08*	1.61
	Jun	19.80*	0.59	18.62	2.85	19.88	2.85	26.27*	3.13
	Jul	18.01	0.93	16.18	1.38	17.97	0.96	16.91	1.26
	Aug	19.09	0.52	19.06	2.00	19.72	2.00	19.80	1.23

*Significant differences from the grave (One Way ANOVA, α=0.05).

Figure 4.25 illustrates the 2203.5 nm band of the SASI images (the closest to the OH^- absorption) collected over the 2013 and 2014 growing seasons. A change in OH^- indicators is observed between the data collections. Prior to site setup, June 2013, there is no clay present over the sites in comparison with the imagery taken two weeks post-disturbance, in July 2013. Furthermore, a decrease in exposed clay is seen three months post-disturbance, in September 2013 (Figure 4.34.D). The most exposed soil is denoted early in both the disturbance stage, July 2013(Figure 4.34.B), and in the growing season, May 2014 (Figure 4.34.E). By July 2014, the 2203.5 nm band shows little to no exposed soil on top of the disturbed sites (Figure 4.34.G).

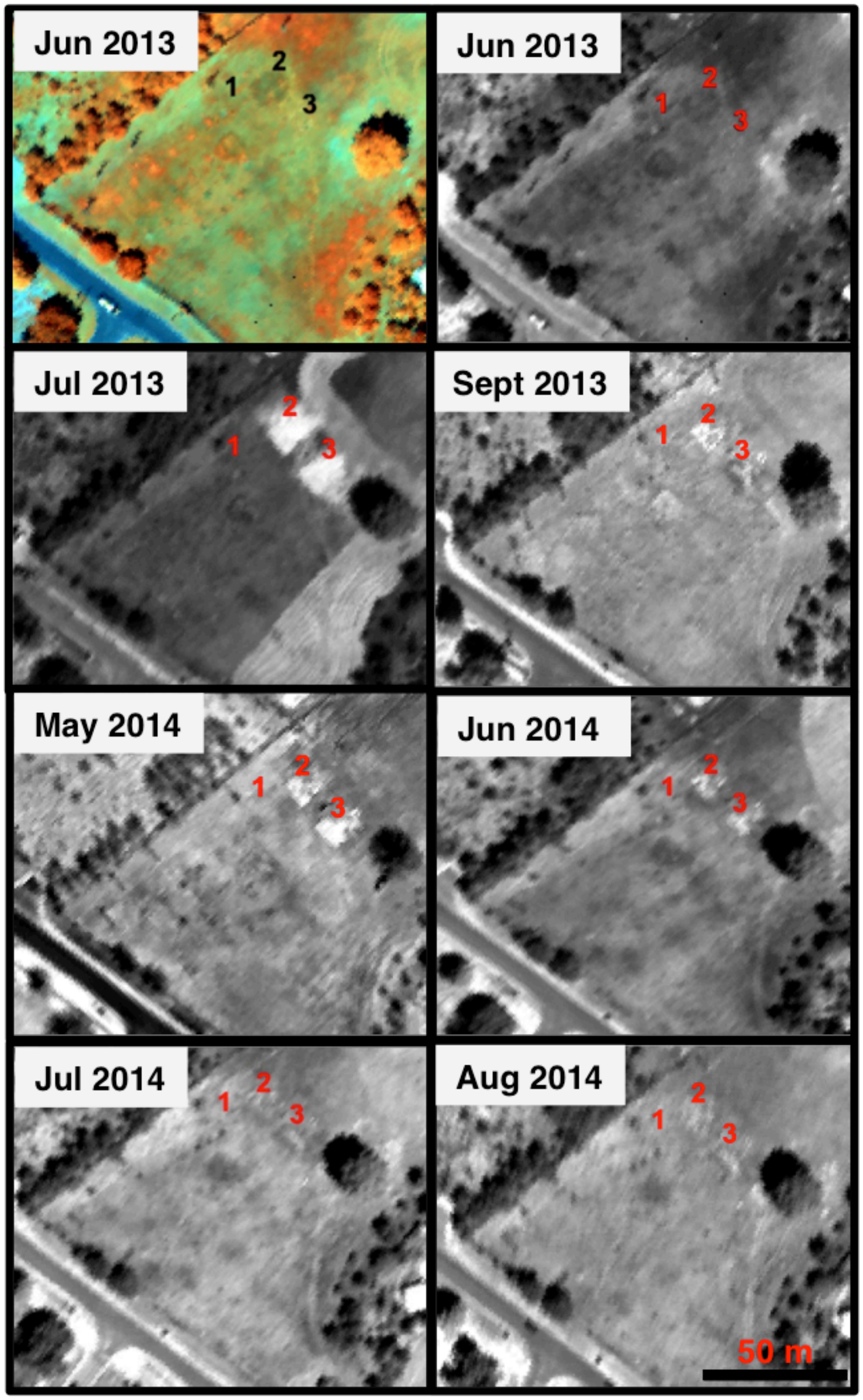

Figure 4.25. Georectified SASI imagery displaying the 2203.3 mn band against false colors. Legend: (1) control; (2) reference; (3) grave and gap. First figure shows the study sites in false color composite (R: 1052 nm G: 1624 nm B: 2122 nm) prior to experiment set-up on June 20th, 2013.

4.5.4. Vegetation Indices

To test the separability of the grave from the non-graves, a series of vegetation indices were computed on the acquired CASI imagery. Appendix E shows the average and standard deviation for the vegetation indices computed. Overall, the control is the most separable from the other sites over the study period. A significant difference between the control and disturbed sites for all computed vegetation indices was found for May 2014 ($p<0.01$). The vegetation indices showing a significant difference between the grave and reference are: NDPI ($p<0.01$), PSRI ($p<0.01$), REP ($p=0.001$), RVSI ($p=0.033$), VOG1 ($p=0.004$), and VOG2 ($p=0.009$). However, based on their high standard deviation, low confidence differences are observed between the two sites. Figure E.1, located in Appendix E, illustrates the computed vegetation indices of the May 2014 imagery. Overall, a separation is observed between the control and disturbed sites. Out of the computed indices, NDPI, REP, and RVSI show the lowest contrast between the control and disturbed sites. The only index showing a visual difference between the grave and reference is NDPI (Figure 4.49.B), where the reference has a lower value at 0.41 in comparison with the grave at 0.45.

Similar to May 2014, the control is significantly different from the disturbed sites ($p<0.05$) in June and July 2014 (Table E.2 and Table E.3). The gap is not significantly different from the grave and the reference in June 2014 ($p>0.05$). The grave is significantly different from the reference for 10 out of 11 vegetation indices in June 2014 ($p<0.05$). The only index not showing a difference between the two sites is VOG1 ($p>0.05$). For instance, the grave has a NDVI value of 0.61 and a SIPI value of 1.37, while the reference is at a value of 0.53 and 1.33 respectively. The high variability of within site shows low confidence differences between the grave and reference. Figure E.2 illustrates the vegetation indices computed for the imagery collected in June 2014. Overall, the location of the disturbed sites can be identified against the control. No distinction can be made between the grave, gap, and reference.

In July 2014, all computed indices show significant differences between the grave and reference ($p<0.05$). The grave shows a NDVI value of 0.75 and a SIPI value of 1.07, while the reference is at 0.63 and 1.14 respectively. Six out of 11 indices also show significant differences between the gap and grave ($p<0.05$). In comparison, significant differences are seen between the gap and reference for NDPI ($p=0.037$), REP ($p<0.001$), and SGI ($p=0.026$). Based on the recorded high standard deviation, small differences are assumed between the disturbed sites. By

July 2014, the grave's distinction from the reference and control is less visible (Figure E.3). For instance, the REP and RVSI indices show no indication of the grave location against the background at this point in the disturbance.

In August 2014, the separation between sites decreases (Table E.4). Even though the statistical test shows significant differences, their high standard deviation reveals a low separation between sites. It is observed that the grave is still significantly different from the reference ($p<0.05$), with the exception of NDPI, REP, and RVSI. At this stage the grave shows a NDVI value of 0.67, in composition with the reference at 0.58. Five out of 11 vegetation indices show significant differences between the grave and gap: NDVI1 ($p=0.011$), RENDVI ($p=0.005$), VOG1 ($p<0.001$), and VOG2 ($p=0.002$). A lower number of vegetation indices show significant differences between the gap and control, and reference, while overall there are significant differences between the control and grave. The vegetation indices computed for the imagery collected 14 months post-disturbance show less separability between the disturbed sites and the control (Figure E.4). None of the computed vegetation indices indicate the separation of the grave from the control and reference.

To further explore the separation of the grave from the non-graves based on their spectral reflectance, the forward features selection algorithm was applied to the vegetation indices computed on the 2014 imagery. Table 4.11 illustrates the indices showing the greatest separation between sites. The separability between sites is dependent on the stage in the disturbance and the time of acquisition. The highest separability between sites is seen using five vegetation indices peaking at 0.82 in July 2014 and dropping to 0.70 by August 2014.

Table 4.12. Vegetation indices computed of the 2014 airborne imagery and their respective separability (Crit.) following the forward feature selection algorithm. Highlighted values represent the indices at which there is the highest recorded separability.

May		June		July		August	
Index	**Crit.**	**Index**	**Crit.**	**Index**	**Crit.**	**Index**	**Crit.**
NDVI1	0.62	NDPI	0.51	NDVI1	0.55	NDVI1	0.53
PSRI	0.74	NDVI2	0.65	NDPI	0.78	NDVI2	0.66
RENDVI	0.76	VOG1	0.75	VOG2	0.78	RENDVI	0.67
NDPI	0.77	RENDVI	0.76	NDVI2	0.80	<u>PSRI</u>	<u>0.70</u>
VOG1	0.78	<u>PSRI</u>	<u>0.77</u>	<u>SIPI</u>	<u>0.82</u>	VOG2	0.67
VOG2	0.79	VOG2	0.75	PSRI	0.82	SIPI	0.67
<u>NDVI2</u>	<u>0.80</u>	NDVI1	0.74	RENDVI	0.82	NDPI	0.64
SIPI	0.72	SIPI	0.73	VOG1	0.81	VOG1	0.61
SGI	0.58	REP	0.48	SGI	0.47	SGI	0.41
REP	0.78	SGI	0.51	REP	0.67	RVSI	0.48
RVSI	0.76	RVSI	0.61	RVSI	0.77	REP	0.51

The Jeffries – Matusita test was performed on vegetation indices that were found to show a high separability between the study sites. The tested indices were NDPI and NDVI1 for May 2014, NDPI, NDVI2, PSRI for June 2014, NDVI, SIPI and VOG2 for July 2014, and NDVI2, PSRI and RENDVI for August 2014. Overall there is a high separability between the control and disturbed sites with values at and greater than 1.80 (Table 4.12). The distinction between the graves and reference is peaking in July 2014, 13 months post-disturbance, at 1.22. In August 2014, a lower distinction is generally observed, where the gap shows the highest separation from the control at 1.80 and the grave – reference pair recording a separation of 0.83. Figure 4.26 shows the scatter plots of site spectral separability based on the tested vegetation indices. As indicated by the Jeffries – Matusita test, the greatest separability is revealed between the control and disturbed sites (i.e. grave, gap, and reference). A weak separation in airborne spectral reflectance between the grave and reference is observed in July 2014.

Table 4.13. Jefferies – Matusita pair separability of site ROI using the indices that show the highest spectral separation between the control, grave, gap, and reference of the CASI imagery collected over the 2014-growing season. The Jeffries – Matusita values range between 0 and 2 where a value of 1.90 indicates a high separability between sites.

Pair Separation	May	June	July	August
Gap and Control	1.99	1.99	1.99	1.80
Grave and Control	1.90	1.99	1.87	1.39
Grave and Gap	1.44	0.43	1.58	0.66
Grave and Reference	1.15	0.79	1.22	0.83
Reference and Control	1.99	1.99	1.87	1.34
Reference and Gap	1.73	1.05	1.51	0.52

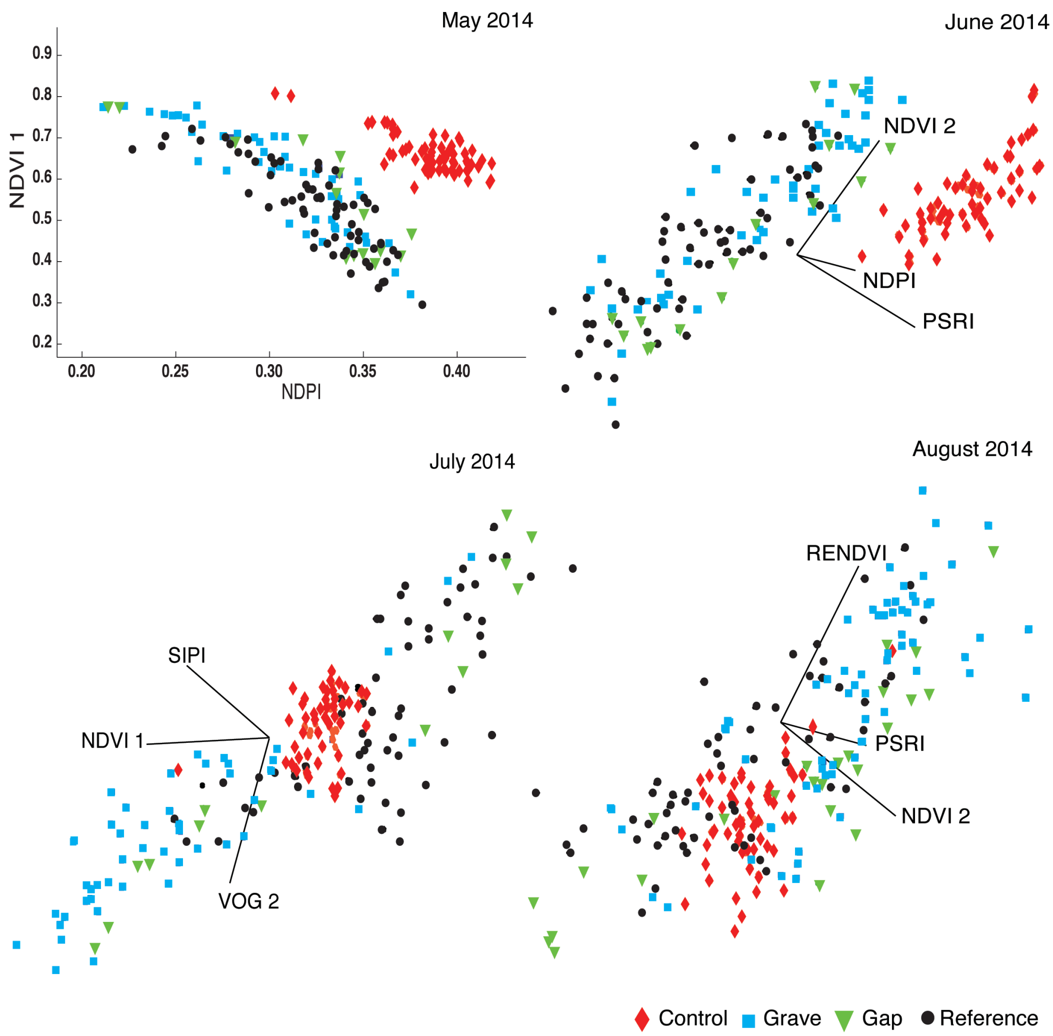

Figure 4.26. Visualization of 2-D (May 2014) and 3-D (June, July and August 2014) scatter plots showing the relationship between (red) control, (blue) grave, (green) gap, and (black) reference based on the vegetation indices indicating the highest spectral separation between sites over the 2014-growing season.

5. Discussion

The premise of this study is that the cadaver decomposition process leads to changes in soil chemistry, due to the release of nutrients into the soil matrix. Therefore, these changes might be captured at the soil level and also using remote sensing derived data at different spatial scales. By measuring vegetation reflectance at the leaf and *in-situ* level (spectroscopy and hyperspectral airborne) scales, it was also hypothesized that chemical and biophysical changes in vegetation would be captured. In terms of soils chemistry between a deep mass grave (i.e. approximately 1.0 – 1.5 m) and a non-grave site the results of this study are inconclusive, however some trends are worth discussing. Due to the depth of burial (i.e. approximately 1.0 – 1.5 m) and environmental conditions, the release of nutrients into the soil matrix may be delayed and/or undetected in surface soil samples. At the end of the sixth month post-disturbance, November 2013, significant differences were found in Ca and Mn concentrations between the grave and reference and in Ca and Mg between the control and disturbed sites (i.e. grave, gap, and reference). Furthermore, the grave records higher Mn concentrations in comparison with the other sites. This finding agrees with the previous work of Snirer (2014) and Carter et al. (2007) where higher concentrations of Mn and Ca in surface grave soil were revealed. Snirer (2014) reports a Ca and Mn concentration of 1.76 ± 1.43 % and 2907.00 ± 1034.00 ppm for deep graves (i.e. 1.2 m) four months post-disturbance, in comparison with this study where concentrations of 1.36 ± 0.22 % and 1147.00 ± 185.90 ppm, respectively, were found five months after burial (Table 4.3). Differences between the two studies can be attributed to differences in soil type. The release of nutrients during the decomposition process has an impact on the surrounding environment as a distinctive grave soil is formed as nutrients from soft tissue and bone are leached into the soil matrix (Carter et al. 2007; Damann et al. 2012; Forbes 2008).

Soils chemistry patterns also indicate that changes in NH_4, NO_3, and available P concentrations are emerging towards the end of the 2014-growing season. Overall, no significant differences were found in available P between the grave and reference over the 2014-growing season until November when a significant difference is found between the two sites (Figure 4.4). The concentration of available P of soil samples collected from the top of the grave increases over time (Figure 4.4). A seasonal fluctuation is revealed between May and October 2014 in NH_4, NO_3, and available P concentrations for the control site, which also has the highest recorded concentrations over the study period. A smaller seasonal fluctuating NH_4 concentration, which peaks in October 2014, is also observed for the disturbed sites. Significant differences have been found in NH_4 between the grave and reference in August and November 2014. The NO_3 concentration is peaking in August 2014 with the control recording higher values up to this date. Starting with September 2014, the grave shows higher concentration of NO_3. Moreover, significant differences were found in NO_3 between the grave and reference in October and November 2014. Low available P, NH_4, and NO_3 concentrations found for the disturbed sites in comparison with the control, more specifically for the grave, could be attributed to the disturbance effect. The regrowth in vegetation requires more uptake of nutrients resulting in lower concentrations in soil chemistry. In contrast, the control is characterized by undisturbed vegetation that does not require as much nutrient uptake for growth. Significant differences in total nitrogen concentrations were found between surficial graves and non-graves grey-brown podsolic soil in the first 14 days post-disturbance in a temperate environment, which returned to basal levels after 100 days post-disturbance (Stokes et al. 2009). The same study also reveals that control sites recorded higher overall concentrations of total nitrogen. Other studies also report an increase in total nitrogen (Hopkins et al. 2000; Melis et al. 2007) and extractable P (Stokes et al. 2009) in grave soil. Phosphorus can be found in body components such as proteins comprising nucleic acids and coenzymes, sugar phosphorus and phospholipids (Dent et al. 2004). Increasing NH_4 concentration, followed by decreasing values over time, has been found in sandy clay loam and loamy grave sand (Stokes et al. 2009). No nitrification has been revealed in heavy clay soil (Hopkins et al. 2000); meanwhile, rapid nitrification has been reported in temperate forest soils in Poland (Melis et al. 2007).

The clay present at the base of the grave (see stratigraphic section 3.2.3 in methods) may lead to a slow decomposition as it may delay the release of gases or nutrients into the soil matrix (Tumer et al. 2013). Moreover, the depth of burial plays an import role in the decomposition process and on how the release of nutrients affects the surrounding soil and vegetation. Other studies on carcass decomposition support the results of this study, where they reveal that buried carcasses show slow decomposition and mass loss rates in comparison with shallow and aboveground graves (Carter et al. 2007). Tumer et al. (2013) reveal a slower decomposition process in shallow graves (0.50 m) characterized by clay and sandy soil, in comparison with graves characterized by loamy and organic soils. Deep graves with coarse-textured soil and low moisture content have been found to promote desiccation, while fine textured clay soil has been reported to inhibit the carcasses breakdown and slow the decomposition process (Hopkins et al. 2000). A formation of adipocere around a body has been reported in deep graves resulting in slower decomposition rates (Dent et al. 2004).

It is important to note that soil samples were collected within 15 cm of the surface, which may play an important role in the results of this study as the pig carcasses were buried at approximately 1 m depth. The effect of the release of nutrients on vegetation may depend on the depth of their roots. The found differences in soil chemistry can also be associated with the disturbance effect. Taking into consideration that the base of the burial site is characterized by clay, it is a challenge to determine exactly how the nutrients react in the soil matrix and affect surrounding vegetation. As stated by Stokes et al. (2009), the complexity of a burial environment and the numerous chemical changes occurring in the soil due to the decomposition of a body pose a challenge to the task of clearly assigning variability to a single factor in decomposition experiments.

Examining the patterns in soil chemistry of a grave reveals that primary changes can, at the time scale of this study, be attributed to the disturbance effect, especially earlier in the study. The 2014 soil chemistry results also suggest that changes are starting to emerge towards the end of the study period. Thereby, insufficient decomposition might have occurred to affect soil chemistry and surrounding vegetation over the study period.

In terms of vegetation pigmentation, differences in chlorophyll and carotenoid concentrations can be attributed to the overall disturbance effect rather than to release of nutrients during the cadaver decomposition process in the first 13 months post-disturbance. Starting with the 13th month point, July 2014, significant differences in chlorophyll and carotenoid have been found between the grave and reference. The vegetation collected from the grave shows higher concentrations of chlorophyll and significant differences from the other sites between July and September 2014 (Figure 4.12). The differences in leaf pigmentation can be triggered by the disturbance effect or the availability of more nutrients for the surrounding vegetation. Snirer (2014) found that soil disturbance could greatly affect the vegetation pigmentation, possibly more than the chemicals released during the cadaver decomposition in shallow (0.6 m) and deep (1.2 m) single graves. Meanwhile, de Gea (2012) reveals higher total chlorophyll concentrations, between 50.00 and 60.00 μg cm^{-2} of mature large commingled grave vegetation from control site vegetation with concentrations between 20.00 and 40.00 μg cm^{-2}, at different times in the growing season. In comparison, this study reveals total chlorophyll concentrations between 11.61 and 54.15 μg cm^{-2} for the experimental mass grave and 20.00 to 30.00 μg cm^{-2} for the control site in the first 15 months post-disturbance (Figure 4.9). Snirer (2014) also reports total chlorophyll concentrations ranging between 20.00 and 80.00 μg cm^{-2} for single deep graves four months after burial in a temperate environment. The differences in chlorophyll for the current study may be attributed to the disturbance effect in the first 17 months since burial or the increase in soil nutrient availability as the main source of nutrients to plants is from the soil matrix through root uptake of nutrients, such as nitrogen and phosphorus (Clemens et al. 2002) and the internal structure and pigmentation of the surrounding vegetation can be influenced by the nutrients absorbed from the soil matrix (Kabata-Pendias and Mukherjee 2007).

In the first 15th months post burial, the mass grave shows incomplete vegetation cover. Because of the size of the disturbance (i.e. 10 x 5 m), the regeneration of vegetation sufficient to cover the affected site is believed to take longer than on aboveground and shallow graves (Caccianiga et al. 2012; Kalacska et al. 2009). Kalacska et al. (2009) reveal an incomplete vegetation cover of an experimental mass grave in the first 16 months since disturbance in a tropical forest environment. Caccianiga et al. (2012) also found that the main factor affecting vegetation cover on a deep grave (i.e. between 0.8 and 0.9 m) is the disturbance effect. Because changes in soil chemistry of the study site in this work are starting to show towards the end of the collection period, the differences in vegetation pigmentation of the mass grave may be caused by the disturbance effect. However, incomplete vegetation may also be caused by the inhibition of regrowth due to the release of decomposition compounds in the soil (Carter et al. 2007). The release of too many nutrients can create a toxic environment resulting in little to no vegetation on top of the grave (Carter et al. 2007; Kalacska et al. 2009). As mentioned, because of the complexity of a grave's microenvironment it is a challenge to attribute the dynamics of vegetation cover to an isolated factor such as depth, or how the soil was placed back after the placement of the carcasses.

The results of the spectral reflectance collected of the study sites using leaf, *in-situ*, and airborne data reveal that overall differences in spectral signatures can be attributed to the disturbance effect in the first 13 months since burial. Similarly to the vegetation pigmentation results, spectral changes are occurring starting with the 13th month point in the disturbance. The regrowth in vegetation leads to dynamic changes for the disturbed sites in comparison with the control over a growing season. At the leaf and *in-situ* spatial scales, differences in shape and amplitude are observed over the study period. The spectral differences between the control and disturbed sites change and decrease over time as there is a regrowth in vegetation. At the *in-situ* spatial scale, more significant differences were found in amplitude over the 925 – 1371 nm and 1500 – 1700 nm ranges in comparison with the 400 – 917 nm range. These ranges have been associated with changes in leaf structure (750 – 1300 nm) and internal cellular structure (1300 – 2500 nm) (Peñuelas and Filella 1998). The computed amplitude and shape metrics also reveal a high within site variability for the grave and reference site, further indicating the disturbed sites as dynamic environments that are characterized by a transition vegetation regrowth. Other study found spectral differences in amplitude and shape between background, surface graves, and shallow and deep burials (Snirer 2014).

The forward feature selection algorithm shows that the best separable bands between the grave and reference depend on spatial scale, disturbance stage and time in the growing season (Figure 4.16, Figure 4.24, and Figure 4.32). Overall, the spectra collected at the leaf spatial scale show a clustering of best separable bands between sites along the 400 – 700 nm range and smaller ones in the 1300 – 1500 nm range later in the disturbance stage, 13 months post-disturbance. These ranges have been found to be characteristic of changes occurring at the vegetation pigmentation level (Peñuelas and Filella 1998). Moreover, a clustering in the 400 – 700 nm range is shown in October 2013 and between July 2014 and September 2014 (Figure 4.16), which are months when a significant difference in total chlorophyll is revealed (Figure 4.12). For the *in-situ* data, a clustering is observed in the 400 – 700 nm range in 2013 and in May and August 2014. A different clustering of separable bands between the grave and reference is revealed in the 700 to 1000 nm range in July and September 2014. A cluster of optimal bands was also found in the 2100 – 2400 nm range early in the disturbance stage, July 2013, and at the 13^{th} month post-burial July 2014. The 2200 - 2500 wavelength range is associated with changes in soil clay composition (Ben-Dor et al. 1997). The airborne images show different separable bands between the grave and reference in the 500 – 700 nm range in June 2014 and the 700 – 800 nm range in July 2014. The 500 nm to 650 nm wavelength range has been reported when differentiating between plants grown in fertilized soil and those grown with animal liver tissue (Herzog 2014) and between a mature grave and control (de Gea 2012) and in the 450 – 500 nm and 570 – 600 nm ranges in recent single graves detection (Snirer 2014). The results of the current and previous studies suggest that the use of separable wavelengths can show a differentiation between a grave and a reference that can depend primarily on seasonal patterns and grave age. A recent grave (less than one year) can show separability in the soil characteristic ranges, while a more mature grave (older than one year) can be differentiated from a false grave in the visible range (450 to 750 nm) where changes in chlorophyll and anthocyanin can be highlighted.

The computed vegetation indices show that the highest spectral separability between the grave and reference is occurring in July 2014 – at the 13th month post-disturbance for the leaf, *in-situ*, and airborne data. Due to incomplete vegetation cover, the computed vegetation indices show high variability for the disturbed sites leading to low confidence differences and separation of the grave from reference solely based on vegetation indices. Depending on the stage of disturbance and site vegetation dynamics a separation between the sites can be attempted. Overall, the main differences are found between the control and disturbed sites. Various vegetation indices, such as NDPI, NDVI, SIPI, and VOG, show significant difference between the grave and reference site at the leaf spatial scale. For the *in-situ* and airborne data, the mix of soil and vegetation spectral characteristics of the disturbed sites leads to high variability and inconclusive separation between the grave and non-graves. No significant differences in vegetation indices were found starting with June 2014, 12 months post-disturbance at the *in-situ* spatial scale. For instance, NDPI shows significant differences between the grave and reference in May 2014 for the leaf and *in-situ* data. The SGI index is the only one showing a significant difference between the grave and reference for the *in-situ* spectral reflectance in August 2014. When looking at the airborne data, the SGI index shows a ranging value of 0.67 - 0.89 for the mass grave (Appendix E). Meanwhile, Leblanc et al. (2014) reports an SGI value ranging between 0.60 and 0.80 for a single surface grave. Similar results are revealed by Snirer (2014), where vegetation indices were able to differentiate between deep single graves and reference. In comparison, the application of PSRI index and of RENDVI in a chlorophyll prediction curve has successfully detected the location of mature animal graves and their separability from false graves in a temperate environment (de Gea 2012). The study reports a similar PSRI average of -0.10 for a mature grave as it was found in the current one (ranging between -0.15 and -0.28) at the leaf spatial scale.

As reported, a step in the detection of potential location of graves in a temperate climate is to compute the relative distribution of hydroxyl (Leblanc et al. 2014). The hydroxyl (OH^-) ion, characterized by a diagnostic absorption at 2200 nm reflectance, is an indicator of clay presence on the scene; the activity of grave excavation is expected to leave traces of clay on the surface (Leblanc et al. 2014). The results of hydroxyl mapping show that a differentiation can be made between the control and disturbed sites early in the disturbance, July 2013, and early in the growing season, May 2014, where the presence of clay on the disturbed sites is at its highest. Similar characteristics are found in the *in-situ* spectra collected around the same time, where the signatures of the disturbed sites are those characteristics of a mix of soil and vegetation. The utility of the 2200 nm wavelength has been emphasized in the detection of clandestine burial sites using hyperspectral remote sensing (Leblanc et al. 2014; Snirer 2014).

The results of the current study also reveal that the detectability of a graves using vegetation indices is not dependent only on one index but on multiple that indicate a common target location. Given that each vegetation index highlights certain characteristics of the site, by combining multiple ones the detection of potential target location increases. By combining different indicators such as the 2200nm wavelength, and various vegetation indices the separability of the grave from the gap, reference and control can be increased. The results of this study show that the combination of indices also depends on the time in the disturbance and in the growing season. The indices showing the greatest separation between sites were NDPI and NDVI1 in May, NDPI, NDVI2, PSRI in June, NDVI, SIPI and VOG2 in July, and NDVI2, PSRI and RENDVI in August for the imagery collected over the 2014-growing season (Figure 4.26 and Table 4.12). Leblanc et al. (2014) also applied the 2200 nm band, NDVI, SGI, and SIPI indicators in the detection of the clandestine single surface graves in a temperate environment. Their study reports a better separability using the Jeffries-Matusita's test at 1.97 between grave and mixed herbaceous and at 1.88 between grave and exposed soil. In comparison, the current study shows separability between 0.79 and 1.22 for the grave and reference, and a higher one for the grave and control at values between 1.39 and 1.90 (Table 4.13). As mentioned by Leblanc et al. (2014) different indicators can be applied in different settings and environments.

Overall, the results of the current study indicated that the use of spectral reflectance for deep mass graves detection depends on the disturbance stage. Mature graves are characterized by a more advanced decomposition stage leading to more nutrients released into the soil matrix and affecting the surrounding vegetation. Given that the detection of burial sites using hyperspectral remote sensing depends on changes in soil and vegetation characteristics, environmental factors also play an important role in its application in a temperate environment. Furthermore, the application of hyperspectral remote sensing in gravesite detection is limited to information collected during the growing season, between April and November, as temperature and snow has been noted as one of the most influential factors of decomposition (Gill-King 1996). Table 5.1 summarizes the main findings of the current study in terms of differences found between the study sites in soil chemistry, vegetation pigmentation, leaf, *in-situ* and airborne spectral reflectance.

Table 5.1. Table summarizing the main findings of the current study.

Data Type	Results Summary
Soil chemistry	▪ Significant differences in Ca ($p=0.018$) and Mn ($p=0.004$) concentrations between grave and reference, along with significant differences in Ca and Mg concentrations between the control and disturbed sites (i.e. grave, gap, and reference) five months post disturbance ($p<0.01$) (Table 4.2) ▪ Significant differences in available P, NH_4, and NO_3 concentrations between the control and disturbed sites (i.e. grave, gap, and reference) in 2014 (Table 4.4, Table 4.5, Table 4.6.) ▪ Significant differences in available P concentration between grave and reference in November 2014 ($p<0.0001$) (Table 4.4) ▪ Significant differences in NH_4 concentration between grave and reference in May, August and November 2014 ($p<0.025$) (Table 4.5) ▪ Significant differences in NO_3 concentration between grave and reference in October and November 2014 ($p<0.01$) (Table 4.6) ▪ The robust nominal cluster analysis shows a separation between control, grave, gap, and reference in Ca, Fe, and Mg concentrations five months post disturbance (Figure 4.4) ▪ The k-mean clustering analysis shows a separation between control and all other sites based on available P, NH_4, and NO_3 concentrations (Figure 4.5)
Leaf pigmentation	▪ Overall significant differences in leaf pigmentation between control and disturbed sites ($p<0.05$) (Figure 4.6, Figure 4.7, Figure 4.8, Figure 4.9) ▪ Significant differences between grave and reference for July 2014 ($p=0.164$) and August 2014 ($p<0.001$) in carotenoids concentration (Figure 4.6) ▪ Significant differences between grave and reference from July 2014 to September 2014, with the grave showing higher values, in chlorophyll A (Figure 4.7), chlorophyll B (Figure 4.8), and Total chlorophyll concentrations ($p<0.001$) (Figure 4.9)

Table Continued.

Data Type	Results Summary
Leaf spectral reflectance	▪ Overall differences in average spectral signature between control and disturbed sites (Figure 4.10, Figure 4.11) ▪ Best separable wavelengths between grave and reference revealed mainly along the 400 – 800 nm and 1400 – 1600 nm ranges (Figure 4.13) ▪ Collected grave leaf spectral reflectance shows higher NDVI1, RENDVI values. Vegetation indices showing a difference between grave and reference are: NDPI, NDVI, RENDVI, SGI, SIPI and VOG (Appendix C)

Field spectrometry	▪ Overall difference in average spectral signatures between control and disturbed sites (Figure 4.17, Figure 4.18)
	▪ Best separable wavelengths between grave and reference found along the 400 – 1000 nm range (Figure 4.20)
	▪ Computed vegetation indices showing significant differences between control and disturbed sites ($p<0.05$) with high standard deviation (Appendix D)
	    ▪ Showing significant differences between grave and reference in the early stages of disturbance, August and September 2013, are NDVI ($p<0.01$), RENDVI ($p\leq0.01$), SGI ($p<0.01$), SIPI ($p=0.03$), and VOG ($p<0.02$).
	    ▪ PSRI in August 2013 ($p=0.015$), at 0.16 for the grave and 0.26 for the reference, and in May 2014 at 0.33 and 0.28 respectively ($p<0.01$)
	    ▪ The NDPI indicates a significant difference in May 2014 between the grave, at 0.36, and reference at 0.31 ($p<0.01$)
	    ▪ A significant difference between the grave and reference is shown by SGI in August 2014 ($p=0.003$)

Airborne Hyperspectral Imagery	▪ Best separable wavelengths between grave and reference along the 900 – 1000 nm and 2000 – 2400 nm ranges in July 2013 and along the 900 to 1200 nm in September 2013 (Figure 4.24) ▪ Best separable wavelengths between grave and reference for the year 2014 along the 400-700 nm and 2100 – 2400 nm, with a cluster in the 400 – 800 nm for August; the greatest separation is seen in the 400s nm and 900s nm ranges ▪ Significant differences between control, reference and grave in hydroxyl distribution (2203.5 nm band) in July 2013, September 2013, and May and June 2014 ($p<0.05$) (Table 4.11) ▪ Vegetation indices showing a weak separation between grave and reference are NDPI and NDVI1 for May 2014, NDPI, NDVI2, PSRI for June 2014, NDVI, SIPI and VOG2 for July 2014, and NDVI2, PSRI and RENDVI for August 2014 (Table 4.13, Figure 4.26)

6. Conclusions

The results of this research study show that differences in spectral reflectance depend on spatial scale, disturbance stage and time in the growing season for the application of hyperspectral remote sensing as a complementary tool in the detection of deep mass graves. Overall differences were found between the grave and control in soil chemistry, vegetation pigmentation and spectral reflectance throughout the study period. In the first 13 months post-disturbance, differences in soil chemistry, vegetation pigmentation (i.e. chlorophyll and carotenoids), and spectral reflectance between the mass grave, control, and reference can be attributed to the overall site disturbance and not due to the decomposition process. Starting with the 13th month post-disturbance, differences in soil chemistry (i.e. ammonium, nitrate, and available phosphorus), vegetation pigmentation and spectral reflectance are starting to occur between the grave and reference. In terms of leaf spectral reflectance, differences were found along the 400 – 700 nm wavelength range between the grave and reference during this period. Furthermore, the results suggest that a combination of various vegetation indices increases the separation between the grave and non-graves depending on the disturbance stage. Indices that started to show a separation in spectral reflectance between sites are NDPI and NDVI1 in May 2014, NDPI, NDVI2, PSRI in June 2014, NDVI, SIPI and VOG2 in July 2014, and NDVI2, PSRI and RENDVI in August 2014 on the collected airborne imagery.

Given that potential changes between the grave and reference are occurring towards the end of the study period, no definitive conclusions can be made in regards to the application of hyperspectral remote sensing in deep mass grave detection using spectral indices and band separability. New studies take advantage of the richness of hyperspectral data, for example through wavelet decomposition from which better results can be obtained regarding biochemical and biophysical characteristics of vegetation (Kalacska et al. 2015).

Nevertheless, hyperspectral remote sensing shows promise as a complementary tool in the detection of clandestine graves by narrowing down search area and highlighting the disturbance areas. Due to the fact that variations in spectral reflectance between the grave and reference are potentially starting to be revealed only after 13 months post-disturbance, surficial expressions of a deep grave may either muted or delayed under these conditions. Further analyses in the second and third year post-disturbance, 2015 and 2016, is recommended to test whether the decomposition process is advanced enough to affect surrounding soil and vegetation.

References

Adlam, R.E., & Simmons, T. (2007). The Effect of Repeated Physical Disturbance on Soft Tissue Decomposition—Are Taphonomic Studies an Accurate Reflection of Decomposition? *Journal of Forensic Sciences, 52*(5), 1007-1014

Agren, G.I., & Andersson, F.O. (2012). Terrestrial Ecosystem Ecology Principles and Applications. *The Forestry Chronicle, 88*(3), 363-364

Aljazeera. (2011). More Bodies Recovered from Mexico Mass Graves. Retrieved on October 15 2015 from: http://www.aljazeera.com/news/americas/2011/04/201142211610296198.html

Aljazeera. (2013). Mass Grave Found near Mali military Base. Retrieved on October 15 2015 from: http://www.aljazeera.com/news/africa/2013/12/mass-grave-found-near-mali-military-base-2013124164418437438.html

Aljazeera. (2014). Mass Grave of Hundreds Unearthed in Bolivia. Retrieved on October 15 2015 from: http://www.aljazeera.com/news/americas/2014/07/mass-grave-hundreds-unearthed-bolivia-2014727124738777584.html

Aljazeera. (2012). Mass Grave Found in Kenya's Delta Region. Retrieved October 15 2015 from: http://www.aljazeera.com/news/africa/2012/09/2012918182747902279.html

Allux, S., & Leblanc, G. (2010). Post-Radiometric Processing of SASI Hyperspectral Data. (p. 26). Flight Research Laboratory, National Research Council Canada

Ambos, E.L., & Larson, D.O. (2002). Verification of Virtual Excavation Using Multiple Geophysical Methods. Case Studies from Navan Port, County Amagh, Northen Ireland. *The Society of American Archaeology Archaeological Record, 2*(1), 32-38

Amnesty International (AMR). (1998). Guatemala: All the Truth, Justice for All. (p. 35). *Amnesty International*. Amnesty International Ltd: Peter Benenson House: London

Amnesty International (AMR). (2008). Annual Report 2008 – Enforced Disappearance Update Selected Extracts on Enforced Disappearance. (p. 6). *Amnesty International*. Amnesty International Ltd: Peter Benenson House: London

Amnesty International (AMR). (2014). Nigeria: More than 1500 Killed in Armed Conflict in North-Eastern Nigeria in Early 2014. (p. 31). *Amnesty International*. Amnesty International Ltd: Peter Benenson House: London

Amnesti International (AMR). (2015). The State of World's Human Rights. (p. 423). *Amnesty International*. Amnesty International Ltd: Peter Benenson House: London

Anderson, B., Meyer, J., & Carter, D.O. (2013). Dynamics of Ninhydrin-Reactive Nitrogen and Ph in Gravesoil During the Extended Postmortem Interval. *Journal of Forensic Sciences, 58*(5), 1348-1352

Anderson, G., & Cervenka, V. (2001). Insects Associated with the Body: Their Use and Analyses. In W.D. Haglund, & M.H. Sorg (Eds.), *Advances in Forensic Taphonomy* (pp. 173-200). New York: CRC Press

Arnon, D.I. (1949). Copper Enzymes in Isolated Chloroplasts. Polyphenoloxidase in Beta Vulgaris. *Plant Physiology, 24*(1), 1-15

Babic, J., Cupkovic, T., & Bosiocic, N. (2000). The Application of Remote Sensing and It in Research of Mass Graves in the System of Jasenovac Ustasha Camps. Retrieved on May 5 2015 from: http://www.jasenovac-info.com/projekti/rsgis_jasenovac_eng.pdf

Bachmann, J., & Simmons, T. (2010). The Influence of Preburial Insect Access on the Decomposition Rate. *Journal of Forensic Sciences, 55*(4), 893-900

Barber, B., and Epstein, S. (2004). Iraq's Legacy of Terror: Mass Graves. (p. 16). United States Agency for International Development

Barnes, E.M., Sudduth, K.A., Hummel, J.W., Lesch, S.M., Corwin, D.L., Yang, C., Daughtry, C.S., & Bausch, W.C. (2003). Remote-and Ground-Based Sensor Techniques to Map Soil Properties. *Photogrammetric Engineering & Remote Sensing, 69*(6), 619-630

Bartel, B. (1982). A Historical Review of Ethnological and Archaeological Analyses of Mortuary Practice. *Journal of Anthropological Archaeology, 1*(1), 32-58

Bartley, G.E., & Scolnik, P.A. (1995). Plant Carotenoids: Pigments for Photoprotection, Visual Attraction, and Human Health. *The Plant Cell, 7*(7), 1027-1038

Bureau of Democracy Human Rights and Labor (BDHRL). (2013). Mexico 2013 Human Rights Report. (p. 47). United States Department of State

Beazeley, G.A. (1919). Air Photography in Archaeology. *Geographical Journal, 53*(5), 330-335

Behmann, J., Steinrücken, J., & Plümer, L. (2014). Detection of Early Plant Stress Responses in Hyperspectral Images. *ISPRS Journal of Photogrammetry and Remote Sensing, 93*(0), 98-111

Ben-Dor, E. (2002). Quantitative Remote Sensing of Soil Properties. *Advances in Agronomy, 75*(0), 173-243

Ben-Dor, E., & Banin, A. (1995). Near-Infrared Analysis as a Rapid Method to Simultaneously Evaluate Several Soil Properties. *Soil Science Society of America Journal, 59*(2), 364-372

Ben-Dor, E., Inbar, Y., & Chen, Y. (1997). The Reflectance Spectra of Organic Matter in the Visible near-Infrared and Short Wave Infrared Region (400–2500 nm) During a Controlled Decomposition Process. *Remote Sensing of Environment, 61*(1), 1-15

Benner, S., & Brodkey, R. (1984). Underground Detection Using Differential Heat Analysis. *Archaeometry, 26*(1), 21-36

Benninger, L.A., Carter, D.O., & Forbes, S.L. (2008). The Biochemical Alteration of Soil beneath a Decomposing Carcass. *Forensic Science International, 180*(2), 70-75

Bergen-Belsen (2015). Stalag Xic (311) and Kz Bergen-Belsen, a History from 1935. Retrieved on October 15 2015 from: http://www.bergenbelsen.co.uk/index.html

Berkhoff , K.C. (2004). Babi Yar. In D.L. Shelton, H. Adelman, F. Chalk, A. Kiss, & W.A. Schabas (Eds.), *Encyclopedia of Genocide and Crimes Against Humanity* (pp. 109 - 111). New York: Macmillan Reference, Thomson Gale

Berlin, G.L., Ambler, J.R., Hevly, R.H., & Schaber, G.G. (1977). Identification of a Sinagua Agricultural Field by Aerial Thermography, Soil Chemistry, Pollen/Plant Analysis, and Archaeology. *American Antiquity, 42*(4), 588-600

Bevan, B.W. (1983). Electromagnetics for Mapping Buried Earth Features. *Journal of Field Archaeology, 10*(1), 47-54

Bevan, B.W. (1991). The Search for Graves. *Geophysics, 56*(9), 1310-1319

Blau, S., & Skinner, M. (2005). The Use of Forensic Archaeology in the Investigation of Human Rights Abuse: Unearthing the Past in East Timor. *The International Journal of Human Rights, 9*(4), 449-463

Boehnke, M. (2013). Body of Evidence: UT Using Donated Corpses in Mass Grave Project with International Aspirations. Knoxville News Sentinal. Retrieved on August 21 2015 from: http://www.knoxnews.com/news/local-news/body-of-evidence-ut-using-donated-corpses-in

Bouckaer, P. (2003). Iraq - The Mass Graves of Al-Mahawil: The Truth Uncovered. *Human Rights Watch*, *15*(5), 18

Brilis, G.M., Gerlach, C.L., & Waasbergen, R.J.v. (2000). Remote Sensing Tools Assist in Environmental Forensics. Part I: Traditional Methods. *Environmental Forensics, 1*(2), 63-67

Brilis, G.M., Van Waasbergen, R., Stokely, P., & Gerlach, C. (2001). Remote Sensing Tools Assist in Environmental Forensics: Part II--Digital Tools. *Environmental Forensics, 2*(3), 223-229

Brown, J.A. (1971). *Approaches to the Social Dimensions of Mortuary Practices*. *Memoir, 1*. (p. 112). Washington, DC: Society for American Archaeology

Buck, S.C. (2003). Searching for Graves Using Geophysical Technology: Field Tests with Ground Penetrating Radar, Magnetometry, and Electrical Resistivity. *Journal of Forensic Sciences, 48*(1), 5-11

Caccianiga, M., Bottacin, S., & Cattaneo, C. (2012). Vegetation Dynamics as a Tool for Detecting Clandestine Graves. *Journal of Forensic Sciences, 57*(4), 983-988

Cambardella, C.A., Moorman, T.B., Parkin, T.B., Karlen, D.L., Novak, J.M., Turco, R.F., & Konopka, A.E. (1994). Field-Scale Variability of Soil Properties in Central Iowa Soils. *Soil Science Society of America Journal, 58*(5), 1501-1511

Carter, D.O., & Tibbett, M. (2006). Microbial Decomposition of Skeletal Muscle Tissue (Ovis Aries) in a Sandy Loam Soil at Different Temperatures. *Soil Biology and Biochemistry, 38*(5), 1139-1145

Carter, D.O., & Tibbett, M. (2008). Cadaver Decomposition and Soil. In M. Tibbett, & D.O. Carter (Eds.), *Soil Analysis in Forensic Taphonomy* (pp. 29-51). Boca Raton, Florida: CRC Press: Taylor & Francis Group

Carter, D.O., Yellowlees, D., & Tibbett, M. (2007). Cadaver Decomposition in Terrestrial Ecosystems. *Naturwissenschaften, 94*(1), 12-24

Carter, D.O., Yellowlees, D., & Tibbett, M. (2008a). Temperature Affects Microbial Decomposition of Cadavers (Rattus Rattus) in Contrasting Soils. *Applied Soil Ecology, 40*(1), 129-137

Carter, D.O., Yellowlees, D., & Tibbett, M. (2008b). Using Ninhydrin to Detect Gravesoil. *Journal of Forensic Sciences, 53*(2), 397-400

Carter, D.O., Yellowlees, D., & Tibbett, M. (2010). Moisture Can Be the Dominant Environmental Parameter Governing Cadaver Decomposition in Soil. *Forensic Science International, 200*(1–3), 60-66

Documentation Center of Cambodia (CDCAM). (2015). List of Mass Graves(p. 24). Documentation Center of Cambodia. Retrieved October 15 2015 from: http://www.d.dccam.org/Projects/Maps/List_of_Burial_Site_Most_Updated.pdf

Chalk, F.R., Jonassohn, K., Mazal Holocaust, C., & Montreal Institute for Genocide, S. (1990). The History and Sociology of Genocide : Analyses and Case Studie*s*. (p. 461). New Haven: Yale University Press

Chang, C. W., Laird, D.A., Mausbach, M.J., & Hurburgh, C.R. (2001). Near-Infrared Reflectance Spectroscopy–Principal Components Regression Analyses of Soil Properties. *Soil Science Society of America Journal, 65*(2), 480-490

Cheetham, P. (2005). Forensic Geophysical Survey. In J. Hunter, & M. Cox (Eds.), *Forensic Archaeology: Advances in Theory and Practice* (pp. 62-92). New York: Routledge

Christodulou, A. (2004). Appendix 4: Memorials, Mass Graves and Other Sites. In Witness to Truth: Report of the Sierra Leone. (p. 72). Truth and Reconsiliation Commmission. Retrieved on October 15 2015 from: http://www.sierraleonetrc.org/index.php/view-the-

final-report/download-table-of-contents/appendices/item/appendix-4-memorials-mass-graves-and-other-sites
Clemens, S., Palmgren, M.G., & Krämer, U. (2002). A Long Way Ahead: Understanding and Engineering Plant Metal Accumulation. *Trends in Plant Science, 7*(7), 309-315
Congram, D.R. (2008). A Clandestine Burial in Costa Rica: Prospection and Excavation. *Journal of Forensic Sciences, 53*(4), 793-796
Congram, D.R. (2010). Spatial Analysis and Predictive Modelling of Clandestine Graves from Rearguard Repression of the Spanish Civil War.(p. 299). PhD Dissertation, Simon Fraser University
Cox, M. (2008). *The Scientific Investigation of Mass Graves: Towards Protocols and Standard Operating Procedures*. (pp. 183-267): Cambridge University Press
Curran, P.J. (1988). The Semivariogram in Remote Sensing: An Introduction. *Remote Sensing of Environment, 24*(3), 493-507
Curran, P.J., Windham, W.R., & Gholz, H.L. (1995). Exploring the Relationship between Reflectance Red Edge and Chlorophyll Concentration in Slash Pine Leaves. *Tree Physiology, 15*(3), 203-206
Daily Mail. (March 31, 2011). Zimbabwe's Killing Fields: Mass Grave of over 600 Bodies Found in Mine Shaft. Retrieved on October 2015 2015 from: http://www.dailymail.co.uk/news/article-1372034/Zimbabwes-killing-fields-Mass-grave-600-bodies-shaft.html
Dallaire, R., & Beardsley, B. (2005). Shake Hands with the Devil : The Failure of Humanity in Rwanda. (p.571). New York: Carroll & Graf ; Distributed by Publishers Group West
Dalva, M., Kalácska, M., Moore, T.R., & Costopoulos, A. (2012). Detecting Graves with Methane. *Geoderma, 189–190*, 18-27
Dalva, M., Moore, T., Kalacska, M., Leblanc, G., & Costopoulos, A. (2015). Nitrous Oxide, Methane and Carbon Dioxide Dynamics from Experimental Pig Graves. *Forensic Science International, 247*, 41-47
Damann, F.E., Tanittaisong, A., & Carter, D.O. (2012). Potential Carcass Enrichment of the University of Tennessee Anthropology Research Facility: A Baseline Survey of Edaphic Features. *Forensic Science International, 222*(1), 4-10
Dammer, K.-H., & Wartenberg, G. (2007). Sensor-Based Weed Detection and Application of Variable Herbicide Rates in Real Time. *Crop Protection, 26*(3), 270-277
Danis Jr, R., Durnik, C., & Rogan, J. (1992). Final Report of the United Nations Commission of Experts Established Pursuant to Securite Council Resolution 780. Annex X. Mass Graves. (p. 106). United Nations
Davenport, G.C., Griffin, T.J., Lindemann, J., & Heimmer, D. (1990). Geoscientists and Law-Enforcement Professionals Work Together in Colorado. *Geotimes, 35*(7), 13-15
Davenport, G.C., Lindemann, J.W., Griffin, T.J., & Borowski, J. (1988). Crime Scene Investigation Techniques. *The Leading Edge, 7*(8), 64-66
Davies, P. (2004). Nutrient Processes and Chlorophyll in the Estuaries and Plume of the Gulf of Papua. *Continental Shelf Research, 24*(19), 2317-2341
de Gea, J. (2012). Discriminating between Grave Sites and Non-Gravesites Using Conventional Remote Sensing Methods. (p. 39). Honours Thesis, McGill University
Dekeirsschieter, J., Verheggen, F.J., Gohy, M., Hubrecht, F., Bourguignon, L., Lognay, G., & Haubruge, E. (2009). Cadaveric Volatile Organic Compounds Released by Decaying Pig

Carcasses (Sus Domesticus L.) in Different Biotopes. *Forensic Science International, 189*(1–3), 46-53
Dent, B.B., Forbes, S., & Stuart, B. (2004). Review of Human Decomposition Processes in Soil. *Environmental Geology, 45*(4), 576-585
Dupras, T.L., Schultz, J.J., Wheeler, S.M., & Williams, L.J. (2011). *Forensic Recovery of Human Remains: Archaeological Approaches*. (pp. 83-195): CRC Press
Argentine Forensic Anthoropology Team (EAAF). (1997). Bolivia: Biannual Report. (p. 140). Argentine Forensic Anthoropology Team
Argentine Forensic Anthoropology Team (EAAF). (2006). Annual Report: Namibia. (p. 4). Argentine Forensic Anthoropology Team
Gagne, D. (2015). Mass Graves Found on Venezuela-Colombia Border. Insight Crime: Investigation and Analysis of Organized Crime. Retrieved from: http://www.insightcrime.org/news-briefs/mass-graves-found-on-venezuela-colombia-border
Eismann, M.T. (2012). *Hyperspectral Remote Sensing*. (pp. 2-10). Bellingham: SPIE Press
Ellis, S., & Mellor, A. (1995). *Soils and Environment*. (pp. 9-54). New York: Routledge
Environment Canada, C. (2015). Climate Data. Retrieved on March 1 2015 from: http://climate.weather.gc.ca/index_e.html - access
Fang, Z., Bouwkamp, J.C., & Solomos, T. (1998). Chlorophyllase Activities and Chlorophyll Degradation During Leaf Senescence in Non-Yellowing Mutant and Wild Type of Phaseolus Vulgaris L. *Journal of Experimental Botany, 49*(320), 503-510
Fassnacht, F.E., Stenzel, S., & Gitelson, A.A. (2015). Non-Destructive Estimation of Foliar Carotenoid Content of Tree Species Using Merged Vegetation Indices. *Journal of Plant Physiology, 176*, 210-217
Fischbach, M.R. (2004). Iraq. In D.L. Shelton, H. Adelman, F. Chalk, A. Kiss, & W.A. Schabas (Eds.), *Encyclopedia of Genocide and Crimes Against Humanity* (pp. 583 - 586). New York: Macmillan Reference, Thomson Gale
Fondebrider, L., & Doretti, M. (2004). Forensics. In D.L. Shelton, H. Adelman, F. Chalk, A. Kiss, & W.A. Schabas (Eds.), *Encyclopedia of Genocide and Crimes Against Humanity*. (pp. 376-382). New York: Macmillan Reference, Thomson Gale
Forbes, S.L. (2008). Decomposition Chemistry in a Burial Environment. In M. Tibbett, & D.O. Carter (Eds.), *Soil Analysis in Forensic Taphonomy* (pp. 203-223). Boca Raton, Florida: CRC Press: Taylor and Francis Group
Forbes, S.L., Stuart, B.H., & Dent, B.B. (2005). The Effect of the Burial Environment on Adipocere Formation. *Forensic Science International, 154*(1), 24-34
Fox, F. (1999). *God's Eye: Aerial Photography and the Katyn Forest Massacre*. (pp. 7-31). Pennsylvania: West Chester University Press
France, D.L., Griffin, T.J., Swanburg, J.G., Lindemann, J.W., Davenport, G.C., Trammell, V., Armbrust, C.T., Kondratieff, B., Nelson, A., & Castellano, K. (1992). A Multidisciplinary Approach to the Detection of Clandestine Graves. *Journal of Forensic Sciences, 37*(6), 1445-1458
France, D.L., Griffin, T.J., Swanburg, J.G., Lindemann, J.W., Davenport, G.C., Trammell, V., Travis, C.T., Kondratieff, B., Nelson, A., Castellano, K., Hopkins, D.W., & Adair, T. (1996). Necrosearch Revisited: Further Multidiciplinary Approaches to the Detection of Clandestine Graves. In W.D. Haglund, & M.H. Sorg (Eds.), *Forensic Taphonomy: The Postmortem Fate of Human Remains* (pp. 497-510). Boca Raton, Florida: CRC Press

Galloway, A. (1996). The Process of Decomposition: A Model from the Arizona-Sonoran Desert. In W.D. Haglund, & M.H. Sorg (Eds.), *Forensic Taphonomy: The Postmortem Fate of Human Remains* (pp. 139-150). Boca Raton, Florida: CRC Press

Gates, D.M., Keegan, H.J., Schleter, J.C., & Weidner, V.R. (1965). Spectral Properties of Plants. *Applied Optics, 4*(1), 11-20

Gibson, K.D., Dirks, R., Medlin, C.R., & Johnston, L. (2004). Detection of Weed Species in Soybean Using Multispectral Digital Images. *Weed Technology, 18*(3), 742-749

Gill-King, H. (1996). Chemical and Ultrastructural Aspects of Decomposition. In W.D. Haglund, & M.H. Sorg (Eds.), *Forensic Taphonomy: The Postmortem Fate of Human Remains* (pp. 93-107). Boca Raton, Florida: CRC Press

Gitelson, A., & Merzlyak, M.N. (1994). Quantitative Estimation of Chlorophyll-a Using Reflectance Spectra: Experiments with Autumn Chestnut and Maple Leaves. *Journal of Photochemistry and Photobiology, 22*(3), 247-252

Gleason, M. (February 2008). The Search for Human Remains in the Search and Rescue Environment. (p. 33). Virginia: Search and Rescue Tracking Institute

Goetz, A.F. (2009). Three Decades of Hyperspectral Remote Sensing of the Earth: A Personal View. *Remote Sensing of Environment, 113*, S5-S16

Gojanović, M.D., & Sutlović, D. (2007). Skeletal Remains from World War Ii Mass Grave: From Discovery to Identification. *Croatian Medical Journal, 48*(4), 520-527

Gordon, K.M. (2010). A Comparative Analysis of the Deterioration of Textiles and Their Role in Determining Post-Mortem Interval. (p. 87). Master of Science Thesis, Louisiana State University

Grip, W.M., Grip, R.W., & Morrison, R.D. (2000). Application of Aerial Photography and Photogrammetry in Environmental Forensic Investigations. *Environmental Forensics, 1*(3), 121-129

Guatame, L.A. (2010). Remote Sensing Analysis Proposal for the Location of Clandestine Cemeteries Next to the Casanare River in Colombia. In Methodological Proposals for Documenting and Searching for Missing Persons in Columbia. (pp. 43-52). Equitas – International Centre for Human Rights Education

Haglund, W.D. (2001). Recent Mass Graves, an Introduction. In W.D. Haglund, & M.H. Sorg (Eds.), *Advances in Forensic Taphonomy: Method, Theory, and Archaeological Perspectives* (pp. 243-262). New York: CRC Press

Haglund, W.D., Connor, M., & Scott, D.D. (2001a). The Archaeology of Contemporary Mass Graves. *Historical Archaeology, 35*(1), 57-69

Haglund, W.D., Connor, M., & Scott, D.D. (2001b). The Effect of Cultivation on Buried Human Remains. In W.D. Haglund, & M.H. Sorg (Eds.), *Advances in Forensic Taphonomy: Method, Theory, and Archaeological Perspectives* (pp. 133-150). New York: CRC Press

Hansen, J.D., Pringle, J.K., & Goodwin, J. (2014). Gpr and Bulk Ground Resistivity Surveys in Graveyards: Locating Unmarked Burials in Contrasting Soil Types. *Forensic Science International, 237*, e14-e29

Harrison, M., & Donnelly, L. (2009). Locating Concealed Homicide Victims: Developing the Role of Geoforensics. In K. Ritz, L. Dawson, & D. Miller (Eds.), *Criminal and Environmental Soil Forensics* (pp. 197-220). London, UK: Springer

Haslam, T.C., & Tibbett, M. (2009). Soils of Contrasting Ph Affect the Decomposition of Buried Mammalian (Ovis Aries) Skeletal Muscle Tissue. *Journal of Forensic Sciences, 54*(4), 900-904

Herzog, C. (2014). A Study of the Effects of Cadaveric Decomposition on Hyperspectral Signatures of Soil and Vegetation. (p. 105). Master of Science Thesis, McGill University

Hiscox, J., & Israelstam, G. (1979). A Method for the Extraction of Chlorophyll from Leaf Tissue without Maceration. *Canadian Journal of Botany, 57*(12), 1332-1334

Hopkins, D.W., Wiltshire, P.E.J., & Turner, B.D. (2000). Microbial Characteristics of Soils from Graves: An Investigation at the Interface of Soil Microbiology and Forensic Science. *Applied Soil Ecology, 14*(3), 283-288

Human Rights Watch (HRW). (1992). Brazil Annual Report.(p.15). Human Rights Watch, New York. Retrieved October 15 2015 from: https://www.hrw.org/reports/1992/WR92/AMW-02.htm

Human Rights Watch (HRW). (2011). Hold Your Hearth: Waiting for Justice in Kenya's Mt. Elgon Region. (p. 66). Human Rights Watch, New York

Huang, W., Lamb, D.W., Niu, Z., Zhang, Y., Liu, L., & Wang, J. (2007). Identification of Yellow Rust in Wheat Using in-Situ Spectral Reflectance Measurements and Airborne Hyperspectral Imaging. *Precision Agriculture, 8*(4-5), 187-197

Huber, S., Kneubühler, M., Psomas, A., Itten, K., & Zimmermann, N.E. (2008). Estimating Foliar Biochemistry from Hyperspectral Data in Mixed Forest Canopy. *Forest Ecology and Management, 256*(3), 491-501

Huggins, R. (1985). Some Design Considerations for Undertaking a Magnetic Survey for Archaeological Resources. *Geophysics, 50*(2), 209-212

International Commision on Missing Persons (ICMP). (2001). Exhumations in Serbia. Belgrad. Retrieved May 2013 from: http://www.ic-mp.org/wp-content/uploads/2008/02/batajnica-2001-eng.pdf

International Commision on Missing Persons (ICMP). (2004). Batajnica Summary Report: Forensic Monitoring Activities. Sarajevo. Sarajevo. Retrieved May 15 2013 from: http://www.ic-mp.org/wp-content/uploads/2008/02/icmp-fsd-16-04-2-doc.pdf

Jessee, E. (2003). Exhuming Conflict: Some Recommentions for the Creation of a Series of Experimental Mass Grave and Mass-Grave Related Test Sites. (p. 150). Master of Arts Thesis, Simon Fraser University

Jessee, E., & Skinner, M. (2005). A Typology of Mass Grave and Mass Grave-Related Sites. *Forensic Science International, 152*(1), 55-59

Jones, H.G., & Vaughan, R.A. (2010). *Remote Sensing of Vegetation: Principles, Techniques, and Applications*. (pp. 36-76). New York: Oxford University Press

Juhl, K. (2005). The Contribution by Forensic Archaeologists to Human Rights Investigations of Mass Graves. (p. 67). Museum of Archaeology: Stavenger

Kabata-Pendias, A. (2010). *Trace Elements in Soils and Plants*. (pp. 93-122). Boca Raton, Florida: CRC press

Kabata-Pendias, A., & Mukherjee, A.B. (2007). *Trace Elements from Soil to Human*. (pp. 85-86). Berlin Heidelberg: Springer Science & Business Media

Kamcilla, P. and Mingoma, N. (2015). Mass Graves Found on KZN Farm. Retrieved October 15 from: http://beta.iol.co.za/news/crime-courts/mass-graves-found-on-kzn-farm-1832544

Kalacska, M., & Bell, L. (2006). Remote Sensing as a Tool for the Detection of Clandestine Mass Graves. *Canadian Society of Forensic Science Journal, 39*(1), 1-14

Kalacska, M., Lalonde, M., & Moore, T. (2015). Estimation of Foliar Chlorophyll and Nitrogen Content in an Ombrotrophic Bog from Hyperspectral Data: Scaling from Leaf to Image. *Remote Sensing of Environment, 169*, 270-279

Kalacska, M.E., Bell, L.S., Arturo Sanchez-Azofeifa, G., & Caelli, T. (2009). The Application of Remote Sensing for Detecting Mass Graves: An Experimental Animal Case Study from Costa Rica. *Journal of Forensic Sciences, 54*(1), 159-166

Killam, E.W. (2004). *The Detection of Human Remains*. (pp. 160-184). Springfield, Illinois: Charles C Thomas Publisher Ltd

Kim, D.S., & Pyen, M.W. (2011). Extraction of Changed Pixels for Hyperion Hyperspectral Images Using Range Average Based Buffer Zone Concept. *Journal of the Korean Society of Surveying Geodesy Photogrammetry and Cartography, 29*(5), 487-496

Knipling, E.B. (1970). Physical and Physiological Basis for the Reflectance of Visible and near-Infrared Radiation from Vegetation. *Remote Sensing of Environment, 1*(3), 155-159

Langner, H.R., Bottger, H., & Schmidt, H. (2006). A Special Vegetation Index for the Weed Detection in Sensor Based Precision Agriculture. *Environmental Monitoring and Assessment, 117*(1-3), 505-518

Larson, D.O., & Ambos, E.L. (1997). New Developments in Geophysical Prospecting and Archaeological Research: An Example from the Navan Complex, County Armagh, Northern Ireland. *Bulletin of the Society for American Archaeology, 15*(1), 10-14

Larson, D.O., Lipo, C.P., & Ambos, E. (2003). Application of Advanced Geophysical Methods and Engineering Principles in an Emerging Scientific Archaeology. *First Break, 21*, 51-62

Larson, D.O., Vass, A.A., & Wise, M. (2011). Advanced Scientific Methods and Procedures in the Forensic Investigation of Clandestine Graves. *Journal of Contemporary Criminal Justice, 27*(2), 149-182

Leblanc, G., Kalacska, M., & Soffer, R. (2014). Detection of Single Graves by Airborne Hyperspectral Imaging. *Forensic Science International, 245*, 17-23

Lichtenthaler, H.K. (1987). Chlorophylls and Carotenoids: Pigments of Photosynthetic Biomembranes. *Methods Enzymology, 148*, 350-382

Lobell, D.B., & Asner, G.P. (2003). Comparison of Earth Observing-1 Ali and Landsat Etm+ for Crop Identification and Yield Prediction in Mexico. *IEEE Transactions on Geoscience and Remote Sensing, 41*(6), 1277-1282

Looft, C. (2012). Honduras Officials Find Mass Grave, Suspect More Will be Found. Insight Crime: Investigation and Analysis of Organized Crime. Retrieved October 15 2015 from: http://www.insightcrime.org/news-briefs/honduras-officials-find-mass-grave-suspect-more-will-be-found

Malley, D.F., McClure, C., Martin, P.D., Buckley, K., & McCaughey, W.P. (2005). Compositional Analysis of Cattle Manure During Composting Using a Field-Portable near-Infrared Spectrometer. *Communications in Soil Science and Plant Analysis, 36*(4-6), 455-475

Mant, A.K. (1950). A Study in Exhumation Data. (p. 55). PhD Dissertation, University of London

Mant, A.K. (1987). Knowledge Acquired from Post-War Exhumations. In A.N. Garland, & R.C. Janaway (Eds.), *Death, Decay and Reconstruction: Approaches to Archaeology and Forensic Science* (pp. 65-78). Manchester: Manchester University Press

Marjanović, D., Durmić-Pašić, A., Kovačević, L., Avdić, J., Džehverović, M., Haverić, S., & Primorac, D. (2009). Identification of Skeletal Remains of Communist Armed Forces Victims During and After World War II: Combined Y-chromosome Short Tandem Repeat (STR) and MiniSTR Approach. *Forensic Science*, *50*(3), 296-304

Mathews, H., Cunningham, R., & Petersen, G. (1973). Spectral Reflectance of Selected Pennsylvania Soils. *Soil Science Society of America Journal, 37*(3), 421-424

Maynard, D.G., & Kalra, Y.P. (1993). Nitrate and Exchangeable Ammonium Nitrogen. In M.R. Carter (Ed.), *Soil Sampling and Methods of Analysis* (pp. 25-32). Boca Raton, Florida: Lewis Publishers

McLachlan, G.J., & Peel, D. (1998). Robust Cluster Analysis Via Mixtures of Multivariate T-Distributions. *Advances in Pattern Recognition* (pp. 658-666). Berlin: Springer

Melis, C., Selva, N., Teurlings, I., Skarpe, C., Linnell, J.C., & Andersen, R. (2007). Soil and Vegetation Nutrient Response to Bison Carcasses in Białowieża Primeval Forest, Poland. *Ecological Research, 22*(5), 807-813

Mellah, S. (2004). The Massacres in Algeria. (p. 65). Justice Commission for Algeria, Algeria Watch: Information on Junam Rights Situation in Algeria

Merton, R., & Huntington, J. (1999). Early Simulation Results of the Aries-1 Satellite Sensor for Multi-Temporal Vegetation Research Derived from Aviris. In, *Proceedings of the Eighth Annual JPL Airborne Earth Science Workshop* (pp. 8-14): NASA, JPL Pasadena, CA

Merzlyak, M.N., Gitelson, A.A., Chivkunova, O.B., & Rakitin, V.Y. (1999). Non-Destructive Optical Detection of Pigment Changes During Leaf Senescence and Fruit Ripening. *Physiologia Plantarum, 106*(1), 135-141

Meyer, J., Anderson, B., & Carter, D.O. (2013). Seasonal Variation of Carcass Decomposition and Gravesoil Chemistry in a Cold (Dfa) Climate. *Journal of Forensic Sciences, 58*(5), 1175-1182

Miller, J., Wu, J., Boyer, M., Belanger, M., & Hare, E. (1991). Seasonal Patterns in Leaf Reflectance Red-Edge Characteristics. *International Journal of Remote Sensing, 12*(7), 1509-1523

Miller, P.S. (1996). Disturbances in the Soil: Finding Buried Bodies and Other Evidence Using Ground Penetrating Radar. *Journal of Forensic Sciences, 41*(4), 648-652

Moore, I.D., Gessler, P., Nielsen, G., & Peterson, G. (1993). Soil Attribute Prediction Using Terrain Analysis. *Soil Science Society of America Journal, 57*(2), 443-452

Morton, R., J., & Lord, W., D. (2001). Detection and Recovery of Abducted and Murdered Children. In W.D. Haglund, & M.H. Sorg (Eds.), *Advances in Forensic Taphonomy: Method, Theory, and Archaeological Perspectives* (pp. 151-172). New York: CRC Press

Nagy, M.A. (2010). Environmental Factors Affecting an Experimental Low-Density Mass Grave near Edmonton, Alberta, Canada.(p. 181). Master of Science Thesis, University of Alberta

Nobes, D.C. (1999). Geophysical Surveys of Burial Sites: A Case Study of the Oaro Urupa. *Geophysics, 64*(2), 357-367

Nobes, D.C. (2000). The Search for" Yvonne": A Case Example of the Delineation of a Grave Using near-Surface Geophysical Methods. *Journal of Forensic Sciences, 45*(3), 715-721

Orengo, H.A. (2006). Detection of Body Dump Sites and Clandestine Burials: A Gis-Based Landscape Approach. In, *Digital Discovery, Exploring New Frontiers in Human Heritage. Computer Applications and Quantitative Methods in Archaeology. Proceedings of the 34th Conference, Fargo, United States* (pp. 185-190)

Peñuelas, J., & Filella, I. (1998). Visible and near-Infrared Reflectance Techniques for Diagnosing Plant Physiological Status. *Trends in Plant Science, 3*(4), 151-156

Penuelas, J., Filella, I., Lloret, P., Munoz, F., & Vilajeliu, M. (1995). Reflectance Assessment of Mite Effects on Apple Trees. *International Journal of Remote Sensing, 16*(14), 2727-2733

Perisset, M., & Tabbagh, A. (1981). Interpretation of Thermal Prospection on Bare Soils. *Archaeometry, 23*(2), 169-187

Physicians for Human Rights (PHR). (2008). Preliminary Assessment of Alleged Mass Graves in the Area of Mazar-I-Sharif, Afghanistan. (p. 16). Physicians for Human Rights, Boston: Washington DC

Powell, K.J. (2006). The Detection of Buried Human Skeletal Remains in the Australian Environment. Doctoral Dissertation, University of Adelaide

Price, J.C. (1994). How Unique Are Spectral Signatures? *Remote Sensing of Environment, 49*(3), 181-186

Primorac, D., Anđelinović, Š., Definis-Gojanović, M., & Drmić-Hofman, I. (1996). Identification of War Victims From Mass Graves in Croatia, Bosnia and Herzegovina by the Use of Standard Forensic Methods and DNA Typing. *Journal of forensic sciences*, *41*(5), 891-894

Pringle, J., Ruffell, A., Jervis, J., Donnelly, L., McKinley, J., Hansen, J., Morgan, R., Pirrie, D., & Harrison, M. (2012a). The Use of Geoscience Methods for Terrestrial Forensic Searches. *Earth-Science Reviews, 114*(1), 108-123

Pringle, J.K., Holland, C., Szkornik, K., & Harrison, M. (2012b). Establishing Forensic Search Methodologies and Geophysical Surveying for the Detection of Clandestine Graves in Coastal Beach Environments. *Forensic Science International, 219*(1–3), e29-e36

Pringle, J.K., & Jervis, J.R. (2010). Electrical Resistivity Survey to Search for a Recent Clandestine Burial of a Homicide Victim, Uk. *Forensic Science International, 202*(1–3), e1-e7

Pueschel, R.F., & Noll, K.E. (1967). Visibility and Aerosol Size Frequency Distribution. *Journal of Applied Meteorology, 6*(6), 1045-1052

Ramsey, G. (2011). Insight Map: Mexico's 'Narco-Graves'. Insight Crime: Investigation and Analysis of Organized Crime. Retrieved on October 15 2015 from: http://www.insightcrime.org/news-analysis/insight-map-mexicos-mass-graves-or-narcofosas

Raymond, N.A., Card, B.L., & Baker, I.L. (2014). A New Forensics: Developing Standard Remote Sensing Methodologies to Detect and Document Mass Atrocities. *Genocide Studies and Prevention: An International Journal, 8*(3), 33-48

Rebmann, A., & David, E. (2000). *Cadaver Dog Handbook: Forensic Training and Tactics for the Recovery of Human Remains*. Boca Raton, Florida: CRC Press

Reed Jr, H. (1958). A Study of Dog Carcass Communities in Tennessee, with Special Reference to the Insects. *American Midland Naturalist, 59*(1), 213-245

Ren, H.-Y., Zhuang, D.-F., Pan, J.-J., Shi, X.-Z., & Wang, H.-J. (2008). Hyper-Spectral Remote Sensing to Monitor Vegetation Stress. *Journal of Soils and Sediments, 8*(5), 323-326

Rouse Jr, J.W., Haas, R., Schell, J., & Deering, D. (1974). Monitoring Vegetation Systems in the Great Plains with Erts. In S.C. Freden, E.P. Mercanti, & M.A. Becker (Eds.), *Third Earth Resources Technology Satellite-1 Symposium- Volume I: Technical Presentations*: NASA Special Publication

Ruffell, A., & McKinley, J. (2005). Forensic Geoscience: Applications of Geology, Geomorphology and Geophysics to Criminal Investigations. *Earth-Science Reviews, 69*(3–4), 235-247

Ruffell, A., & McKinley, J. (2008). *Geoforensics*. Belfast, UK: John Wiley & Sons Ltd

Schmitt, S. (2001). Mass Graves and the Collection of Forensic Evidence: Genocide, War Crimes, and Crimes against Humanity. In W.D. Haglund, & M.H. Sorg (Eds.), *Advances in Forensic Taphonomy: Method, Theory, and Archaeological Perspectives* (pp. 277-292). New York: CRC Press

Schut, L.W., & Wilson, E.A. (1987). *Soils of the Regional Municipality of Ottawa-Carleton (Excluding the Ottawa Urban Fringe)*. Ottawa: Ministry of Agriculture and Food, Agriculture Canada

Secker, J., Staenz, K., Gauthier, R.P., & BudkewitSch, P. (2001). Vicarious Calibration of Airborne Hyperspectral Sensors in Operational Environments. *Remote Sensing of Environment, 76*(1), 81-92

Signoli, M., Ardagna, Y., Adalian, P., Devriendt, W., Lalys, L., Rigeade, C., Vette, T., Kuncevicius, A., Poskiene, J., & Barkus, A. (2004). Discovery of a Mass Grave of Napoleonic Period in Lithuania (1812, Vilnius). *Comptes Rendus Palevol, 3*(3), 219-227

Simmons, T. (2001). Taphonomy of a Karstic Cave Execution Site at Hrgar, Bosnia-Herzegovina. In W.D. Haglund, & M.H. Sorg (Eds.), *Advances in Forensic Taphonomy : Method, Theory, and Archaeological Perspectives* (pp. 263-276). New York: CRC Press

Simmons, T., Adlam, R.E., & Moffatt, C. (2010). Debugging Decomposition Data—Comparative Taphonomic Studies and the Influence of Insects and Carcass Size on Decomposition Rate. *Journal of Forensic Sciences, 55*(1), 8-13

Skinner, M. (1987). Planning the Archaeological Recovery of Evidence from Recent Mass Graves. *Forensic science international, 34*(4), 267-287

Skinner, M.F., York, H.P., & Connor, M.A. (2001). Postburial Disturbance of Graves in Bosnia-Herzegovina. In W.D. Haglund, & M.H. Sorg (Eds.), *Advances in Forensic Taphonomy: Method, Theory, and Archaeological Perspectives* (pp. 293-308). New York: CRC Press

Snirer, E. (2014). Hyperspectral Remote Sensing of Individual Gravesites – Exploring the Effects of Cadaver Decomposition on Vegetation and Soil Spectra. (p. 148). Master of Science Thesis, McGill University

Solberg, S., Næsset, E., Lange, H., & Bollandsås, O.M. (2004). Remote Sensing of Forest Health. In M. Thies, B. Koch, H. Spiecker, & H. Weinacke (Eds.), *Laser-Scanners for Forest and Landscape Assessment* (pp. 161-166). Freiburg, Germany: International Archives of Photogrammetry, Remote Sensing and Spatial Information

Stadler, S., Stefanuto, P.-H., Brokl, M., Forbes, S.L., & Focant, J.-F.o. (2012). Characterization of Volatile Organic Compounds from Human Analogue Decomposition Using Thermal Desorption Coupled to Comprehensive Two-Dimensional Gas Chromatography–Time-of-Flight Mass Spectrometry. *Analytical Chemistry, 85*(2), 998-1005

Statheropoulos, M., Agapiou, A., Spiliopoulou, C., Pallis, G., & Sianos, E. (2007). Environmental Aspects of Vocs Evolved in the Early Stages of Human Decomposition. *Science of the Total Environment, 385*(1), 221-227

Statheropoulos, M., Spiliopoulou, C., & Agapiou, A. (2005). A Study of Volatile Organic Compounds Evolved from the Decaying Human Body. *Forensic Science International, 153*(2), 147-155

Sterenberg, J. (2002). Archaeological Techniques and Methods for the Excavation and Recording of Contemporary Primary and Secondary Mass Graves. (p. 125). Master of Science Thesis, Bournemouth University

Stokes, K., Forbes, S., Benninger, L., Carter, D., & Tibbett, M. (2009). Decomposition Studies Using Animal Models in Contrasting Environments: Evidence from Temporal Changes in Soil Chemistry and Microbial Activity. In K. Ritz, L. Dawson, & D. Miller (Eds.), *Criminal and Environmental Soil Forensics* (pp. 357-377): Springer Netherlands

Stokes, K.L., Forbes, S.L., & Tibbett, M. (2013). Human Versus Animal: Contrasting Decomposition Dynamics of Mammalian Analogues in Experimental Taphonomy. *Journal of Forensic Sciences, 58*(3), 583-591

Stoll, D. (2004). Guatemala. In D.L. Shelton, H. Adelman, F. Chalk, A. Kiss, & W.A. Schabas (Eds.), *Encyclopedia of Genocide and Crimes Against Humanity* (pp. 419-422). New York: Macmillan Reference, Thomson Gale

Stylinski, C., Gamon, J., & Oechel, W. (2002). Seasonal Patterns of Reflectance Indices, Carotenoid Pigments and Photosynthesis of Evergreen Chaparral Species. *Oecologia, 131*(3), 366-374

Summers, D., Lewis, M., Ostendorf, B., & Chittleborough, D. (2011). Visible near-Infrared Reflectance Spectroscopy as a Predictive Indicator of Soil Properties. *Ecological Indicators, 11*(1), 123-131

Tainter, J.A. (1978). Mortuary Practices and the Study of Prehistoric Social Systems. *Advances in Archaeological Method and Theory, 1*, 105-141

Tans, P., & NOAA/ESRL (2015). Esrl Global Monitoring Division – Global Greenhouse Gas Reference Network. Retrieved on January 10 2015 from: http://www.esrl.noaa.gov/gmd/ccgg/trends/ - mlo_data

Tibbett, M., & Carter, D. (2009). Research in Forensic Taphonomy: A Soil-Based Perspective. In K. Ritz, L. Dawson, & D. Miller (Eds.), *Criminal and Environmental Soil Forensics* (pp. 317-331): Springer Netherlands

Tibbett, M., Carter, D.O., Haslam, T., Major, R., & Haslam, R. (2004). A Laboratory Incubation Method for Determining the Rate of Microbiological Degradation of Skeletal Muscle Tissue in Soil. *Journal of Forensic Sciences, 49*(3), 560-565

Tran, S.T., & Simard, R.R. (1993). Mehlich III – Extractable Elements. In M.R. Carter (Ed.), *Soil Sampling and Methods of Analysis* (pp. 43-49). Boca Raton, Florida: Lewis Publishers

Tucker, C.J. (1979). Red and Photographic Infrared Linear Combinations for Monitoring Vegetation. *Remote Sensing of Environment, 8*(2), 127-150

Tumer, A.R., Karacaoglu, E., Namli, A., Keten, A., Farasat, S., Akcan, R., Sert, O., & Odabaşi, A.B. (2013). Effects of Different Types of Soil on Decomposition: An Experimental Study. *Legal Medicine, 15*(3), 8

Turner, W., Spector, S., Gardiner, N., Fladeland, M., Sterling, E., & Steininger, M. (2003). Remote Sensing for Biodiversity Science and Conservation. *Trends in Ecology & Evolution, 18*(6), 306-314

United Nations (UN). (1999). Situation of Human Rights in Somalia. Forensic Report: Preliminary Assessment of Mass Graves in the Vicinity of Hargeisa, Somalia. (p. 16). Economic and Social Council of United Nations: Commision on Human Rights, Geneva

United Nations (UN). (2005). Report of the International Commission of Inquiry on Darfur 2005. Pursuant to Security Council Resolution 1564. (p. 176). United Nations, Geneva

United Nations (UN). (2010). Report of the Mapping Exercise Documenting the Most Serious Violations of Human Rights and International Humanitarian Law Committed within the Territory of the Democratic Republic of the Congo between March 1993 and June 2003. (p. 575). United Nations, Geneva

United Nations (UN). (2014). Report on the Human Rights Situation in Ukraine. (p. 49). Office of the United Nations: High Commissioner for Human Rights, Geneva

Vass, A.A., Smith, R.R., Thompson, C.V., Burnett, M.N., Dulgerian, N., & Eckenrode, B.A. (2008). Odor Analysis of Decomposing Buried Human Remains. *Journal of Forensic Sciences, 53*(2), 384-391

Vass, A.A., Smith, R.R., Thompson, C.V., Burnett, M.N., Wolf, D.A., Synstelien, J.A., Dulgerian, N., & Eckenrode, B.A. (2004). Decompositional Odor Analysis Database. *Journal of Forensic Sciences, 49*(4), 760-769

Vaughan, C.J. (1986). Ground-Penetrating Radar Surveys Used in Archaeological Investigations. *Geophysics, 51*(3), 595-604

Vogelmann, J., Rock, B., & Moss, D. (1993). Red Edge Spectral Measurements from Sugar Maple Leaves. *Remote Sensing, 14*(8), 1563-1575

Williams, C.A. (2009). Exile History: An Ethnography of the Swapo Camps and the Namibian Nation. (p. 353). Doctoral Dissertation, University of Michigan

Wilson, A.S., Janaway, R.C., Holland, A.D., Dodson, H.I., Baran, E., Pollard, A.M., & Tobin, D.J. (2007). Modelling the Buried Human Body Environment in Upland Climes Using Three Contrasting Field Sites. *Forensic Science International, 169*(1), 6-18

Wilson, D.R. (1982). *Air Photo Interpretation for Archaeologists*. (p. 256). London: Batsford

Wright, R., Hanson, I., & Sterenberg, J. (2005). The Archaeology of Mass Graves. In J. Hunter, & M. Cox (Eds.), *Forensic Archaeology: Advances in Theory and Practice* (pp. 137-158). New York: Routledge: Taylor & Francis Group

Wulder, M.A., Dymond, C.C., White, J.C., Leckie, D.G., & Carroll, A.L. (2006). Surveying Mountain Pine Beetle Damage of Forests: A Review of Remote Sensing Opportunities. *Forest Ecology and Management, 221*(1), 27-41

Wynn, J.C. (1986). A Review of Geophysical Methods Used in Archaeology. *Geoarchaeology, 1*(3), 245-257

Yang, C.C., Prasher, S.O., & Goel, P.K. (2004). Differentiation of Crop and Weeds by Decision-Tree Analysis of Multi-Spectral Data. *Transactions of the ASEA, 47*(3), 873-879

Zarco-Tejada, P.J., Miller, J., Mohammed, G., Noland, T., & Sampson, P. (2002). Vegetation Stress Detection through Chlorophyll A + B Estimation and Fluorescence Effects on Hyperspectral Imagery. *Journal of environmental quality, 31*(5), 1433-1441

Zwiggelaar, R. (1998). A Review of Spectral Properties of Plants and Their Potential Use for Crop/Weed Discrimination in Row-Crops. *Crop Protection, 17*(3), 189-206

Żychowski, J. (2011). Geological Aspects of Decomposition of Corpses in Mass Graves from WWI and WWII, Located in SE Poland. *Environmental Earth Sciences, 64*(2), 437-448

Appendix A

Table A.1. Table summarizing mass graves characteristics found across the literature. Location and number of victims displayed in Figure 2.1.

Country	Site Location	Site size (width x length x depth)	Number of individuals	Other characteristics*	Reference
Bosnia and Herzegovina	Tavoscici		30		Skinner et al. (2001)
	Batkovic Prison Camp, Bijeljina	50 m x 10 m	15	Mass density of 2.12 kg/m^2	Danis Jr et al. (1992)
	Blagaj, Bosanski Novi	2 sites, 2 m apart : 100 m x 50 cm x 1 m	200	Mass density of 14.16 kg/m^2	
	Bimex Agricuiltural Complex, Brcko	30 m x 3m/4m x 2 m	200	Mass density of 78.66 kg/m^2	
	Prhovo, Kljuc	3 m x 4 m x 2.5 m	200	Mass density of 472 kg/m^2	
	Velagici	20 m x 30 m	282	Mass density of 33.28 kg/m^2	
	Marino Selo, Pakrac	3m x 2m x 1.5 m	12	Mass density of 94.40 kg/m^2	
	Pakracka Poljana site B	1.5 m x 1.8 m	unknown		
	Pakracka Poljana site C	4 m x 20 m	19	Mass density of 22.42 kg/m^2	
	Open Pit Mine, Stara Cesta Road, Ljubija	12 m diameter x 6 m	20 to 25	Mass density of 19.66 kg/m2 to 24.58 kg/m^2	
	Redak & Kruska Pits	2 x (3 m x 3 m x 2.5 m)	200	Mass density of 314.66 kg/m^2	
	Stara Rijeka	4 m x 2.5 m	9	Mass density of 63.72 kg/m^2	
Somalia	Milk Factory site, Hargeisa	3.5-6m x 2-3m x 1m	5	Minimum of 40 mass graves	UN (1999)
	Malko Durduro	8m x 2.5-3m x 70 cm	3	Minimum of 15 to 20 mass graves located in the area	
	Badhka site	3.5 m x 2.5 m x 1m	2	29 mass graves 10 mass graves intermingled with formal cultural graves	

Table Continued.

Country	Site Location	Site size (width x length x depth)	Number of individuals	Other characteristics*	Reference
Croatia	Dalmatian hinterland, near the village of Zagvozd	4 m x 3.10 m x 0.32 m	18 complete skeletons	Artifacts found	Gojanović and Sutlović (2007)
	Vukovar, the Ovcara grave		264	Mass density of 102.77 kg/m^2	Haglund et al. (2001a)
East Timor	Hera, Dili	7.5 m x 9m x 1.8 m	25	Mass density of 11.83 kg/m^2	Blau and Skinner (2005)
Former Yugoslavia	Srebrenica	> 39 mass graves: 17 fully excavated	>6000		Jessee (2003)
Guatemala	Chichupac	Site II: 2.7 m x 1.35 m Site III: 1.3 m x 1.8 m Depth: 90 cm to 125 cm	Site I: 3 individuals Site II: 13 individuals Site III: 14 individuals		Schmitt (2001)
Iraqui Kurdistan		2 mass grave sites	27 individuals executed by firing squad	Bodies were prepared and wrapped in burial shroud according to Muslim custom and buried in a mass grave by surviving relatives	Jessee (2003)
Lithuania	Vilnus	Site 1: 10 m (6 m SW and 8m NE) x 40 m (39 – 42 m) x 1 -1.5 m Site 2: 6 m x 30 m x 3m (skeletons appeared at a depth of 2 m) Site 3: not stated	Area 1: 886 Area 2: 979 Area 3:1000 44 non-attributed Total number of individuals: 3269	Based on femoral diaphysis Bodies in close contact Individuals buried at the same time Mass density of 156.82 kg/m^2 for site no. 1 and 256.72 kg/m^2 for site no. 2	Signoli et al. (2004)
Rwanda	Roman Catholic Church site near Kibuye	The bottom of the grave was trenched 40-80 cm below the last remains	53 skeletons complete individuals and isolated bones 493 individuals		Haglund et al. (2001a)
Ukraine	Sernyky	60 m x 5 m x 2 m with a ramp descending from the eastern wall	July – August 1941: 100 August 1942: 850	Bodies were placed orderly and face down in the northern extent of the site and disorganized in the southern extent of the site	Jessee and Skinner (2005)
USA	Crow Creek Massacre site, South Dakota	6.6 m x 6 m x 1 m	500 commingled skeletons		Skinner (1987)

Table Continued.

Country	Site Location	Site size (width x length x depth)	Number of individuals	Other characteristics*	Reference
Poland	Blonie	30 m x 100 m	312	Mass density of 7.71 kg/m^2	Żychowski (2011)
	Bochnia	30 m x 22 m	417	Mass density of 46.82 kg/m^2	
	Brzesko	70 m x 45 m	507	Mass density of 11.93 kg/m^2	
	Niepolomice	20 m x 10 m	700	Mass density of 259.35 kg/m^2	
	Nowy Sacz	10 m x 20 m	400	Mass density of 148 kg/m^2	
	Rajbrot	60 m x 30 m	530	Mass density of 21.82 kg/m^2	
	Barwinek	5 m x 26 m	500	Mass density of 272.31 kg/m^2	
Serbia	Barajnica1	3 m x 3 m x 2m	36	Mass density of 148.2 kg/m^2	ICMP (2001)
	Petrovo Selo 1	3 m x 3m x 3.5 m	16	Mass density of 37.64 kg/m^2	ICMP (2004)
	Petrovo Selo 2	3 m x 3m x 1.5 m	59	Mass density of 323.84 kg/m^2	
	Barajnica 2	15 m x 10 m x 2.8 m	Min of 269	Mass density of 47.46 kg/m^2	
	Derventa Canyon	4 m x 6 m x 1.5 m	min of 48	Mass density of 98.80 kg/m^2	
	Batajnica 3	16.7 m x 2.8 m x 2.5 m	39	Mass density of 24.72 kg/m^2	
	Batajnica 5	25 m x 2.8/2.9 m x 1.5/2m	287	Mass density of 202.54 kg/m^2	
Germany	Hassee, Kiel	3 m x 3 m x 6 m	46	Mass density of 60.31 kg/m^2	Mant (1950)
Argentina	Cordoba	Between 2 and 3 m in diameter, 3 m depth	Between 9 and 28 per site	11 single graves 19 mass graves	Fondebrider and Doretti (2004)

Table A.2. Table of countries and number of victims found in mass graves reported across the literature. Mass graves locations and numbers of victims are displayed in in Figure 2.1.

Country	Site location	Number of Victims	Reference
Guatemala	Los Dos Erres	350	AMR (1998)
Guatemala	Agua Fria	100	AMR (1998)
Guatemala	Panzos	36	AMR (1998)
Guatemala	Cuarto Pueblo	300	AMR (1998)
Guatemala	Parraxtut	300	AMR (1998)

Table Continued.

Country	Site location	Number of victims	Reference
Guatemala	San Francisco	320	AMR (1998)
Bosnia and Herzegovina	Kamenica	616	AMR (2008)
Colombia	Bogota	100	AMR (2008)
India	Baramulla	1051	AMR (2008)
Guatemala	Rio Negro	444	AMR (2002)
Congo	Kasese	200	UN (2010)
Congo	Baraka	3	UN (2010)
Congo	Kamituga	12	UN (2010)
Congo	Bukavu	100	UN (2010)
Congo	Katala	100	UN (2010)
Congo	Luvungi	20	UN (2010)
Congo	Luberizi	370	UN (2010)
Congo	Luberizi	220	UN (2010)
Congo	Bwegera	72	UN (2010)
Congo	Ngendo	100	UN (2010)
Congo	Sange	13	UN (2010)
Congo	Ruzia	600	UN (2010)
Congo	Mpwe	180	UN (2010)
Congo	Kigulube	200	UN (2010)
Congo	Mugunga	40	UN (2010)
Congo	Pangi	200	UN (2010)
Congo	Wanie Rukula	470	UN (2010)
Congo	Obilo	80	UN (2010)
Congo	Biaro	100	UN (2010)
Congo	Mbandaka	200	UN (2010)
Congo	Tebero	760	UN (2010)
Congo	Kinigi	310	UN (2010)
Congo	Kausa	460	UN (2010)
Congo	Nyakariba	160	UN (2010)
Congo	Muheto	50	UN (2010)
Congo	Kyavinyonge	184	UN (2010)
Congo	Kidoti	50	UN (2010)
Congo	Kaziba	36	UN (2010)
Congo	Uvira	126	UN (2010)
Congo	Vabesu	7	UN (2010)
Somalia	Hargeisa	190	UN (1999)
El Salvador	El Mozote	767	Juhl (2005)
El Salvador	Los Toriles	22	Juhl (2005)
Iraqi Kurdistan	Koreme	27	Juhl (2005)

Table Continued.

Country	Site location	Number of victims	Reference
Germany	Bergen-Belsen	23200	Bergen-Belsen (2015)
Iraq	Al-Basrah	200	Barber and Epstein (2004)
Chile	Lonquen	15	Wilson et al. (2009)
South Korea	Jeju	100	Wilson et al. (2009)
Greece	Lesvos	13	Wilson et al. (2009)
Zimbabwe	Harare	640	Daily Mail (2011)
Rwanda	Kibuye	454	Juhl (2005)
Iraq	Iraq	3000	Juhl (2005)
Iraq	Al-Mahawi	2500	Bouckaer (2003)
Iraq	Al-Hillah	40	Barber and Epstein (2004)
Sudan	Molli, Gharb Darfur	64	UN (2005)
Sudan	Nurei, Gharb Darfur	67	UN (2005)
Sudan	Mallaga, Gharb Darfur	18	UN (2005)
Sudan	Kulbus	59	UN (2005)
Ukraine	Donetsk	9	UN (2014)
Ukraine	Sloviansk	12	UN (2014)
Ukraine	Mykolaivka	3	UN (2014)
Afghanistan	Mazar-I-Sharif	500	PHR (2008)
Afghanistan	Mazar-I-Sharif	10	PHR (2008)
Afghanistan	Mazar-I-Sharif	50	PHR (2008)
Afghanistan	Mazar-I-Sharif	4	PHR (2008)
Afghanistan	Mazar-I-Sharif	80	PHR (2008)
Afghanistan	Mazar-I-Sharif	70	PHR (2008)
Afghanistan	Mazar-I-Sharif	30	PHR (2008)
Mexico	Tlalmanalco	12	BDHRL (2013)
Mexico	Iguala	28	Ramsey (2015)
Mexico	Chihuahua	20	Ramsey (2015)
Mexico	Sonora	5	Ramsey (2015)
Mexico	Juarez_Nuevo_Leon	73	Ramsey (2015)
Mexico	Tamaulipas	217	Ramsey (2015)
Mexico	Mazatlan	9	Ramsey (2015)
Mexico	Santa Maria	4	Ramsey (2015)
Mexico	Morelos	12	Ramsey (2015)
Mexico	Morelos	55	Ramsey (2015)
Mexico	Guerrero	129	Ramsey (2015)
Mexico	Tunzingo	18	Ramsey (2015)
Mexico	Durango	50	Aljazeera (2011)
Venezuela	Tachira	12	Gagne (2015)
Honduras	Tela	25	Looft (2012)

Table Continued.

Country	Site location	Number of victims	Reference
Sierra Leone	Katombo	10	Christodulou (2004)
Sierra Leone	Koinadugu	18	Christodulou (2004)
Sierra Leone	Lengekoro	9	Christodulou (2004)
Sierra Leone	Falaba	8	Christodulou (2004)
Sierra Leone	Mogbomo	18	Christodulou (2004)
Sierra Leone	Bendu Malen	264	Christodulou (2004)
Sierra Leone	æSahn Malen	36	Christodulou (2004)
Cambodia	La-ang Phnom Kuoy Yum	100	CGCAM (2015)
Cambodia	Chamkar Ta Ling	660	CGCAM (2015)
Cambodia	Tuol Roung Chrey	400	CGCAM (2015)
Cambodia	Wat Samrong	1008	CGCAM (2015)
Cambodia	Tuol Ta San	20	CGCAM (2015)
Cambodia	Prey Roung Khla	10	CGCAM (2015)
Cambodia	Koh Sleng	2000	CGCAM (2015)
Cambodia	Phnom Daun Penh	7000	CGCAM (2015)
Cambodia	Wat Tuo	600	CGCAM (2015)
Cambodia	Prey Sokhon	12000	CGCAM (2015)
Bolivia	Vallegrande	7	EAAF (1997)
Bolivia	Potosi	400	Aljazeera (2014)
Brazil	Perus	1048	HRW (1992)
Kenya	Kilelengwani	38	HRW (2011)
Kenya	Mt_Elgon	1074	Aljazeera (2012)
Nigeria	Chibok	640	AMR (2015)
Bosnia	Tomasica	435	AMR (2015)
Pakistan	Totak_Balochistan	100	AMR (2015)
Cyprus	Cyprus	564	AMR (2015)
Serbia	Raska	53	AMR (2015)
Slovenia	Lovrenska	11	Marjanovic et al. (2009)
Bosnia	Kupres	61	Primorac et al. (1996)
Namibia	Oshana	3	EAAF (2006)
Angola	Cassinga	400	Williams (2009)
South Africa	Dududu	100	Kamcilla and Mingoma (2015)
Algeria	Setif	10000	Mellah (2004)
Mali	Diago	21	Aljazeera (2013)
Nigeria	Kaleri	100	AMR (2014b)

Appendix B

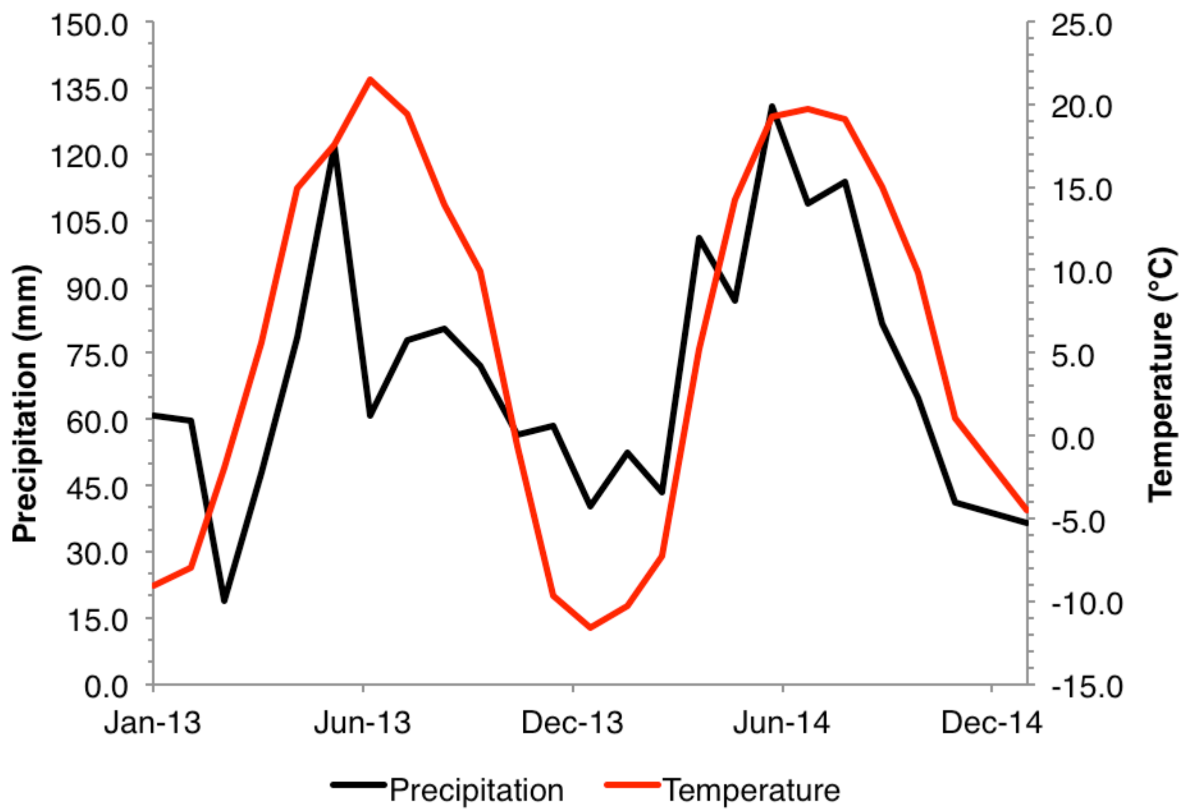

Figure B.1. Recorded average monthly precipitation (mm) and temperature (°C) at the nearby MacDonald Cartier International Airport, Ottawa, ON, over the study period. Records retrieved from Environment Canada database (Environment Canada 2015).

Appendix C

Table C.1. Mean (μ) and standard deviation (σ) of the vegetation indices computed of the leaf spectral reflectance collected two weeks post disturbance on August 13th, 2013.

Index	Control		Grave		Gap		Reference	
	μ	**σ**	**μ**	**σ**	**μ**	**σ**	**μ**	**σ**
NDPI*	-0.01	0.04	-0.06	0.03	-0.07	0.01	-0.02	0.02
NDVI1	0.67	0.05	0.73	0.04	0.69	0.08	0.78	0.04
NDVI2	0.68	0.04	0.73	0.04	0.69	0.08	0.78	0.04
PSRI	-0.22	0.03	-0.19	0.02	-0.18	0.03	-0.18	0.02
RENDVI	0.42	0.04	0.53	0.04	0.52	0.07	0.56	0.02
REP	0.23	0.02	0.34	0.04	0.35	0.01	0.36	0.04
RVSI	0.21	0.02	0.31	0.04	0.32	0.02	0.33	0.03
SGI	0.09	0.01	0.11	0.01	0.12	0.03	0.10	0.01
SIPI*	0.99	0.02	0.98	0.01	0.97	0.02	0.99	0.01
VOG1	1.26	0.05	1.41	0.07	1.44	0.09	1.43	0.05
VOG2	0.65	0.03	0.73	0.04	0.75	0.05	0.74	0.02

*Significant differences between grave and reference (Wilcoxon rank sum, α=0.05).

Table C.2. Mean (μ) and standard deviation (σ) of the vegetation indices of the leaf spectral reflectance collected on September 13th, 2013.

Index	Control		Grave		Gap		Reference	
	μ	**σ**	**μ**	**σ**	**μ**	**σ**	**μ**	**σ**
NDPI*	-0.12	0.04	-0.06	0.03	-0.02	0.04	-0.11	0.03
NDVI1*	0.73	0.04	0.71	0.05	0.68	0.08	0.75	0.02
NDVI2*	0.74	0.04	0.71	0.04	0.68	0.08	0.75	0.02
PSRI	-0.29	0.01	-0.18	0.04	-0.21	0.05	-0.20	0.03
RENDVI	0.42	0.05	0.53	0.06	0.43	0.07	0.51	0.02
REP*	0.37	0.04	0.35	0.02	0.17	0.06	0.39	0.02
RVSI*	0.35	0.06	0.32	0.02	0.16	0.05	0.37	0.02
SGI	0.15	0.03	0.12	0.02	0.06	0.02	0.13	0.00
SIPI*	0.95	0.02	0.97	0.01	0.99	0.02	0.96	0.01
VOG1*	1.26	0.06	1.48	0.13	1.33	0.09	1.40	0.05
VOG2*	0.65	0.03	0.77	0.07	0.69	0.05	0.72	0.03

*Significant differences between grave and reference (Wilcoxon rank sum, α=0.05).

Table C.3. Mean (μ) and standard deviation (σ) of the vegetation indices of leaf spectral reflectance collected on October 18th, 2013.

Index	Control		Grave		Gap		Reference	
	μ	**σ**	**μ**	**σ**	**μ**	**σ**	**μ**	**σ**
NDPI	-0.09	0.01	-0.05	0.04	-0.04	0.03	-0.04	0.03
NDVI1	0.66	0.09	0.65	0.06	0.71	0.05	0.68	0.04
NDVI2	0.67	0.08	0.68	0.06	0.72	0.05	0.69	0.04
PSRI	-0.26	0.01	-0.28	0.04	-0.23	0.04	-0.22	0.04
RENDVI*	0.40	0.07	0.39	0.04	0.45	0.05	0.44	0.04
REP*	0.25	0.05	0.37	0.02	0.39	0.04	0.41	0.05
RVSI*	0.23	0.04	0.35	0.02	0.36	0.04	0.38	0.04
SGI	0.10	0.01	0.16	0.02	0.14	0.02	0.15	0.02
SIPI	0.95	0.02	0.97	0.02	0.98	0.02	0.98	0.02
VOG1*	1.25	0.05	1.24	0.05	1.30	0.07	1.31	0.05
VOG2*	0.64	0.03	0.63	0.03	0.67	0.04	0.67	0.03

*Significant differences between grave and reference (Wilcoxon rank sum, α=0.05).

Table C.4. Mean (μ) and standard deviation (σ) of the vegetation indices of the leaf spectral reflectance collected on November 8th, 2013.

Index	Control		Grave		Gap		Reference	
	μ	**σ**	**μ**	**σ**	**μ**	**σ**	**μ**	**σ**
NDPI	-0.09	0.03	-0.03	0.08	0.02	0.05	-0.01	0.09
NDVI1	0.68	0.05	0.72	0.04	0.74	0.04	0.73	0.04
NDVI2	0.69	0.05	0.73	0.04	0.75	0.03	0.74	0.03
PSRI	-0.05	0.01	-0.02	0.02	-0.01	0.01	-0.02	0.02
RENDVI	0.39	0.03	0.43	0.04	0.44	0.04	0.45	0.04
REP	0.18	0.02	0.22	0.07	0.26	0.06	0.27	0.05
RVSI	0.26	0.04	0.32	0.11	0.37	0.09	0.39	0.08
SGI	0.11	0.01	0.11	0.03	0.13	0.03	0.14	0.03
SIPI	0.95	0.02	0.98	0.03	1.01	0.02	0.99	0.03
VOG1	1.25	0.03	1.28	0.04	1.27	0.04	1.31	0.06
VOG2	0.64	0.02	0.65	0.02	0.65	0.02	0.67	0.04

*Significant differences between grave and reference (Wilcoxon rank sum, α=0.05).

Table C.5. Mean (μ) and standard deviation (σ) of the vegetation indices of the leaf spectral reflectance collected on May 29th, 2014.

Index	Control		Grave		Gap		Reference	
	μ	**σ**	**μ**	**σ**	**μ**	**σ**	**μ**	**σ**
NDPI	-0.06	0.05	-0.09	0.03	-0.07	0.02	-0.08	0.03
NDVI1	0.72	0.04	0.79	0.03	0.79	0.03	0.76	0.05
NDVI2	0.73	0.03	0.78	0.03	0.80	0.02	0.76	0.05
PSRI	-0.24	0.05	-0.20	0.04	-0.22	0.04	-0.22	0.04
RENDVI*	0.46	0.05	0.54	0.04	0.54	0.04	0.51	0.06
REP*	0.36	0.06	0.36	0.04	0.40	0.01	0.40	0.02
RVSI*	0.33	0.05	0.33	0.03	0.37	0.01	0.37	0.02
SGI*	0.13	0.02	0.11	0.02	0.12	0.01	0.13	0.02
SIPI	0.97	0.02	0.97	0.01	0.98	0.01	0.97	0.02
VOG1	1.30	0.07	1.40	0.06	1.40	0.07	1.37	0.08
VOG2	0.67	0.04	0.72	0.03	0.72	0.04	0.71	0.05

*Significant differences between grave and reference (Wilcoxon rank sum, α=0.05).

Table C.6. Mean (μ) and standard deviation (σ) of the vegetation indices of the leaf spectral reflectance collected on June 19th, 2014.

Index	Control		Grave		Gap		Reference	
	μ	**σ**	**μ**	**σ**	**μ**	**σ**	**μ**	**σ**
NDPI*	-0.04	0.05	-0.08	0.04	-0.05	0.02	-0.03	0.03
NDVI1*	0.73	0.02	0.78	0.02	0.79	0.02	0.80	0.02
NDVI2*	0.74	0.02	0.78	0.02	0.80	0.02	0.79	0.02
PSRI	-0.25	0.04	-0.19	0.04	-0.20	0.04	-0.18	0.03
RENDVI	0.45	0.04	0.54	0.04	0.54	0.03	0.55	0.04
REP	0.39	0.01	0.38	0.02	0.38	0.01	0.39	0.02
RVSI	0.37	0.01	0.35	0.02	0.35	0.01	0.36	0.02
SGI	0.15	0.01	0.11	0.02	0.11	0.01	0.11	0.02
SIPI*	0.98	0.02	0.98	0.02	0.99	0.01	0.99	0.01
VOG1	1.29	0.05	1.41	0.07	1.40	0.06	1.44	0.08
VOG2	0.66	0.03	0.73	0.04	0.72	0.03	0.75	0.04

*Significant differences between grave and reference (Wilcoxon rank sum, α=0.05).

Table C.7. Mean (μ) and standard deviation (σ) of the vegetation indices of the leaf spectral reflectance collected on July 25th, 2014.

Index	Control		Grave		Gap		Reference	
	μ	**σ**	**μ**	**σ**	**μ**	**σ**	**μ**	**σ**
NDPI	0.03	0.04	-0.07	0.03	-0.06	0.04	-0.05	0.06
NDVI1*	0.71	0.06	0.78	0.03	0.78	0.03	0.75	0.04
NDVI2*	0.74	0.04	0.77	0.02	0.77	0.02	0.75	0.03
PSRI*	-0.02	0.01	-0.16	0.04	-0.18	0.04	-0.21	0.04
RENDVI*	0.39	0.08	0.56	0.05	0.54	0.05	0.50	0.05
REP*	0.19	0.03	0.36	0.02	0.39	0.01	0.38	0.02
RVSI*	0.28	0.05	0.33	0.02	0.36	0.01	0.35	0.02
SGI*	0.11	0.03	0.10	0.02	0.11	0.02	0.12	0.02
SIPI	1.01	0.01	0.98	0.01	0.98	0.02	0.98	0.02
VOG1*	1.23	0.08	1.44	0.08	1.42	0.07	1.36	0.07
VOG2*	0.63	0.05	0.75	0.04	0.73	0.04	0.70	0.04

*Significant differences between grave and reference (Wilcoxon rank sum, α=0.05).

Table C.8. Mean (μ) and standard deviation (σ) of the vegetation indices of the leaf spectral reflectance collected on August 21st, 2014.

Index	Control		Grave		Gap		Reference	
	μ	**σ**	**μ**	**σ**	**μ**	**σ**	**μ**	**σ**
NDPI	0.07	0.03	-0.02	0.05	-0.03	0.06	0.01	0.05
NDVI1	0.76	0.05	0.80	0.03	0.80	0.04	0.79	0.04
NDVI2	0.77	0.02	0.78	0.03	0.78	0.03	0.78	0.04
PSRI*	-0.24	0.08	-0.15	0.03	-0.17	0.04	-0.20	0.03
RENDVI*	0.46	0.10	0.57	0.03	0.56	0.05	0.52	0.04
REP	0.38	0.02	0.36	0.01	0.35	0.02	0.36	0.01
RVSI	0.35	0.02	0.33	0.01	0.32	0.02	0.34	0.01
SGI*	0.12	0.03	0.09	0.01	0.09	0.02	0.11	0.02
SIPI	1.02	0.01	0.99	0.01	0.99	0.02	1.00	0.01
VOG1*	1.31	0.12	1.47	0.06	1.43	0.08	1.39	0.06
VOG2*	0.67	0.07	0.76	0.04	0.74	0.05	0.72	0.03

*Significant differences between grave and reference (Wilcoxon rank sum, α=0.05).

Table C.9. Mean (μ) and standard deviation (σ) of the vegetation indices of the leaf spectral reflectance collected on September 25th, 2014.

Index	Control		Grave		Gap		Reference	
	μ	**σ**	**μ**	**σ**	**μ**	**σ**	**μ**	**σ**
NDPI*	0.03	0.02	-0.05	0.05	-0.02	0.05	0.01	0.02
NDVI1*	0.77	0.02	0.83	0.01	0.82	0.03	0.80	0.01
NDVI2*	0.77	0.02	0.82	0.01	0.82	0.03	0.79	0.01
PSRI	-0.24	0.03	-0.19	0.03	-0.21	0.04	-0.23	0.06
RENDVI	0.47	0.04	0.57	0.03	0.54	0.05	0.50	0.06
REP*	0.35	0.02	0.35	0.00	0.36	0.02	0.37	0.02
RVSI*	0.33	0.02	0.32	0.01	0.33	0.02	0.35	0.02
SGI*	0.12	0.02	0.09	0.01	0.10	0.02	0.11	0.02
SIPI*	1.01	0.01	0.99	0.01	0.99	0.01	1.00	0.00
VOG1	1.31	0.04	1.43	0.07	1.39	0.07	1.35	0.09
VOG2	0.68	0.02	0.74	0.04	0.72	0.04	0.70	0.05

*Significant differences between grave and reference (Wilcoxon rank sum, α=0.05).

Table C.10. Mean (μ) and standard deviation (σ) of the vegetation indices of the leaf spectral reflectance collected on October 24th, 2014.

Index	Control		Grave		Gap		Reference	
	μ	**σ**	**μ**	**σ**	**μ**	**σ**	**μ**	**σ**
NDPI	-0.01	0.02	-0.06	0.04	-0.04	0.03	-0.02	0.05
NDVI1	0.78	0.04	0.80	0.03	0.79	0.03	0.81	0.03
NDVI2	0.76	0.04	0.79	0.03	0.78	0.03	0.80	0.04
PSRI	-0.19	0.02	-0.20	0.05	-0.19	0.02	-0.20	0.04
RENDVI	0.52	0.04	0.53	0.06	0.52	0.04	0.54	0.04
REP	0.37	0.02	0.37	0.01	0.38	0.01	0.37	0.02
RVSI	0.34	0.02	0.34	0.01	0.35	0.01	0.34	0.02
SGI	0.11	0.02	0.11	0.01	0.11	0.01	0.10	0.01
SIPI	1.00	0.01	0.98	0.01	0.99	0.01	0.99	0.02
VOG1	1.40	0.06	1.41	0.10	1.38	0.05	1.40	0.05
VOG2	0.72	0.03	0.73	0.06	0.71	0.03	0.72	0.03

*Significant differences between grave and reference (Wilcoxon rank sum, α=0.05).

Table C.11. Mean (μ) and standard deviation (σ) of the vegetation indices of the resampled leaf spectral reflectance collected on November 14th, 2014.

Index	Control		Grave		Gap		Reference	
	μ	**σ**	**μ**	**σ**	**μ**	**σ**	**μ**	**σ**
NDPI	-0.05	0.05	-0.08	0.05	-0.08	0.06	-0.02	0.06
NDVI1	0.78	0.06	0.81	0.03	0.78	0.01	0.80	0.03
NDVI2	0.77	0.06	0.81	0.03	0.77	0.02	0.79	0.04
PSRI	-0.26	0.01	-0.21	0.05	-0.19	0.04	-0.21	0.02
RENDVI	0.46	0.05	0.53	0.07	0.52	0.02	0.51	0.02
REP	0.37	0.04	0.37	0.03	0.37	0.03	0.38	0.01
RVSI	0.35	0.05	0.34	0.03	0.34	0.03	0.35	0.01
SGI	0.13	0.02	0.10	0.02	0.11	0.00	0.11	0.01
SIPI	0.98	0.02	0.98	0.02	0.98	0.02	0.99	0.02
VOG1	1.29	0.05	1.39	0.12	1.39	0.06	1.36	0.04
VOG2	0.66	0.03	0.72	0.07	0.72	0.03	0.70	0.02

*Significant differences between grave and reference (Wilcoxon rank sum, α=0.05).

Appendix D

Table D.1. Mean (μ) and standard deviation (σ) of the vegetation indices computed of the resampled *in-situ* spectral reflectance collected two weeks post disturbance on July 12th, 2013.

Index	Control		Grave		Gap		Reference	
	μ	**σ**	**μ**	**σ**	**μ**	**σ**	**μ**	**σ**
NDPI	0.37	0.04	0.35	0.03	0.35	0.03	0.34	0.04
NDVI1	0.60	0.06	0.05	0.01	0.06	0.01	0.05	0.02
NDVI2	0.67	0.05	0.11	0.02	0.11	0.02	0.11	0.03
PSRI	0.10	0.03	0.38	0.02	0.38	0.02	0.36	0.03
RENDVI	0.40	0.05	0.04	0.01	0.04	0.01	0.03	0.02
REP	0.14	0.02	0.21	0.03	0.19	0.03	0.21	0.03
RVSI	0.17	0.03	0.21	0.03	0.19	0.03	0.21	0.03
SGI	0.05	0.00	0.14	0.02	0.13	0.02	0.15	0.02
SIPI	1.15	0.04	3.97	0.48	3.89	0.46	4.03	0.71
VOG1	1.32	0.05	1.03	0.01	1.03	0.01	1.02	0.01
VOG2	0.70	0.03	0.52	0.01	0.52	0.00	0.52	0.01

*Significant differences between grave and reference (Wilcoxon rank sum, α=0.05).

Table D.2. Mean (μ) and standard deviation (σ) of the vegetation indices of the resampled *in-situ* spectral reflectance collected on August 19th, 2013.

Index	Control		Grave		Gap		Reference	
	μ	**σ**	**μ**	**σ**	**μ**	**σ**	**μ**	**σ**
NDPI	0.37	0.02	0.27	0.08	0.24	0.10	0.29	0.04
NDVI1*	0.51	0.07	0.42	0.25	0.54	0.27	0.17	0.18
NDVI2*	0.58	0.06	0.45	0.24	0.56	0.25	0.22	0.17
PSRI*	0.14	0.03	0.16	0.13	0.12	0.11	0.26	0.09
RENDVI*	0.33	0.05	0.31	0.19	0.42	0.22	0.13	0.14
REP	0.15	0.03	0.21	0.04	0.22	0.04	0.21	0.03
RVSI	0.18	0.04	0.24	0.05	0.26	0.06	0.22	0.04
SGI*	0.06	0.01	0.11	0.04	0.10	0.03	0.14	0.03
SIPI*	1.23	0.07	1.71	0.92	1.31	0.36	2.74	1.19
VOG1*	1.25	0.04	1.30	0.21	1.44	0.27	1.12	0.14
VOG2*	0.65	0.03	0.68	0.13	0.77	0.17	0.57	0.09

*Significant differences between grave and reference (Wilcoxon rank sum, α=0.05).

Table D.3. Mean (μ) and standard deviation (σ) of the vegetation indices of the resampled *in-situ* spectral reflectance collected on September 27th, 2013.

Index	Control		Grave		Gap		Reference	
	μ	**σ**	**μ**	**σ**	**μ**	**σ**	**μ**	**σ**
NDPI	0.34	0.03	0.29	0.07	0.26	0.09	0.26	0.08
NDVI1*	0.59	0.07	0.55	0.20	0.69	0.11	0.37	0.24
NDVI2*	0.65	0.06	0.58	0.19	0.71	0.09	0.40	0.23
PSRI	0.10	0.03	0.12	0.08	0.06	0.03	0.18	0.11
RENDVI*	0.38	0.04	0.38	0.15	0.47	0.10	0.26	0.18
REP	0.15	0.04	0.20	0.05	0.22	0.05	0.20	0.03
RVSI	0.19	0.05	0.24	0.06	0.27	0.07	0.23	0.04
SGI*	0.05	0.02	0.08	0.03	0.07	0.01	0.10	0.03
SIPI*	1.16	0.05	1.25	0.24	1.09	0.05	1.77	0.91
VOG1*	1.30	0.04	1.33	0.16	1.42	0.13	1.23	0.18
VOG2*	0.68	0.02	0.70	0.10	0.75	0.08	0.64	0.11

*Significant differences between grave and reference (Wilcoxon rank sum, $\alpha=0.05$).

Table D.4. Mean (μ) and standard deviation (σ) of the vegetation indices of the resampled *in-situ* spectral reflectance collected on October 11th, 2013.

Index	Control		Grave		Gap		Reference	
	μ	**σ**	**μ**	**σ**	**μ**	**σ**	**μ**	**σ**
NDPI	0.38	0.08	0.32	0.08	0.34	0.07	0.27	0.10
NDVI1	0.56	0.11	0.52	0.24	0.63	0.20	0.41	0.29
NDVI2	0.62	0.09	0.55	0.22	0.65	0.18	0.44	0.27
PSRI	0.13	0.05	0.14	0.11	0.10	0.09	0.18	0.13
RENDVI	0.37	0.08	0.36	0.18	0.42	0.16	0.29	0.22
REP	0.16	0.09	0.17	0.05	0.25	0.05	0.15	0.05
RVSI	0.20	0.11	0.21	0.08	0.31	0.06	0.18	0.06
SGI	0.06	0.04	0.06	0.02	0.08	0.03	0.07	0.03
SIPI	1.20	0.09	1.37	0.44	1.20	0.25	1.78	0.91
VOG1	1.30	0.08	1.31	0.20	1.37	0.18	1.26	0.23
VOG2	0.69	0.05	0.69	0.12	0.72	0.11	0.66	0.14

*Significant differences between grave and reference (Wilcoxon rank sum, $\alpha=0.05$).

Table D.5. Mean (μ) and standard deviation (σ) of the vegetation indices of the resampled *in-situ* spectral reflectance collected on May 7th, 2014.

Index	Control		Grave		Gap		Reference	
	μ	**σ**	**μ**	**σ**	**μ**	**σ**	**μ**	**σ**
NDPI*	0.37	0.02	0.36	0.02	0.34	0.02	0.31	0.04
NDVI1	0.31	0.08	0.12	0.08	0.19	0.18	0.17	0.18
NDVI2	0.40	0.07	0.19	0.08	0.25	0.18	0.22	0.17
PSRI*	0.22	0.04	0.33	0.05	0.28	0.09	0.28	0.09
RENDVI	0.21	0.05	0.07	0.06	0.13	0.13	0.12	0.13
REP	0.21	0.03	0.20	0.02	0.24	0.03	0.19	0.02
RVSI	0.23	0.04	0.21	0.02	0.25	0.03	0.21	0.02
SGI	0.10	0.02	0.13	0.02	0.15	0.04	0.13	0.03
SIPI	1.52	0.16	2.77	0.64	2.52	1.09	2.73	1.11
VOG1	1.16	0.05	1.06	0.05	1.10	0.11	1.10	0.11
VOG2	0.60	0.03	0.54	0.03	0.57	0.07	0.56	0.07

*Significant differences between grave and reference (Wilcoxon rank sum, α=0.05).

Table D.6. Mean (μ) and standard deviation (σ) of the vegetation indices of the resampled *in-situ* spectral reflectance collected on June 20th, 2014.

Index	Control		Grave		Gap		Reference	
	μ	**σ**	**μ**	**σ**	**μ**	**σ**	**μ**	**σ**
NDPI	0.32	0.10	0.20	0.09	0.23	0.10	0.24	0.08
NDVI1	0.70	0.11	0.65	0.18	0.53	0.31	0.54	0.26
NDVI2	0.73	0.09	0.66	0.17	0.55	0.30	0.56	0.25
PSRI	0.07	0.04	0.06	0.06	0.12	0.12	0.11	0.10
RENDVI	0.47	0.10	0.45	0.14	0.38	0.24	0.39	0.19
REP	0.17	0.04	0.21	0.04	0.17	0.02	0.20	0.04
RVSI	0.22	0.05	0.27	0.05	0.20	0.03	0.24	0.06
SGI	0.05	0.02	0.08	0.02	0.08	0.03	0.09	0.04
SIPI	1.11	0.06	1.13	0.16	1.36	0.40	1.38	0.61
VOG1	1.41	0.19	1.41	0.17	1.34	0.25	1.37	0.22
VOG2	0.75	0.12	0.75	0.10	0.71	0.15	0.72	0.14

*Significant differences between grave and reference (Wilcoxon rank sum, α=0.05).

Table D.7. Mean (μ) and standard deviation (σ) of the vegetation indices of the resampled *in-situ* spectral reflectance collected on July 11th, 2014.

Index	Control		Grave		Gap		Reference	
	μ	**σ**	**μ**	**σ**	**μ**	**σ**	**μ**	**σ**
NDPI	0.36	0.04	0.20	0.11	0.20	0.10	0.24	0.08
NDVI1	0.67	0.08	0.67	0.15	0.57	0.28	0.59	0.19
NDVI2	0.71	0.06	0.69	0.14	0.60	0.26	0.62	0.18
PSRI	0.08	0.03	0.05	0.05	0.09	0.10	0.08	0.07
RENDVI	0.43	0.06	0.48	0.13	0.41	0.22	0.41	0.14
REP	0.18	0.03	0.22	0.05	0.19	0.03	0.19	0.04
RVSI	0.23	0.04	0.27	0.07	0.23	0.04	0.24	0.05
SGI	0.06	0.01	0.08	0.03	0.08	0.03	0.08	0.03
SIPI	1.12	0.05	1.10	0.10	1.26	0.35	1.17	0.19
VOG1	1.35	0.06	1.45	0.19	1.39	0.26	1.37	0.17
VOG2	0.71	0.04	0.77	0.12	0.74	0.16	0.72	0.10

*Significant differences between grave and reference (Wilcoxon rank sum, α=0.05).

Table D.8. Mean (μ) and standard deviation (σ) of the vegetation indices of the resampled *in-situ* spectral reflectance collected on August 6th, 2014.

Index	Control		Grave		Gap		Reference	
	μ	**σ**	**μ**	**σ**	**μ**	**σ**	**μ**	**σ**
NDPI	0.37	0.06	0.31	0.08	0.28	0.07	0.30	0.09
NDVI1	0.62	0.09	0.58	0.17	0.58	0.22	0.55	0.15
NDVI2	0.67	0.07	0.63	0.15	0.62	0.20	0.59	0.13
PSRI	0.10	0.04	0.10	0.07	0.10	0.08	0.11	0.06
RENDVI	0.39	0.06	0.38	0.13	0.39	0.16	0.35	0.12
REP	0.18	0.04	0.16	0.05	0.19	0.06	0.17	0.04
RVSI	0.22	0.05	0.20	0.06	0.23	0.07	0.21	0.05
SGI*	0.06	0.01	0.06	0.02	0.07	0.02	0.07	0.02
SIPI	1.15	0.06	1.19	0.19	1.20	0.19	1.21	0.14
VOG1	1.31	0.06	1.32	0.13	1.33	0.17	1.29	0.14
VOG2	0.69	0.03	0.69	0.08	0.70	0.10	0.68	0.09

*Significant differences between grave and reference (Wilcoxon rank sum, α=0.05).

Table D.9. Mean (μ) and standard deviation (σ) of the vegetation indices of the resampled *in-situ* spectral reflectance collected on September 18th, 2014.

Index	Control		Grave		Gap		Reference	
	μ	**σ**	**μ**	**σ**	**μ**	**σ**	**μ**	**σ**
NDPI	0.36	0.05	0.31	0.09	0.33	0.05	0.32	0.07
NDVI1	0.64	0.09	0.56	0.21	0.45	0.21	0.52	0.17
NDVI2	0.69	0.07	0.61	0.18	0.53	0.18	0.58	0.14
PSRI	0.09	0.03	0.12	0.09	0.17	0.10	0.14	0.09
RENDVI	0.42	0.06	0.38	0.16	0.30	0.15	0.34	0.12
REP	0.20	0.07	0.14	0.06	0.12	0.05	0.15	0.04
RVSI	0.26	0.08	0.17	0.08	0.15	0.06	0.18	0.06
SGI	0.07	0.03	0.05	0.02	0.05	0.02	0.06	0.02
SIPI	1.14	0.05	1.24	0.23	1.37	0.34	1.26	0.23
VOG1	1.34	0.07	1.33	0.17	1.24	0.13	1.28	0.12
VOG2	0.71	0.04	0.70	0.10	0.65	0.07	0.67	0.07

*Significant differences between grave and reference (Wilcoxon rank sum, α=0.05).

Appendix E

Table E.1. Mean (μ) and standard deviation (σ) of the computed vegetation indices for the airborne data collected on May 8th, 2014.

Index	Control		Grave		Gap		Reference	
	μ	**σ**	**μ**	**σ**	**μ**	**σ**	**μ**	**σ**
NDPI*	0.47	0.01	0.45	0.02	0.45	0.02	0.41	0.02
NDVI1	0.44	0.04	0.23	0.07	0.18	0.03	0.22	0.07
NDVI2	0.36	0.05	0.16	0.07	0.12	0.02	0.17	0.07
PSRI*	0.21	0.03	0.33	0.05	0.35	0.01	0.30	0.05
RENDVI	0.24	0.03	0.10	0.05	0.08	0.01	0.12	0.05
REP*	0.29	0.02	0.33	0.01	0.33	0.01	0.32	0.01
RVSI*	0.10	0.01	0.11	0.01	0.11	0.01	0.10	0.01
SGI	0.11	0.01	0.14	0.01	0.15	0.01	0.14	0.01
SIPI	1.46	0.10	2.43	0.56	2.65	0.26	2.27	0.54
VOG1*	1.18	0.03	1.08	0.04	1.07	0.01	1.11	0.05
VOG2*	0.60	0.02	0.55	0.02	0.54	0.01	0.56	0.02

*Significant differences between grave and reference (Wilcoxon rank sum, α=0.05).

Table E.2. Mean (μ) and standard deviation (σ) of the computed vegetation indices for the airborne data collected on June 17th, 2014.

Index	Control		Grave		Gap		Reference	
	μ	**σ**	**μ**	**σ**	**μ**	**σ**	**μ**	**σ**
NDPI*	0.39	0.02	0.31	0.04	0.33	0.05	0.32	0.03
NDVI1*	0.66	0.05	0.61	0.12	0.55	0.14	0.53	0.11
NDVI2*	0.60	0.06	0.57	0.13	0.51	0.15	0.49	0.12
PSRI*	0.10	0.02	0.09	0.05	0.11	0.06	0.12	0.05
RENDVI*	0.39	0.05	0.41	0.09	0.36	0.11	0.35	0.09
REP*	0.22	0.01	0.25	0.02	0.26	0.02	0.25	0.02
RVSI*	0.71	0.06	0.77	0.11	0.82	0.12	0.79	0.11
SGI*	0.67	0.05	0.89	0.16	0.95	0.18	0.96	0.16
SIPI*	1.32	0.06	1.37	0.10	1.32	0.12	1.33	0.10
VOG1	0.67	0.03	0.69	0.06	0.66	0.06	0.67	0.05
VOG2*	0.60	0.02	0.55	0.02	0.54	0.01	0.56	0.02

*Significant differences between grave and reference (Wilcoxon rank sum, α=0.05).

Table E.3. Mean (μ) and standard deviation (σ) of the computed vegetation indices for the airborne data collected on July 10th, 2014.

Index	Control		Grave		Gap		Reference	
	μ	**σ**	**μ**	**σ**	**μ**	**σ**	**μ**	**σ**
NDPI*	0.42	0.02	0.28	0.06	0.27	0.07	0.31	0.04
NDVI1*	0.66	0.03	0.75	0.06	0.66	0.12	0.63	0.06
NDVI2*	0.61	0.04	0.73	0.07	0.64	0.13	0.60	0.07
PSRI*	0.10	0.02	0.04	0.02	0.06	0.05	0.08	0.03
RENDVI*	0.38	0.02	0.52	0.06	0.44	0.12	0.41	0.06
REP*	0.25	0.01	0.27	0.01	0.27	0.02	0.25	0.02
RVSI*	0.86	0.05	0.73	0.09	0.79	0.10	0.76	0.06
SGI*	0.77	0.04	0.78	0.09	0.91	0.09	0.86	0.08
SIPI*	1.16	0.03	1.07	0.04	1.12	0.09	1.14	0.05
VOG1*	1.29	0.03	1.49	0.09	1.40	0.14	1.36	0.07
VOG2*	0.66	0.01	0.76	0.05	0.70	0.08	0.69	0.04

*Significant differences between grave and reference (Wilcoxon rank sum, α=0.05).

Table E.4. Mean (μ) and standard deviation (σ) of the computed vegetation indices for the airborne data collected on August 8th, 2014.

Index	Control		Grave		Gap		Reference	
	μ	**σ**	**μ**	**σ**	**μ**	**σ**	**μ**	**σ**
NDPI	0.41	0.02	0.36	0.04	0.36	0.03	0.36	0.04
NDVI1*	0.60	0.02	0.67	0.07	0.61	0.11	0.58	0.07
NDVI2*	0.53	0.03	0.62	0.07	0.56	0.12	0.52	0.08
PSRI*	0.13	0.01	0.08	0.03	0.10	0.05	0.11	0.03
RENDVI*	0.33	0.02	0.40	0.06	0.35	0.09	0.33	0.06
REP	0.21	0.01	0.21	0.02	0.21	0.02	0.22	0.02
RVSI	0.76	0.05	0.70	0.08	0.74	0.09	0.74	0.08
SGI*	0.71	0.05	0.67	0.09	0.73	0.12	0.78	0.11
SIPI*	1.21	0.02	1.14	0.05	1.20	0.11	1.21	0.08
VOG1*	1.24	0.03	1.34	0.06	1.28	0.08	1.27	0.06
VOG2*	0.63	0.01	0.68	0.03	0.65	0.04	0.64	0.03

*Significant differences between grave and reference (Wilcoxon rank sum, α=0.05).

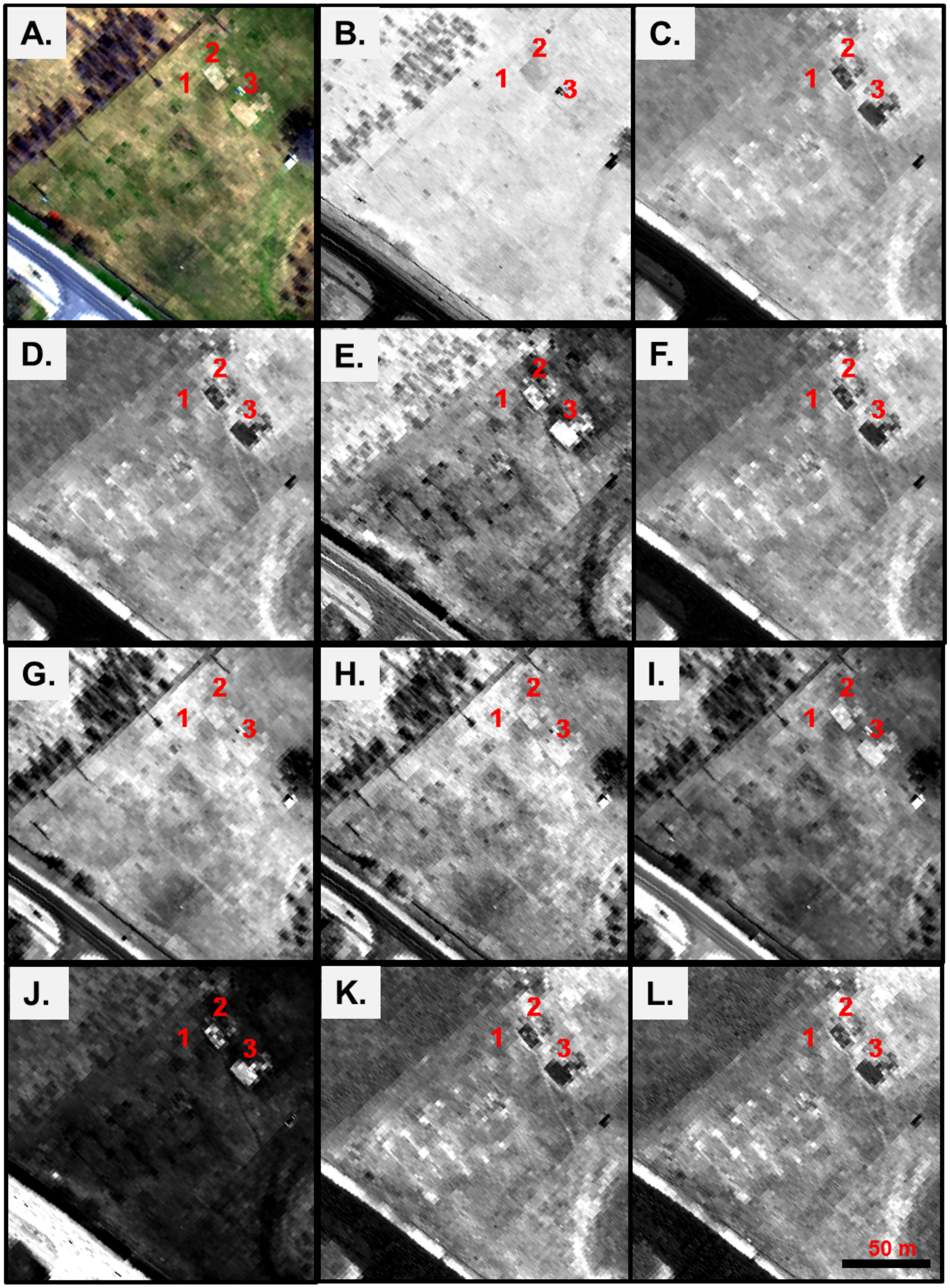

Figure E.1. Georectified CASI imagery displaying the computed vegetation indices for the data collected on May 8th, 2014. Order of indices: (A) True color composite (R: 739 nm G: 698 nm B: 553 nm), (B) NDPI, (C) NDVI1, (D) NDVI2, (E) PSRI, (F) RENDVI, (G) REP, (H) RVSI, (I) SGI, (J) SIPI, (K) VOG1, and (L) VOG2. Numbers on the images represent the study sites: (1) control, (2) reference, (3) grave and gap.

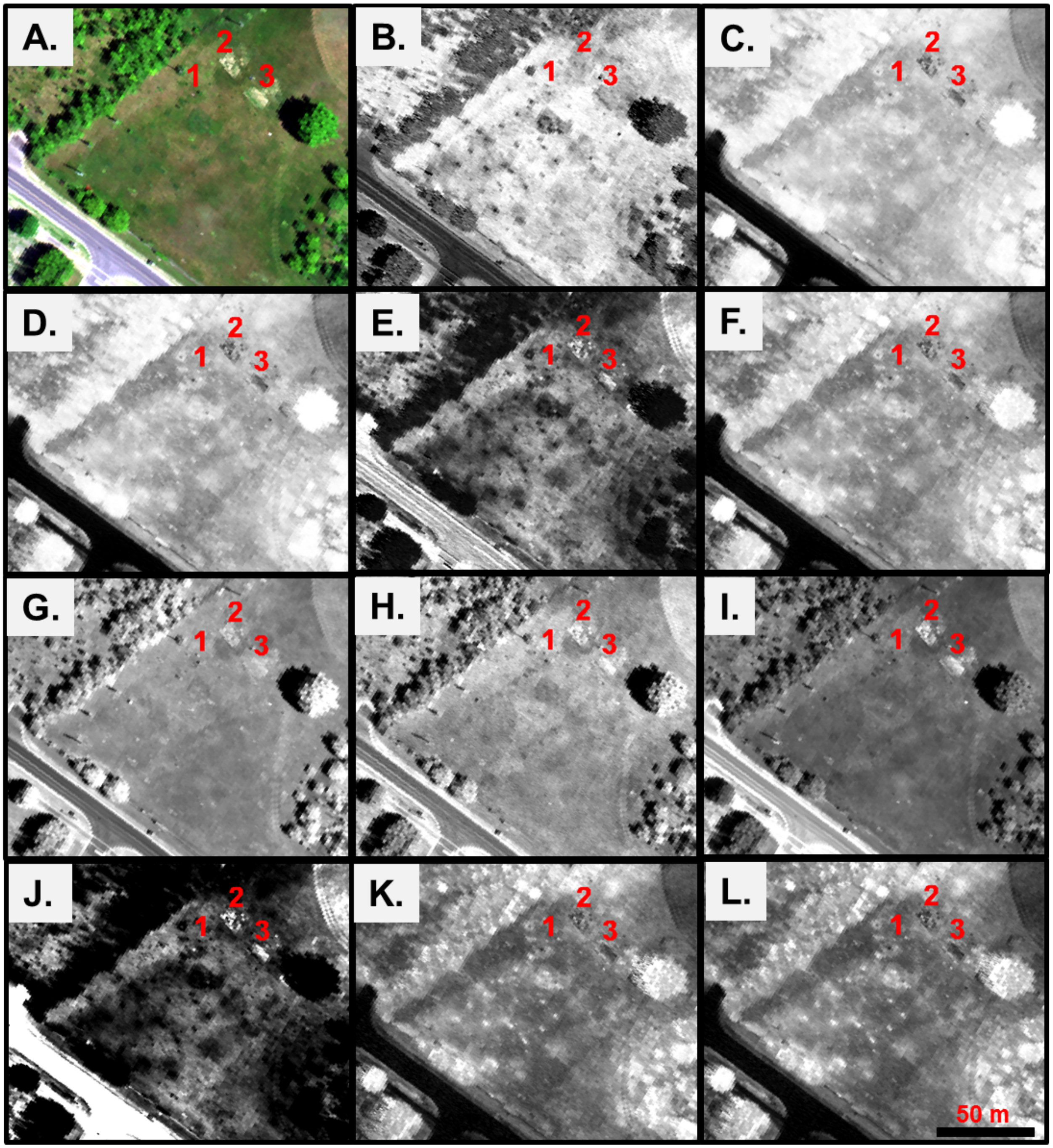

Figure E.2. Georectified CASI imagery displaying the computed vegetation indices for the data collected on June 17th, 2014. Order of indices: (A) True color composite (R: 739 nm G: 698 nm B: 553 nm), (B) NDPI, (C) NDVI1, (D) NDVI2, (E) PSRI, (F) RENDVI, (G) REP, (H) RVSI, (I) SGI, (J) SIPI, (K) VOG1, and (L) VOG2. Numbers on the images represent the study sites: (1) control, (2) reference, (3) grave and gap.

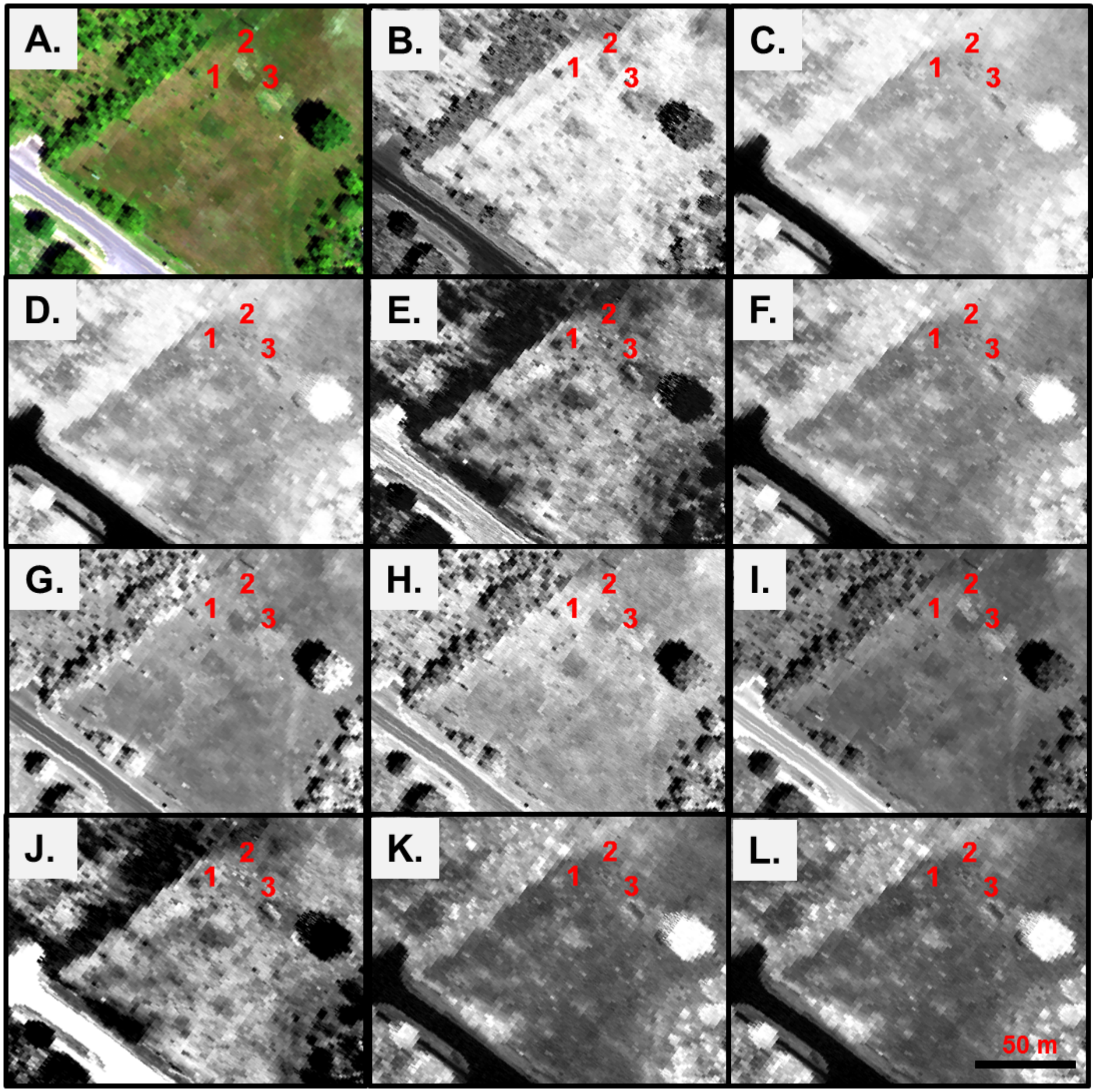

Figure E.3. Georectified CASI imagery displaying the computed vegetation indices for the data collected on July 10th, 2014. Order of indices: (A) True color composite (R: 739 nm G: 698 nm B: 553 nm), (B) NDPI, (C) NDVI1, (D) NDVI2, (E) PSRI, (F) RENDVI, (G) REP, (H) RVSI, (I) SGI, (J) SIPI, (K) VOG1, and (L) VOG2. Numbers on the images represent the study sites: (1) control, (2) reference, (3) grave and gap.

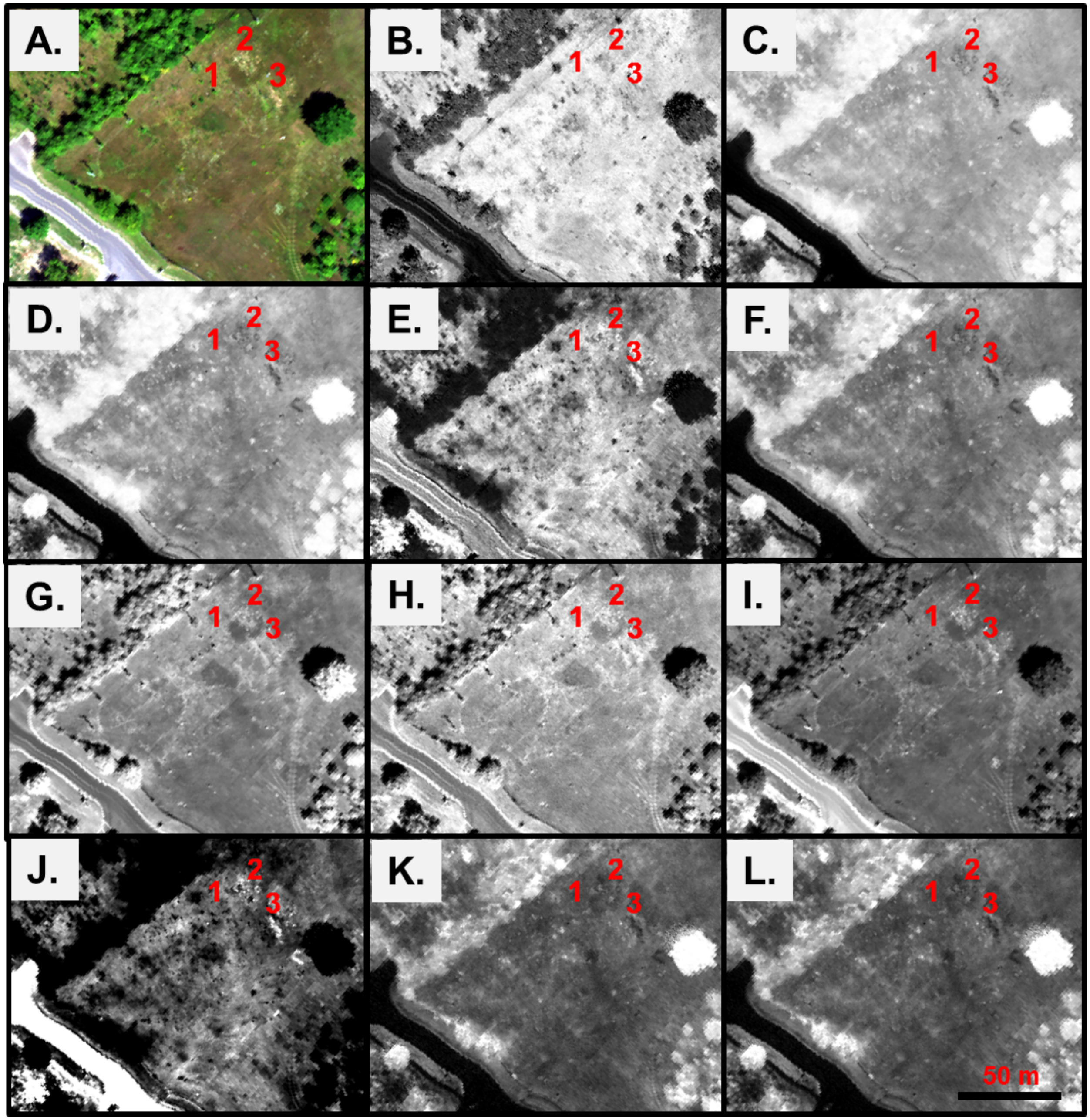

Figure E.4. Georectified CASI imagery displaying the computed vegetation indices for the data collected on August 8th, 2014. Order of indices: (A) True color composite (R: 739 nm G: 698 nm B: 553 nm), (B) NDPI, (C) NDVI1, (D) NDVI2, (E) PSRI, (F) RENDVI, (G) REP, (H) RVSI, (I) SGI, (J) SIPI, (K) VOG1, and (L) VOG2. Numbers on the images represent the study sites: (1) control, (2) reference, (3) grave and gap.